SMHI

Scientific Report for the SAFNWC

Mid Term Review

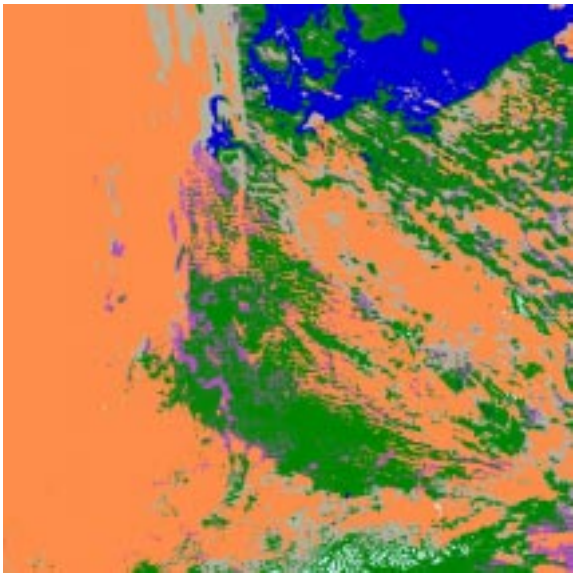
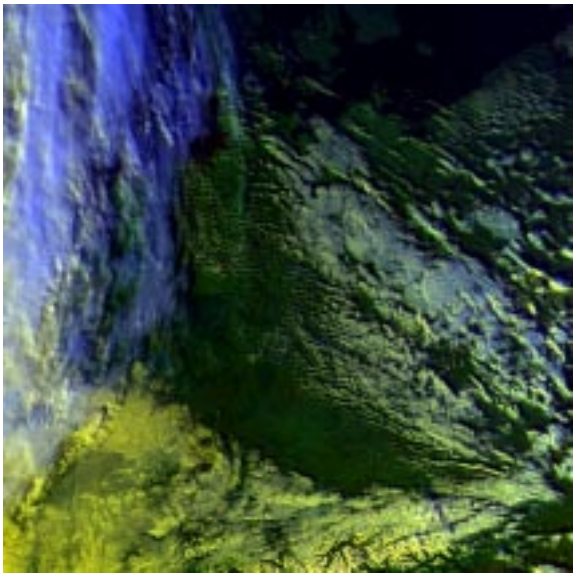
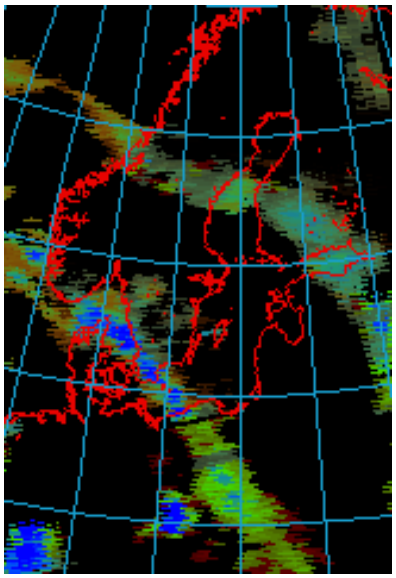
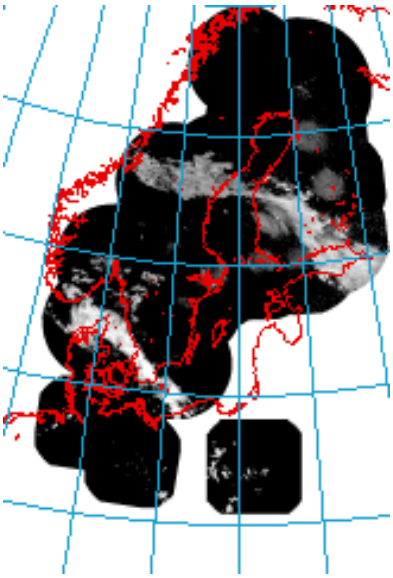

SAF/NWC/SMHI/MTR/SR, Issue 1.1, September, 2000

Prepared by the Swedish Meteorological and Hydrological Institute

Cover: ***Upper-left:*** Cloud Mask prototype.

The five-category cloud mask output (non-procesed is black; cloudfree is green or blue; cloud contaminated is grey; cloud filled is orange; snow cover is white) is here combined with information from the Processing flags. The flag for low-quality is superimposed, thus where there is purple there is particular risk for mis-classifications. (NOAA 14, 14 February 2000, 15:03 UTC).

Upper right: Corresponding AVHRR channel 1,2,4 RGB composite.

Lower right: Precipitating Clouds prototype.
Precipitation probabilities from combined AVHRR/AMSU. Reddish indicates very light, green light to moderate and blue intensive precipitation. (NOAA15, 23 September 1999, 17:24 UTC)

Lower left: Radar composite for 17:30UTC. (NORDRAD)

Scientific Report for the SAFNWC Mid Term Review

Prepared by:

Adam Dybbroe, K.-G. Karlsson, Mats Moberg, Anke Thoss

Swedish Meteorological and Hydrological Institute

SE-601 76 Norrköping, Sweden

Phone: +46 11 4958000

Document change record

Issue/rev.	Document ID	Date	Changes
Draft	SR Draft	January 2000	Draft for review
Issue 1.0	SAF/NWC/SMH/MTR/SR/1.0	21 February 2000	First version
Issue 1.1	Updates based on Mid Term Review	September 2000	Mainly changes as listed in the MTR RID Response Report.

Executive summary

The main tasks for SMHI in the SAF for support to Nowcasting and Very Short Range Forecasting (SAFNWC) are the development of software to produce Cloud Mask, Cloud Type, Cloud Top Temperature and Height and Precipitating Clouds products based on AVHRR data and a Precipitating Clouds product based on SEVIRI data. Prototypes for all products are available with somewhat different status, especially concerning validation. Much effort has been allocated to the thorough prototyping of the Cloud Mask product, as the quality of this is crucial for all the other AVHRR/AMSU products.

Compared to the Project Plan, there is a certain time delay and some tasks are not fulfilled. It is envisaged, though, that by October 2000, SMHI will be in phase with the overall plan with no effects on the final delivery to the integration phase. However, the still not solved issue about the final integration of the EPS Software Package, including common software support elements like a EPS Software Library, is a major obstacle for the further development of the AVHRR based products.

1 Scope of the SMHI MTR Scientific Report

1.1 Objective of the SAFNWC project as regards cloud and precipitation products

The main purpose of the SAFNWC project is to give the weather forecaster and other users in all EUMETSAT member states guidance on the existence and evolution of synoptic and mesoscale weather systems with particular emphasis on the monitoring of severe weather phenomena. In this respect, the monitoring of clouds and precipitation is extremely important.

From a general point of view, SAFNWC products shall be based primarily on data from EUMETSAT satellites (i.e., MSG and EPS) but other satellite data and necessary ancillary data may be used if applicable and if contributing in enhancing the value of the product. The use of NWP data is allowed but must be kept to a minimum in order to ensure that it highlights features in satellite imagery and does not dominate the contents of the product.

Two different aspects of cloud monitoring are covered in SAFNWC. The first one concerns the detection and identification of clouds at the pixel or even at sub-pixel scale. The primary purpose here is to delineate all cloudy or cloud-contaminated pixels in order to prevent mistakes from being made in applications investigating conditions in cloud-free areas. This particular aspect of cloud monitoring is important for the extraction of information on atmospheric stability and moisture content – two crucial parameters used for determining the risk for severe weather. In addition, the derived information on cloud types and the vertical extension of clouds may provide valuable information on the status of ongoing cloud processes (different convection phases, distribution of stratiform and convective clouds, existence of deep convection, etc.). The second aspect of cloud monitoring concerns the interpretation of existing cloud systems or cloud complexes in satellite imagery. Here, cloud systems with horizontal dimensions largely exceeding the pixel scale have to be identified and tracked in order to provide useful information on the current development phase and intensity of each particular weather phenomena.

Precipitation products may be seen as further derivatives of either or both aspects of cloud monitoring. A refined analysis of individual pixel radiances may be used to infer precipitation rates or, alternatively, information on larger-scale cloud system appearances and temporal evolutions may be used for the same purpose.

Table 1-1below shows a summary of all the developed products in SAFNWC sorted in various groups or families according to their different purposes. The first aspect of cloud monitoring is here covered by products denoted as Cloud products while the second aspect concerns the two groups Thunderstorm products and Conceptual Models products. Note also here that the Cloud products in general must be derived prior to the derivation of the group Air Mass products for reasons explained earlier. Finally, Precipitation products as well as Wind products form specific groups in Table 1-1

*Table 1-1***:** *SAFNWC product groups*

Group	Product No.	Acronym
Cloud products (CP)	Products 1 to 3	CMa; CT; CTTH
Precipitation products (PP)	Products 4 and 5	PC; CRR
Air mass products (AMP)	Products 6 to 8 and 12	TPW; LPW; SAI; AMA
Wind product (WP)	Product 9	HRW
Thunderstorm Product (TP)	Product 11	RDT
Conceptual Models product (CMP)	Product 10	ASII

1.2 The role of SMHI in SAFNWC

Historically, SMHI has a long tradition in developing Nowcasting tools for cloud and precipitation monitoring purposes by use of weather satellite imagery. SMHI is consequently involved in the SAFNWC development of products in the Cloud and Precipitation product groups, more specifically products CMa, CT, CTTH and PC as listed in Table 1-1 above.

SMHI is the only participating NMS in SAFNWC representing NMSs from the northern part of Europe where the use of Meteosat and MSG is somewhat limited due to geometrical constraints. This has given SMHI a quite different role in SAFNWC as compared to the roles of other consortium partners. More specifically, in order to ensure valuable SAFNWC products also for NMSs in EUMETSAT member states situated at northern latitudes, SMHI is responsible for the development of products based on data from polar orbiting satellites (NOAA and, in future, EPS). This means that the development of products based on MSG/SEVIRI data is not the main goal for SMHI as opposed to the goals for the other partners in SAFNWC. The SMHI responsibility to also provide the NOAA/EPS cloud mask algorithm for use in SAFOSI emphasises this chosen development priority even further.

However, to be noted here is that among the SMHI tasks in SAFNWC is also the task to harmonise the NOAA/EPS cloud products with the corresponding products from MSG/SEVIRI. In addition, this includes that SMHI shall contribute in the adaptation of the MSG/SEVIRI algorithms to the special conditions prevailing at northern latitudes (e.g., caused by large seasonal changes, very cold surface temperatures, frequent twilight conditions, snow covered ground, etc.).

The development of the cloud products (SAFNWC products 1-3) is shared between SMHI and Meteo-France in the following way: Meteo-France is responsible for the MSG/SEVIRI software modules and SMHI for the NOAA/EPS software modules. Regarding the development of the precipitation product (SAFNWC product 4), SMHI has the full responsibility for both the NOAA/EPS and the MSG/SEVIRI modules.

1.3 SMHI prototyping strategy

As a first priority in the SMHI development, the ambition has been to develop a significantly revised set of cloud and precipitation monitoring products based on polar satellite data as compared to previously available operational tools at SMHI and at other NMSs. In addition, these products must be made compatible and harmonised with corresponding products developed for MSG/SEVIRI in order to facilitate their future use in a Nowcasting system environment.

To accomplish this harmonisation, a very close co-ordination with Meteo-France was conducted during the initial specification of the contents of the cloud products. Later on in the project, a further harmonisation also involving development and implementation of common software elements or algorithms was envisaged. Concerning the precipitation product (PC) where development is conducted exclusively by SMHI, a common product output for the MSG and NOAA/EPS algorithms was defined whereas algorithm differences is expected due to the additional use of microwave data from the AMSU instrument in the NOAA/EPS algorithm.

In summary, SMHI has tried to adopt the following logical steps during the development (as shown in Table 1-2.

Table 1-2: General SMHI development plan in SAFNWC.

Chronological development Step	Development action
Step 1	Produce detailed product specification including a harmonisation of MSG and NOAA/EPS product outputs.
Step 2	Prototype NOAA/EPS algorithms and perform a basic validation of results.
Step 3	Test modifications of the prototyped GOES cloud algorithms to be applied at high latitudes based on experiences from the previous step.
Step 4	Implement the NOAA/EPS algorithms
Step 5	Implement modifications to the MSG/SEVIRI cloud algorithms.
Step 6	Validate and tune the NOAA/EPS and MSG/SEVIRI algorithms.
Step 7	Integrate software and deliver to SAFNWC host

Referring to the SAFNWC project plan (PP), steps 1-3 should be completed before MTR.

1.4 Summary of general achievements

Considerable progress in the prototyping of the NOAA/EPS algorithms has been reached prior to MTR. This concerns especially the CMa, CTy and PC products where considerable efforts have been made during the development work. For the CTTH product, parts of the prototyping work still remains uncompleted. Deviations from the development plan Table 1-2 can also be seen for the activities planned for Step 3. The specific problems here are partly due to the unsolved problem of getting access to GOES imager data for prototyping and partly to the fact that an initial delay of the SMHI prototyping work resulted in severe timing problems for the common SMHI and Meteo-France development work.

It has to be recognised that the commitments to the development of four NOAA/EPS products and one MSG/SEVIRI product in combination with the expected contribution to the three MSG/SEVIRI cloud products have not been completely fulfilled within the given manpower resources. The shortcomings are partly explained by initial staff shortage problems but it seems also evident that initial plans were too optimistic and ambitious in relation to given resources.

Some particular problems regarding the status and development of the NOAA/EPS software packages in SAFNWC have been encountered and this has caused some extra workload for SMHI, see 2.1.

1.5 Outlines of this report

In the following chapters of this report, the results of the SMHI prototyping work are given followed by a discussion on the consequences and plans for the remaining period of the SAFNWC project.

Chapter 2 explains general product conditions and requirements which are common for all four NOAA/EPS products. *Chapters 3-7* describe the prototyping of each individual PGE. Chapters 3-6 deal with cloud and precipitation products for NOAA/EPS while chapter 7 describes the precipitation product for MSG/SEVIRI. Notice here that for the cloud products 1-3 (described in chapters 3-5) a special section discussing the adaptation of the MSG/SEVIRI scheme to high latitude conditions is also included (related to development step 3 in Table 1-2).

Chapter 8 summarises the main conclusions from the prototyping work and discusses how this will affect activities for the remaining period of SAFNWC. The plans for validation and integration activities are detailed and a strategy for solving the remaining prototyping tasks is presented.

Necessary references to applicable documents and publications as well as additional complementing information related to the previous chapters are given in the Appendices A.1-A.11.

2 Common SAFNWC product issues

Several of the product requirements listed in the SP and URD documents are common for all SAFNWC products. The most important of them, related to the cloud and precipitation products covered in this report, are listed in the following sub-sections.

2.1 Software design - software packages

2.1.1 SAFNWC requirements

- All AVHRR modules (products 1b-4b) and the AVHRR-AMSU module (product 4b) shall be integrated into a single software package independent of the SEVIRI software package. (**UR-6.2.3**)
- The SEVIRI and the AVHRR/AMSU Software Packages shall be designed highly modular so that the users' can easily integrate parts of the Software Packages into their own Nowcasting Systems. (**UR-6.2.4**)
- The user shall be able to configure which of the 12 SEVIRI and 4 AVHRR/AMSU products he wishes to process without needing to modify the software, bearing in mind existing product dependencies. (**UR-6.3.4**)

2.1.2 The EUMETSAT EPS program

At the start of the SAFNWC in 1997, the final decision on the development and launch of the EPS satellites had not yet been taken by the EUMETSAT council. As a consequence, the NOAA/EPS package was initially given only the status of an optional and independent part of the SAFNWC software and not a fully integrated one. This decision has lead to rather serious consequences for the SMHI development work. For example, it meant that no common pre-processing or preparation modules for NOAA/EPS would be supplied by the SAFNWC host as a contrast to the case for MSG (see 2.3) Thus, SMHI was by this forced to develop or acquire this software as an additional development task. These circumstances were not clear at the definition and start of the SAFNWC project. Consequently, these additional task for SMHI were not supported by any of the work packages in the SAFNWC PP.

2.1.3 Status of the NOAA/EPS software package

Not until May 1999, at the 4th Project Team meeting, it became obvious that there was a contractual inconsistency regarding the responsibility for the integration of the NOAA/EPS product modules into a Software Package. According to the contract between the SAFNWC host, INM, and EUMETSAT the host is only responsible for the delivery of a MSG Software Package (SWP). On the other hand, the agreement between INM and SMHI states that the latter is only responsible for the delivery of product modules, not the integration of those modules into an EPS SWP with common Library functions, a Task Manger etc. The relation between Software Package and Product elements is illustrated in Figure 2-1

This issue was addressed at the 6th SAFNWC Steering Group meeting in June 1999. The meeting decided that SMHI was to document the status of the software included and the additional activities and tasks needed for a full integration of an AVHRR/EPS package.

At the extra, 7th, SG meeting in September SMHI presented a report (Implications of a separate Software Package for EPS data within the SAFNWC, 7 July 1999) outlining the

tasks and funding necessary for the integration of such an EPS SWP. This report addresses the General considerations for a separate EPS SWP as follows:

> "The overall design criteria for the EPS SW Package should aim at, as far as possible, the re-use of the design, functions, libraries and interfaces from the MSG SW Package. From the end-users point of view, installation, maintenance and use of the package shall be as similar as possible compared to the MSG package. Both packages shall be able to run in parallel on one computer. However, a possible overall integration of the two packages (e.g. a global Task Manager) is beyond the scope of the EPS Package."

The SG approved the ideas outlined in the report but found the estimated costs to high. However, the SG decided to use funding from the Visiting Scientists program for the most urgent task, the documentation phase for the EPS SWP. On the other hand, they postponed any decision on the actual development work of the SWP and the later phase of integration and verification. The present status of the EPS SWP is that the software documentation is available (SRD, ADD, ICD and SVV) but there is no funding for the actual creation of this package during the present development phase.

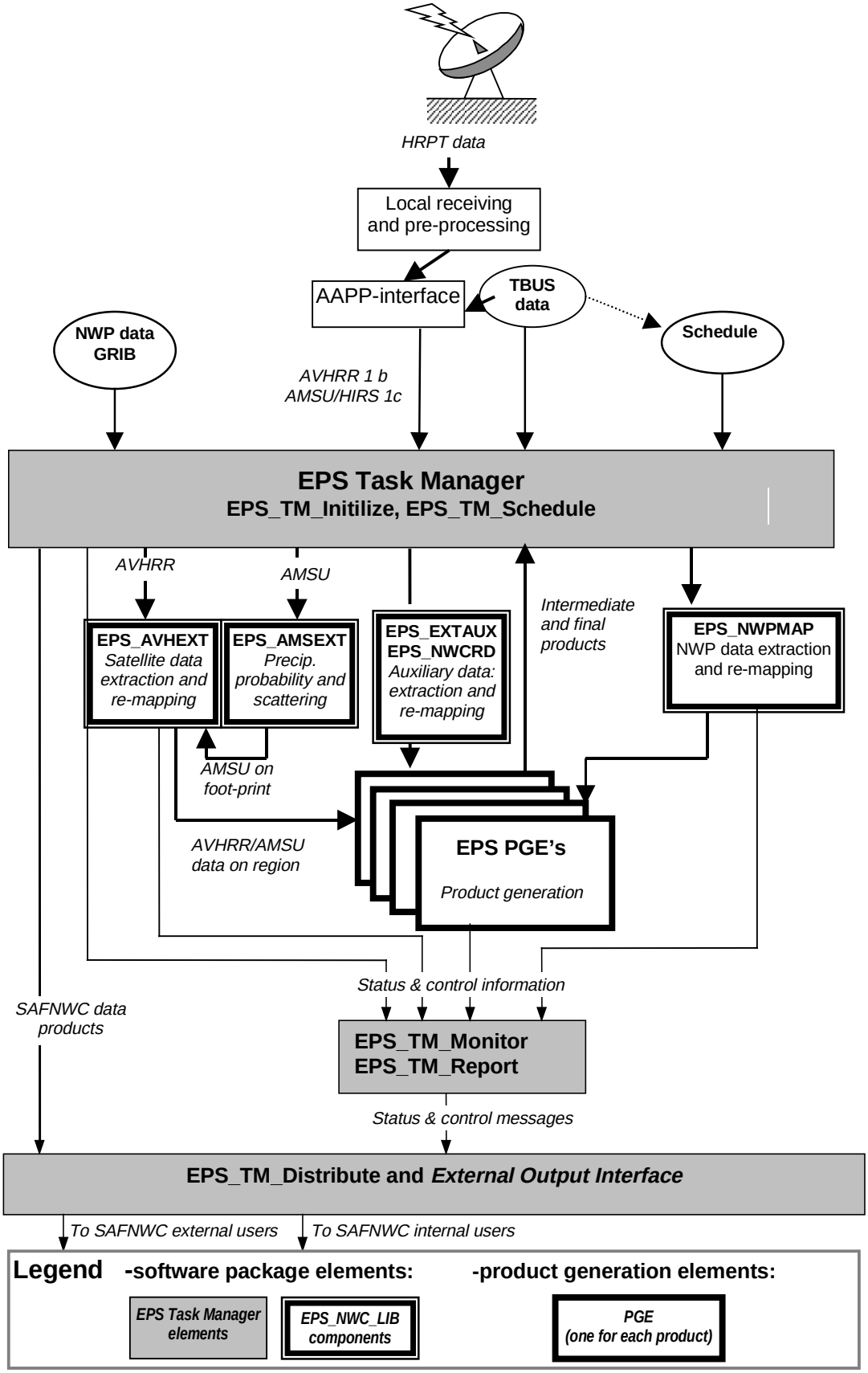

Figure 2-1: The overall concept of the SAFNWC EPS Software Package

2.2 Software design - software recommendations

2.2.1 SAFNWC requirements

- The SEVIRI software shall be coded in ANSI C and/or FORTRAN using the Korn Shell, avoiding proprietary extensions. (**UR-6.8.1**)
- No other Programming Language shall be used, unless it can be demonstrated that such use has no impact on the software portability. (**UR-6.8.2**)
- The Software Package shall not make use of freely available software packages (e.g. "Freeware"), unless explicitly agreed by EUMETSAT. (**UR-6.4.3**)

2.2.2 The use of Python

2.2.2.1 Background

Python was introduced at SMHI in 1995, when the satellite processing system, Prosat, (handling tasks from reception to image presentation), was moved from the VAX to the Unix environment. Now *Python* is an integrated part of both the production and development of satellite applications, and *Python* has spread to other application areas such as those using Weather Radar data. At the Research and Development section, it is being used as a general purpose programming language together with *C* and *Fortran*, and at the same time to a large extent replacing ordinary Shell scripts. From our experience we believe *Python* (in combination with *C* and *Fortran*) will let us concentrate on solving the problems we are facing in the SAFNWC quickly and efficiently, more so than using any other alternative.

2.2.2.2 The Python issue

Quite early in the SAFNWC project the question whether to allow the use of Python in the software to be developed became an issue. Several discussions in the SAFNWC Project Team as well as in the Steering Group accompanied with the production of various written documents (the most comprehensive paper being SMHI_6) have taken place during the past years.

The issue was finally settled with a decision and a recommendation at the 6th STG Science Working Group Meeting (March 1999). The action decided was that SMHI should demonstrate the portability of Python by making a test installation of Python on different platforms. By the end of September 1999, these tests was successfully accomplished at MF/CMS (SUN Solaris platform) and at DNMI (SGI platform). The recommendation was that

> "The SWG encouraged SMHI to continue the software development with Python and recommended to the SAF steering group to favourably consider the SMHI proposal to use the Python language considering that maintenance for at least 5 years will be guaranteed by SMHI"
>
> *(Summary Minutes, STG 6th SWG Meeting, Recommendation 6.12).*

From the user's of EPS-based product perspective, the Python code will be non-transparent, i.e. all configuration is done by the ordinary configuration files. The necessary Python libraries will be a part of the EPS SWP installation. Our PC product for MSG data will not include any use of Python.

2.3 Provision of AVHRR/AMSU level 1b data

2.3.1 SAFNWC requirements

- The Software Packages provided by the SAF shall include all necessary standard modules to pre-process SEVIRI level 1.5 and AVHRR/AMSU level 1b data, i.e. calibration in brightness temperatures and bi-directional reflectances, computation of satellite and solar geometry and geographic reprojection routines (e.g. space view to latitude/longitude). (**UR-6.5.1**)

2.3.2 Provision of AVHRR/AMSU level 1b data

As opposed to SEVIRI level 1.5 data there is presently no EUMETSAT defined standard for the exact format of the corresponding level 1b polar data. Based on an EUMETSAT initiative the AAPP (ATOVS and AVHRR Processing Package) are under development under the auspices of the EUMETSAT AAPP Development Team. This is the most promising, common available, software for the extraction of AVHRR and AMSU data. The SAFNWC EPS products depend solely on the AAPP for the input of AVHRR/AMSU data.

Note that there may be some confusion concerning the term " AVHRR/AMSU level 1b data". According to the EPS Data Level Definition, AVHRR level 1b is defined as

> " Calibrated, earth located and quality controlled data, at the original full instrument resolution as acquired and packaged with needed ancillary, engineering and auxiliary data." (E.g. *EPS End User Requirements Document, 25-Aug-97)*

According to the AAPP documentation, AVHRR level 1b is defined as

> " Instrument counts, calibration and earth location information appended, on an original instrument grid" (corresponding to the EPS Data Level Definition level 1a).
>
> *(ATOVS and AVHRR Processing Package AAPP Design Document, Volume 1, Module Design, Rev. 1, 21-July-97).*

The SAFNWC EPS products will expect AVHRR level 1b input data as defined by AAPP; i.e. a prerequisite for the use of the SAFNWC/EPS Software Package is an installation of the AAPP

In other words, the user is expected to, by means of the recommended version of AAPP and configured as specified by the SAFNWC, furnish the EPS product modules with pixel data in their original position and with navigation and calibration information appended. The actual calibration and navigation to the requested region, in the proper projection, is a task for an EPS Library function. AMSU data input is expected to conform to the AAPP AMSU level 1c definition:

> "Radiances and brightness temperatures, with appended earth location, on original instrument grid."
>
> *(ATOVS and AVHRR Processing Package AAPP Design Document, Volume 1, Module Design, Rev. 1, 21-July-97).*

2.4 Dependency on non-satellite data

As it become clear from the description of the individual products all algorithms make use of auxiliary data as input in addition to the satellite data. The auxiliary data cover both static data and dynamic (content changes from one satellite slot/pass to another). Of typical static data

belong the physiographical data like land-use and digital elevation model (DEM) data, extracted from external sources. The most pronounced source of dynamic data are the outputs from short term NWP forecasts. It is worth mentioning here that the algorithms make use of other dynamic data, namely the information of the sun- and satellite viewing geometry (sun zenith, satellite zenith, and sun-satellite azimuth difference angles). However, these data, being part of the output from the early pre-processing of the satellite data (AAPP), we will refer to as ancillary data to distinguish them from the true auxiliary data not having to do with the satellite.

The use and dependency of NWP data in satellite retrievals is often thought to be critical, and something one should either try to avoid or limit to the absolute minimum. This is because products may be used as input to objective analyse schemes also using (the same) NWP mode data, or more seriously the product will be feed into the local NWP data assimilation giving rise to unrealistic growth of initial model errors (usually referred to as incest).

Therefore we treat the use of NWP data in general here, and for each product we discuss where in the algorithms the dependency on NWP model data (and quality) is particularly topical.

2.4.1 SAFNWC requirements

- The Software Package shall not make use of forecasted meteorological fields whose forecast validation time differs more than 6 hours from the observation time (**UR-6.4.4**) and whose forecast length exceeds 24 hours. (**UR 6.4.5**)
- The dependence of the products on NWP model data shall be limited to the amount that is absolutely necessary to extract the products, i.e. the parameters derived from NWP model output shall not dominate the final products. (**UR-6.4.6**)
- The Software Package shall include standard modules to pre-process ECMWF model output data (e.g. re-mapping of NWP output data onto SEVIRI and AVHRR images). These modules shall be well documented so that the user of the software can easily adapt them to other NWP models (e.g. to the HIRLAM model and the ARPEGE model). (**UR-6.5.2**)

2.4.2 Current status in prototyping

Experiences of the benefits of using Numerical Weather Prediction (NWP) data, in various meteorological satellite classification schemes at several NMS's during a rather long time, have proven that these data increase the performance significantly. The SAFNWC EPS products will all need access to different NWP output parameters, the most dominantly being the surface temperature and the total column integrated water vapour (sometimes also refered to as total precipitable water eventhough we here disregard cloud liquid water). The CMa and CTy products use NWP data in their multi-spectral thresholding schemes, the CTTH for deduction of the cloud heights and the PC product in estimating the surface temperature. As an alternative, the NWP data can be substituted with climatological data for the required parameters if poorer qualities of the products are acceptable.

The acceptable maximum time deviation between the satellite acquisition time and the NWP valid time is configurable within the EPS Task Manager. For the CMa, CTy and CTTH products, the output carries information on the use of NWP data by different flags.

Reading of NWP output data in GRIB format is supported. The final delivery will support reading from HIRLAM and both the ECMWF as well as the ARPEGE model (EPS Library tasks).

In the prototyping development data from the local HIRLAM model has been used. If the user is going to run the algorithms on other NWP model output than the impact on product quality is not likely to be significant, and any possible adaptation to a local NWP model (or one different from HIRLAM) will not be an issue for the user. See further discussions in the sections 3.2.5, 4.2.4, 5.2.3, 6.2.3, and 7.2.4.

2.5 NOAA/EPS coverage and resolution

2.5.1 SAFNWC requirements

- The CMa; CTy, CTTH and PC products is designed for image data generation north of 50 degrees latitude over Northern Europe (including parts of the North Atlantic), but the products are expected to be valid even over middle latitude areas. They will at least be applicable over central Europe.
  The temporal frequency will be governed by the latitude of the local satellite receiving station. In northern Europe and Scandinavia this is likely to be 10-15 NOAA AVHRR scenes per day (grouped around the nominal optimal zenith passage times close to 02, 07, 12 and 18 UTC). (SP, sections 2.2.1.1.2, 2.2.1.2.2, 2.2.1.3.2 and 3.1.1.2)
- The CMa and CTy products shall be derived at a horizontal resolution comparable to the maximum nominal AVHRR resolution (1.1 km). (**UR-7.1.3.2.1, UR-7.2.3.2.1**). The same will be true also for the CTTH and PC products even if the used algorithms have been operating on segments having larger sizes. (**UR-7.3.3.2.1, UR-7.4.3.3.1**)
- The user of the AVHRR/AMSU Software Package shall have the possibility to select a rectangular area of numlin x numele AVHRR IR pixels centered at latpos, lonpos in a given polar stereographic projection where the products are to be generated. (**UR-6.3.5.5**)
- The user of the AVHRR/AMSU Software Package shall have the possibility to process the full AVHRR image without needing to modify the software. (**UR-6.3.5.6**)
- The user of the AVHRR/AMSU Software Package shall have the possibility to define the latitude of the true scale and central meridian of the polar stereographic projection. (**UR-6.3.5.7**)
- The default values for the latitude of the true scale and central meridian of the polar stereographic projection shall be 60 degrees north and 15 degrees east, respectively. (**UR-6.3.5.8**)
- It shall be possible to change the horizontal resolution of the products without reinstallation of the software, i.e. where applicable the processing segment size shall be a modifiable parameter of the software. (**UR-6.3.6**)

2.5.2 Current status in prototyping

As pointed out in the Science Plan, the spatial coverage of AVHRR/EPS data is dependent on the user's radio horizon and the temporal coverage by the user's geographical latitude. Selection criteria for which satellite pass to process is for the user to define and is communicated to the SAFNWC by means of the "EPS/NOAA schedule" (based on TBUS data) which is mandatory input (see EPS ADD for more information).

The AVHRR products will all be mapped to the polar stereographic projection. The exact definition of this is configurable by the user. The parameters to define are the latitude of true scale, the scale, the central parallel and the central meridian. Default for these will be true scale at 60 N, scale 1.0 km, central parallel 60 N and central meridian 15 E.

Users can define regions by specifying the number of pixels (x * y) and the latitude and longitude of the central point. The scale can be chosen totally arbitrary. If a region, covering the whole satellite scene is defined, this whole scene can be processed in whatever scale the user wants. However, the user shall be aware of that to use a large scale on a large area can impose too much load on internal memory and disks, making the execution very slow or perhaps impossible

.

3 Prototyping the Cloud Mask product – CMa

3.1 Overview

3.1.1 Objectives

This product shall provide information on the possible occurrence of clouds within each pixel. The central aim is to delineate all absolutely cloud-free pixels in a satellite scene with a high degree of confidence. In addition, the product will provide information on the presence of aerosols and snow/sea ice, and it will also indicate the presence of thick and semi-transparent clouds.

The main use of this product is to support Nowcasting applications and the remote sensing of continental and oceanic surfaces. As the latter is based on the radiation emitted or reflected by the surface, there must be absolutely no contamination by clouds in the selected pixels. The CMa product will also be used in ocean analysis applications within the framework of the Ocean & Sea Ice SAF (SAFOSI).

The CMa will allow identification of cloud free areas where other products (e.g., total precipitable water, stability index, sea/land surface temperatures, and snow and ice cover delineation) may be derived from the SAFNWC Software Package or from other software packages (e.g., developed by other SAFs). It will also allow identification of cloudy areas where other cloud products (CTy, CTTH, etc.) may be derived.

The objectives are described in the URD, section 7.1.1 (see Appendix A1.1)

3.1.2 Background for SMHI CMa prototyping activities

The SMHI experience of deriving cloud masks from satellite imagery stems mainly from the development and use of the SCANDIA model, a multispectral cloud analysis scheme based on the processing of NOAA AVHRR data (Karlsson and Liljas, 1990 and Karlsson, 1996). SCANDIA is one of several algorithms that was developed worldwide from the late 1980s to the present date. Other schemes of great importance here are APOLLO (Saunders and Kriebel, 1988), LUX (Derrien et al., 1993) and CLAVR (Stowe et al., 1991).

The similarities among the schemes mentioned are quite pronounced. Common for them is their utilisation of the typical differences in cloud appearances in all five spectral channels of the AVHRR instrument by applying sequences of threshold tests. The schemes differ in their way to specify thresholds, how corrections for atmospheric and surface effects are handled and the actual composition of the utilised image features (i.e., how individual spectral channels are combined).

The SCANDIA model was specifically aimed for the use in Nowcasting applications in contrast to the objectives of many of the other schemes mentioned. As a consequence, not only the cloud masking task was addressed, but also the task to identify cloud types and precipitating clouds. The scheme was optimised for near-nadir conditions, meaning that its

ability to handle large viewing angles and strong bi-directional effects is limited. In this respect, the other schemes mentioned are more advanced.

Regarding the method for screening absolutely cloud free pixels, SCANDIA shows some differences compared to the other schemes. SCANDIA threshold tests are coupled, meaning that the identification of a cloud-filled or cloud-contaminated pixel requires that several threshold tests (one for each applicable image feature) all must be passed. As a contrast, other schemes often use several tests for detecting cloud free pixels meaning that if one of the tests fails the pixel is denoted cloudy or cloud-contaminated. The difference here is explained mainly by the ambition to perform also additional tasks than single cloud masking in SCANDIA.

The strategy for the SMHI prototyping of the CMa product has been to develop a significantly revised cloud masking scheme as compared to the previous SCANDIA scheme. There are four main reasons for this:

1. Validation of SCANDIA results have shown some underestimation of total cloudiness indicating some problems in identifying very thin clouds or the existence of sub-pixel cloudiness (Karlsson, 1997).
2. Improved corrections for bi-directional and atmospheric effects are identified as essential.
3. Dynamic thresholds depending on the current atmospheric state and current illumination and viewing conditions must be applied rather than static climatologically determined thresholds.
4. It must be possible to adapt the cloud scheme in a consistent way to future AVHRR sensors.

The first reason implies that the previous SCANDIA model is more tuned to the cloud type identification task than to the cloud masking task. A consequence here is that the alternative concept mentioned for cloud masking, will be applied in the SMHI CMa scheme since this methodology allows a more stringent and restrictive identification of cloud free pixels.

The second and third reasons imply that thresholds must be determined by use of available information on the atmospheric and surface state as given by e.g. NWP models. This is an entirely new strategy as compared to previously developed schemes that basically apply empirically or climatologically defined thresholds.

The third and fourth reason points also at the need for proper tools to simulate or calculate necessary dynamical thresholds. These tools must be able to accurately handle the influence of sensor-related dependencies (in particular, the spectral response) as well as the absorption/scattering effects of both the earth surface and the atmosphere. Access to such tools will also facilitate the adaptation of the algorithm to other satellite sensor datasets, at least if spectral channel differences are not too large.

Our opinion is that the strategy to use NWP model information for the threshold preparation purpose does not violate the recommendation of a restricted use of NWP data as expressed in sections 1.1 and 2.1.3. It is clear that very short forecasts from today's NWP models are capable of providing a much better estimate of the current atmospheric state than the use of a pure climatological estimation. This fact must be recognised and utilised for the further improvement of cloud processing schemes.

Furthermore, the ability to compensate for anomalous deviations from climatological values is especially important for Nowcasting applications. The only option available here is to use what is offered by NWP models and it is our strong belief that this will lead to improved cloud products. The choice of a multispectral thresholding scheme here as opposed to a statistical scheme (including neural network solutions) is also favourable since improvements in NWP models will directly improve results with no need for recalculation of thresholds or other algorithm parameters.

3.1.3 SAFNWC Product requirements

A condensed description of the prescribed SAFNWC Cloud Mask product is given in the following sub-sections referring to the SAFNWC SP (section 2.2.1) and the given descriptions and corresponding user requirements in URD. This should be compared to the final definition of the product which is described in a later section (section 3.1.4).

3.1.3.1 Source

The CMa product shall be derived from the complete AVHRR data set comprising of spectral channels at 0.6 μm, 0.9 μm, 1.6 μm, 3.7 μm, 10.8 μm and 11.9 μm. [TBC] (**UR-7.1.2.2.1**)

3.1.3.2 Product description

Seven different classification categories will be considered, i.e. :

- cloud free
- contaminated by clouds (i.e. semitransparent clouds or partly cloudy)
- cloud filled (i.e. covered by thick clouds)
- contaminated by aerosols
- contaminated by snow or by ice
- unclassified
- non-processed.

(URD, Section 7.1.1).

The CMa product shall identify whether clouds are present in a pixel or not. Pixels even slightly contaminated by thin Cirrus or sub-pixel clouds must be detected. (**UR-7.1.2.2.2**)

3.1.3.3 Quality control

The CMa product shall include a quality flag, which gives information on the conditions under which the product has been derived and informs on the availability of NWP outputs, the illumination conditions and the viewing geometry. (**UR-7.1.4.1**)

For unclassified and unprocessed pixels the quality flag shall give an information on the reason. (**UR-7.1.4.2**)

3.1.3.4 Product output content and format

The product output comprises of the pixel categories given in section 3.1.3.2 and the associated quality flag specified in section 3.1.3.3.

The output format of the CMa product is [TBD]. (**UR-7.1.2.2.3**)

3.1.3.5 Time constraints

The product - for an area of 1024x1024 AVHRR pixels - shall be available within 2 minutes after the end of pre-processing of the EPS data (to generate level 1.b data), provided that the user installs the software on the target hardware, indicated by the SAFNWC Consortium. (**UR-7.1.2.2.4**)

3.1.3.6 Internal product dependency

No dependency on any other SAFNWC product shall exist (CMa is the primary cloud product).

3.1.3.7 Chosen method

The method will be based on a multispectral thresholding scheme. (SP section 2.2.1.2.2)

3.1.3.8 Auxiliary and ancillary data

The chosen scheme will use the following input data for the dynamic definition of essential thresholds:

- Sun and satellite zenith and azimuth angles (four angles in total) associated with the AVHRR image. Mapped on AVHRR images at full horizontal resolution.
- NWP output (analyses or short-term (less than 12 hours) forecasts):

  - *Temperature at several levels (most frequent in the lower troposphere including the surface in order to resolve and detect near-ground temperature inversions).*
  - *Water vapour content (the total amount and for several individual layers, TBC)*
  - *Near-surface wind speed (TBC during prototyping)*
  - *Forecasted snow accumulation (TBC during prototyping).*

  (All NWP data shall be mapped on AVHRR images at full horizontal resolution)

- Static threshold data (previously determined empirically or with the aid of RTM calculations)
- Other auxiliary data sets:
- Land/sea mask (bit map)
- Elevation map
- Snow/ice cover map (TBC)
- Surface type map (TBC) (SP, section 2.2.1.3.1)

3.1.4 Prototype description

A short summary of the Cloud Mask product in its present prototype stage is described in this section. The purpose is mainly to indicate the level of agreement between the specified product and the final prototype version. Deviations from the prescribed product definitions and relevant additional information on the product are briefly mentioned. Unless specifically commented later on in the text, the general product requirements listed previously in section 2.1 have been followed. For clarity, the same ordering of sub-sections as in the previous section 1.1.3 is used. Further details on the prototype version are given later in section 3.2.

3.1.4.1 Source

All channels of the AVHRR/3 are used as prescribed. However, the prototype does not yet include a valid scheme for the 1.6 μm channel (channel 3A). Such a scheme will be added later in conjunction with the availability of operational data from NOAA-L. In addition, the use of AVHRR channel 2 is here treated as optional (awaiting further validation results) since its importance for cloud detection seems to be small in comparison with other spectral channels.

The mandatory channels are
- channel 1
- channel 3B (or 3A)
- channel 4
- channel 5

Thus when channel 2 data are missing the algorithm will not be affected, however if any of the other channels are missing the CMa cannot process.

3.1.4.2 Product description

The prescribed product requirement is followed except for the category “contaminated by aerosols”. This category has instead been shifted to become a separate flag (explained further below). In addition, it must be mentioned that the category “contaminated by snow or ice “ only exist during daytime (i.e, when illumination allows snow and ice detection).

Thus, the main product output consists of the following six categories:
- Unprocessed
- Cloud free
- Cloud contaminated
- Cloud filled
- Snow/Ice contaminated
- Unclassified

From the cloud processing point of view, cloud free land and cloud free sea represent here one and the same category (cloud free pixel). In order to create an output image which shows this distinction, the users have to apply their own land/sea mask or use the information available in the quality flag (bit number 0 - see next section).

The information on excessive aerosol content due to dust clouds or volcanic plumes has been excluded from the main output, due to poor separability using the spectral channels of the AVHRR (agreed upon in personal communication with Herve LeGleau, Meteo-France). Instead, this information will be put in a separate output flag. Five categories are defined to

describe the contamination of an excessive aerosol content due to dust clouds, volcanic plumes and smoke from fires.

Table 3-1 Contents of the five-category output flag for dust clouds or volcanic plumes.

Class #	Class name
0	Non-processed (containing no data or corrupt data)
1	No contamination
2	Volcanic plume or smoke
3	Dust cloud
4	Fire
5	Unclassified (due to known separability problems)

3.1.4.3 Quality control

A large list of various quality flags has been determined. Since not all of these flags are directly coupled to the quality of the product but more to the circumstances prevailing during processing, the choice of the notation ***Processing flag*** has been applied in the following. However, based on validation results such as those presented in section 3.4 establishment of real quality characteristics from the information in the processing flags can be achieved. The processing flags occupies 11 bits (listed in the tables below), and provides the user with valuable information on the conditions under which the cloud mask processing was performed, and on the quality of the thresholding. The information in the processing flags is available for each individual pixel. Thus for example the flag for missing AVHRR channel in bit number 8 (see below) informs whether or not data for one or more channels are missing for the particular pixel. The exact outline of the processing flags is given below.

To describe the illumination and environmental conditions under which the cloud mask was derived seven bits are used (Table 3-2).

Table 3-2: Processing flag for illumination & environmental conditions

Bit #	Meaning of the bit – 1/0
0	Land/Not land
1	Coast/Not coast
2	Night/Not night
3	Twilight/Not twilight
4	Sunglint/No sunglint
5	High terrain/Low terrain
6	Inversion/No inversion (Low level inversion present, or not)

To describe the use and availability of NWP data and the availability of the AVHRR channels, two bits are used (Table 3-3).

Table 3-3: Processing flag for Missing data

Bit #	Meaning of the bit – 1/0
7	NWP data has been used / NWP not used
8	One or more AVHRR channels missing/No channels missing

The quality of the thresholding itself is described by two bits (Table 3-4). If the measurement was close to one of the thresholds of the active test the result will be assigned a low confidence.

Table 3-4: Processing flag for Thresholding quality

Bit #	Meaning of the bit – 1/0
9	Low quality (when the value of a pixel in some feature is close to the threshold determining the output)/High quality
10	Very low quality (when an isolated pixel has been changed from cloudy to cloudfree, or vice-versa, after applying spatial smoothing)/High quality

3.1.4.4 Product output content and format

The AVHRR Cloud Mask output consist of
- Main output (classification categories)
- Quality flags
- A dust/volcanic plume flag

In addition to the above, the output may include a threshold test flag. This flag has been used during prototyping for identifying the decisive threshold tests.

The product output is given in the HDF5 format (HDF5, see http://hdf.ncsa.uiuc.edu/HDF5/ and ICD). It was considered as not relevant to use the HRIT format (as recommended for MSG/SEVIRI products) for the NOAA/EPS products. The HDF5 format was found more attractive since this format has become more or less an international standard in many data applications meaning that a wealth of I/O support modules already exist.

3.1.4.5 Time constraints

The prototype is executed within the prescribed time limits on the current SMHI development hardware. For a 1024 time 1024 regional area it takes about 60-75 seconds of CPU time for the pre-processing step (prior to satellite data reception) and the on-line processing is finished with in 27 seconds of CPU time. See section 3.3.1 for details.

3.1.4.6 Internal product dependency

None.

3.1.4.7 Chosen method

The prescribed method is used.

3.1.4.8 Auxiliary and ancillary data

The auxiliary data used are:
- NWP surface temperature
- NWP 950 hPa temperature
- NWP total precipitable water
- Sun zenith, satellite view zenith, and sun-satellite view relative azimuth difference angles
- 1 km Land use data (including land/sea mask)
- 1 km Digital elevation map

More details on these datasets are given in appendix A.4.

3.2 Detailed algorithm description

3.2.1 Algorithm outline

The algorithm is performed in two separate processing stages: the ***Pre-processing stage*** and the ***On-line processing stage***. This distinction is caused by the fact that some computations can be made in advance of satellite data reception (pre-processing) while others demand access to real satellite data (on-line processing). A natural strategy has been to put as much as possible of the computations in the Pre-processing stage in order to make the product output available as early as possible after satellite data aquisition (see section 3.1.3.5).

The Pre-processing stage, the On-line processing stage and the structure of the core thresholding algorithm is described in the following sub-sections.

3.2.1.1 The pre-processing stage

Figure 3-1 below describes the processing tasks performed in the Pre-processing stage. Four major tasks are carried out:

- Preparation of auxiliary data
  Information on land cover, fraction of land and land elevation above mean sea level is extracted from global and regional databases.

- Preparation of NWP model information.
  The surface temperature and the temperature at several pressure levels are extracted and the total precipitable water is computed.

- Preparation of parameters for description of illumination and viewing geometry.
  The local solar zenith angle, the satellite zenith angle and solar-satellite azimuth angle

difference is computed for each pixel.

- Preparation of thresholds.
  Thresholds for IR and VIS channels are dynamically updated by utilisation of pre-computed tables from RTM simulations.

The fourth processing task (the threshold preparation task - illustrated at the bottom of Figure 3-1) is carried out as the final one since it depends on the output of the other three. This task must be considered as a core task for the algorithm performance. Consequently, large efforts have been put on the definition of the RTM-simulated threshold tables (see discussion later in section 3.2.3 and in Appendix A.8).

To be noticed here is that the output from the pre-processing stage consists of imagery with the same horizontal resolution as corresponding AVHRR imagery (to be produced in the following On-line processing stage). This means that for parameters derived from data sources having a coarser horizontal resolution than AVHRR interpolation methods have been applied. This concerns all parameters derived from NWP model data. The fraction of land is derived from the 1-km land cover data by counting the land covered pixels in a local neighbourhood. More information on these computational aspects and on the basic content in auxiliary databases can be found in Appendix A.4.

3.2.1.2 The on-line processing stage

The tasks carried out in the on-line processing stage are described in Figure 3-2.

Prior to performing the core multispectral thresholding step by using the input data from the previous pre-processing stage and the additional static threshold parameters (comprising of basic threshold offset constants and other tuneable parameters), necessary satellite input imageries must be prepared. This preparation consists of the following two actions (illustrated at the top of Figure 3-2):

- Extraction and re-mapping of AVHRR level 1b data (IR channels being calibrated into brightness temperatures and visible channels calibrated into pseudo reflectances) from satellite projection to the specified product region in polar-stereographic map projection.
- Computation of texture parameters.

The last action is motivated by the fact that all texture computations (based not only on one pixel value but also on pixel values from a number of neighbouring pixels) are computationally intensive. Thus, this kind of image feature is better to calculate once and for all while the calculation of other image features may be calculated when needed from individual AVHRR channel data while computing the cloud mask. The latter calculation strategy is e.g. also applied when investigating channel differences/quotas or even when converting original visible radiance values to bi-directional reflectances.

Original image data is transferred from satellite-projection to polar-stereographic map projections on pre-defined product regions. Image transformations are made by a nearest neighbour re-sampling technique in order to retain original pixel values. The product areas have a nominal horizontal resolution capable of reproducing image data at their maximum horizontal resolution (1 km) but this resolution is configurable.

When performing cloud mask computation, the extraction of the aerosol flag is treated as a separate optional function. A final post-processing step is applied where isolated pixels resulting primarily from noisy AVHRR channel 3b imagery are removed. It is also possible to extract statistical information based on the entire product output data set.

3.2.1.3 Structure of the core thresholding algorithm

The CMa algorithm consists of a large number of multispectral thresholding sub-schemes applied according to prevailing illumination, atmospheric, viewing or geographical conditions. These conditions are determined from the auxiliary, NWP and viewing geometry input data sets supplied by the pre-processing stage. All sub-schemes fetch their applicable thresholds and parameters from the pre-calculated threshold tables and the static threshold parameters provided in configuration files.

An overview of the algorithm showing all sub-scheme branches is given in Figure 3-3. In total, 21 different algorithm sub-schemes can be identified (red bulbs). The primary algorithm divider is the illumination condition which separates the algorithm into the three branches Day, Twilight and Night. These are determined exclusively by the local solar zenith angle. The corresponding dividing solar zenith angles are 95º for night/twilight distinction and 80º for twilight/day distinction.

The three main branches are further divided according to the type of pixel according to the geography classes Land, Sea or Coast. The reason for specifically defining a Coast category is explained by the existence of remaining uncertainties in the navigation of AVHRR imagery (errors of the order of 1-5 km can be expected). These errors may cause specific problems for cloud detection in cases of strong radiance gradients along coast lines. For example, the existence of strong sunglint in sea pixels may easily be misinterpreted as a cloud signature if erroneously assuming the pixel to be a land pixel. The same effect can be seen in the winter season when very large temperature contrasts exist between land and sea surfaces. Thus, a specific coastal region is defined where a combination of tests from the land and from the sea algorithms is applied and where thresholds are chosen more carefully. The definition of the coastal region is made by utilising the pre-computed fraction of land which is computed in segments with a pixel window of 11 pixels. A pixel is defined as a coast pixel where both land and sea pixels are present within such a segment.

For the Sea category, a further division into Sunglint or No Sunglint sub-categories is made. This distinction is made by calculating the probability of sunglint to occur from Cox-Munk theory considering an average distribution of facets as a function of sun and satellite viewing angles (see Berendes et al. 1999). For the Sunglint category to be chosen, the sunglint probability must exceed 0.5 %.

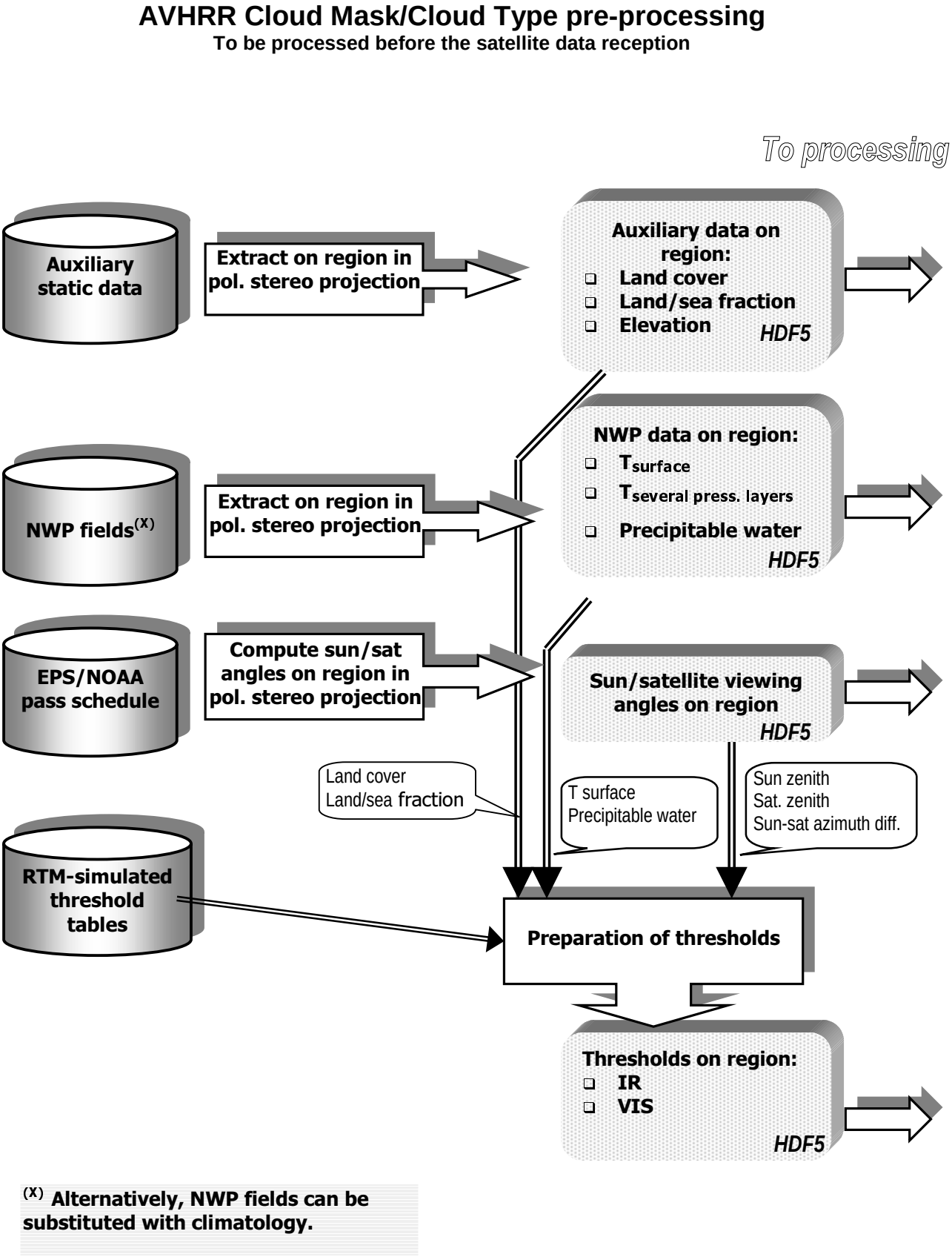

Figure 3-1: AVHRR Cloud Mask/Cloud Type pre-processing.

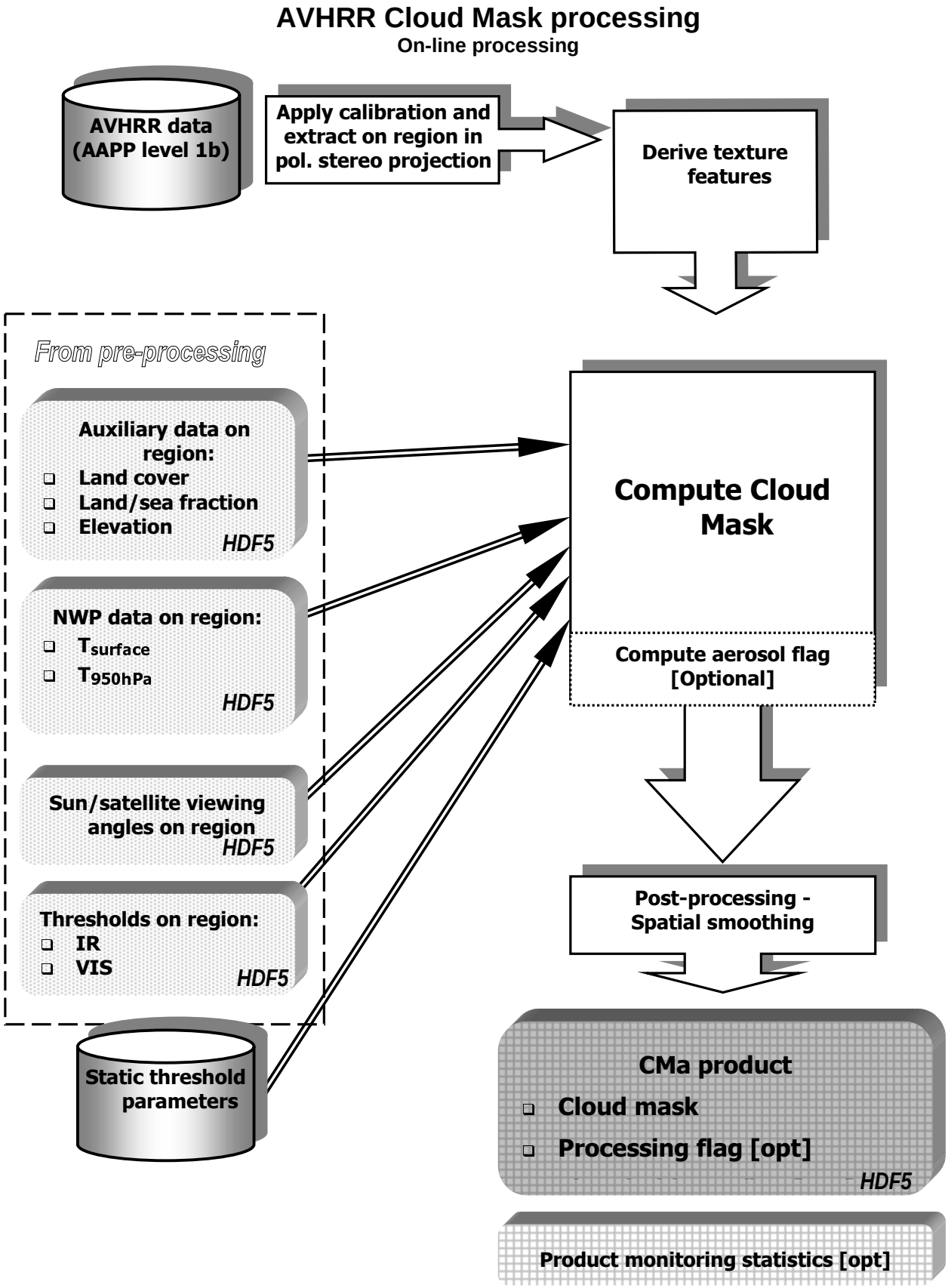

Figure 3-2: AVHRR Cloud Mask processing

Finally, the Land category is further divided according to the elevation and the existence of temperature inversions. For the High terrain category (elevation above 500 m), no inversion treatment is included since the likelihood for inversion occurrence is considered to be small (however not zero) in comparison with the conditions for lower terrain. This category has been defined in order to be more careful when using forecasted temperature thresholds in areas with steep and largely varying orography. For the category Low terrain, a sub-division into an Inversion and a No Inversion category is made by studying if forecasted temperatures at the surface are colder than the corresponding temperatures at 950 hPa (as suggested in VSci-1).

3.2.2 Applied threshold tests

Although a large number of sub-schemes may be chosen according to Figure 3-3, many similarities among them can be found. Each sub-scheme is generally composed by a sequence of basic threshold test components and many of these components are common among the sub-schemes. Differences consist of e.g. applying a varying order of tests, exclusion of some tests or inclusion of a few additional tests. In many cases, the used threshold for a certain test component may be varied according to varying conditions.

Before going into details of sub-schemes and individual test components, a complete list of the fundamental image features is given in Table 3-5. Notice here that one feature (**t11-tsur** – the difference between the AVHRR channel 4 brightness temperature and the forecasted surface temperature) is not derived from satellite imagery alone and it is included here due to its importance. Please observe that the notations of individual image features as given in Table 3-5 will hereafter be used in all remaining sections of this report.

Each sub-scheme for day and twilight conditions contains an initial screening of snow or snow covered ice before screening for cloudy or cloud contamined pixels. This is motivated by the fact that, during the pre-calculation of thresholds, snow- or ice-free surfaces have been assumed in the corresponding RTM simulations. If aiming at using deviations from these thresholds as a sign of cloud presence, snow or ice surfaces must consequently first be identified.

A specific multi-spectral snow and ice detection scheme has thus been developed and it is summarised in Table 3-6. The used thresholds are either static or composed of the simulated snow free thresholds but modified with threshold offsets appropriate for snow surfaces (denoted dynamic thresholds in Table 3-6). Details on how thresholds and offsets have been determined are given later in section 3.2.3. Notice here that all of the conditions must be true for the labelling of a pixel as snow or ice.

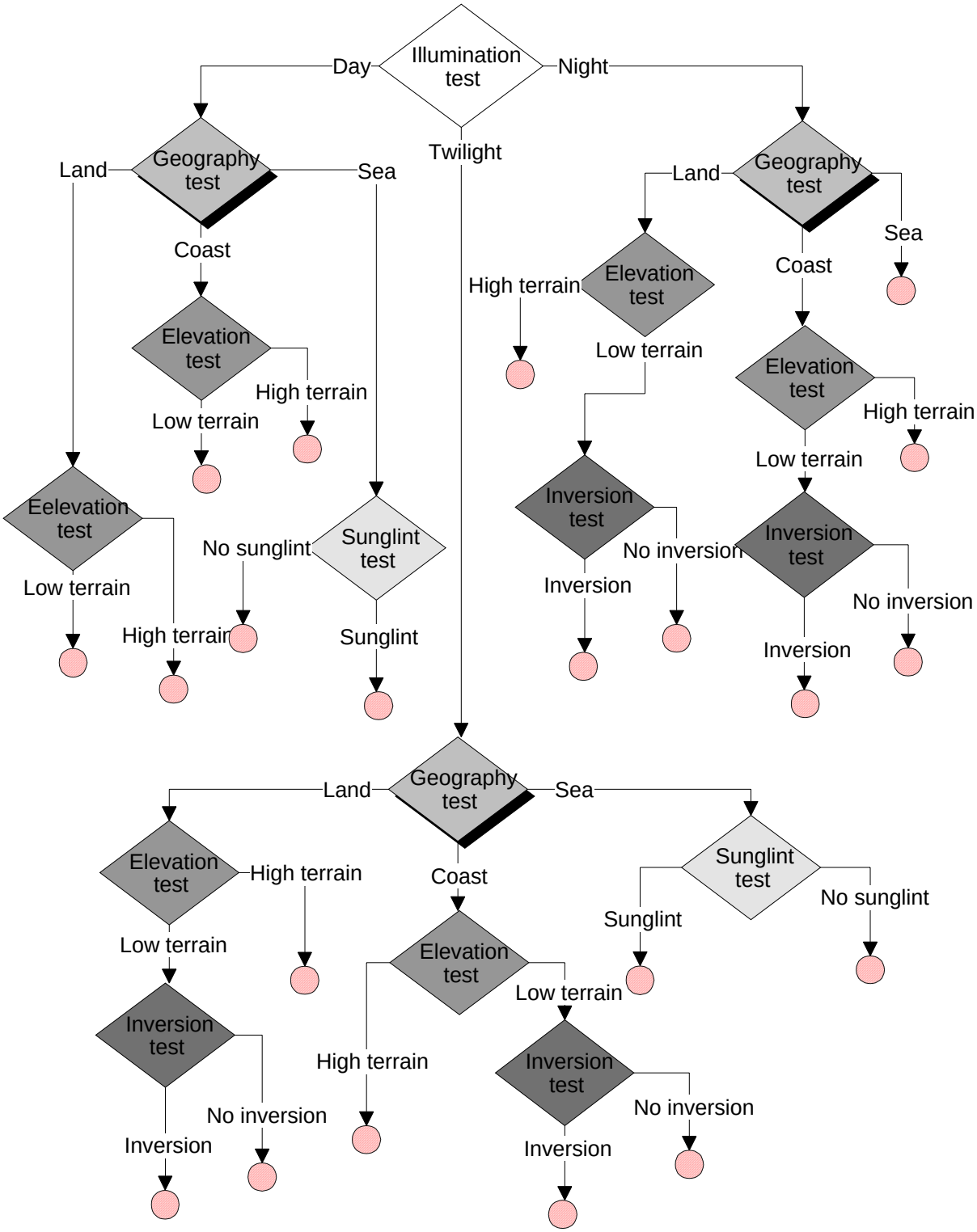

Figure 3-3: Overview of the CMa algorithm structure. Each red bulb defines one of 21 possible versions of the applied CMa thresholding scheme.

Table 3-5: Description of used image features

Image feature	Composition
r06	Bi-directional reflectances for AVHRR channel 1
Pseudo06	Pseudo-reflectances (assuming sun in zenith) AVHRR channel 1
r06_text	Local (5x5 pixels) **r06** standard deviation
r09	Bi-directional reflectances for AVHRR channel 2
r16	Bi-directional reflectances for AVHRR channel 3a
r37	Bi-directional reflectances for AVHRR channel 3b
qr37r06	Reflectance quota between **r37** and **r06**
t37	Brightness temperature for AVHRR channel 3b
t11	Brightness temperature for AVHRR channel 4
t11-t37	Brightness temperature difference between **t11** and **t37**
t11_text	Local (5x5 pixels) **t11** standard deviation
t12	Brightness temperature for AVHRR channel 3b
t11-t12	Brightness temperature difference between **t11** and **t12**
t37-t12	Brightness temperature difference between **t37** and **t12**
t37t12_text	Local (5x5 pixels) **t37-t12** standard deviation
t11-tsur	Difference between **t11** and forecasted surface temperature

The most essential threshold test components for cloud screening is explained in Table 3-7 below. The notation and output (when the test is true), the used image features and the function of each component are described. Notice that many of the described components consist of several or a few coupled threshold tests, a methodology which somewhat resembles the SCANDIA methodology (sometimes denoted “grouped thresholding” – see Baum and Trepte, 1999) previously discussed in section 3.1.2. Generally, it was found too risky to rely on single threshold tests. One illustrating example of this problem is the following case: The use of a single infrared temperature test in cold winter situations, assigning pixels as cloudy if significantly colder than the forecasted surface temperature, leads often to an overestimation of the number of cloudy pixels. This is explained by the fact that the local surface temperature variation within a NWP grid box area is very large in reality in very cold and clear situations.

Each sub-scheme applies a selection of the thresholding components in Table 3-7 in a sequential order. If one test is positive (or rather, far above the threshold(s)) the pixel is labelled cloudy (cloud filled) or cloud contaminated depending on the active test component. Further testing is then stopped. Notice here that all the components based on texture tests will produce the category cloud contaminated. The reason is that the texture features (at least, in the form they are composed here) are only sensitive to radiance gradients valid at the pixel

Table 3-6: The CMa snow- and ice cover detection scheme.
(Notice that for AVHRR/3 on satellites following NOAA-15 the r37 feature will be replaced by the r16 feature, qr37r06 by qr16r06 and t37-t12 will be excluded)

Conditional test (threshold type)	Meaning in the present prototype
t11-tsur > threshold (dynamic)	Snow surfaces are allowed to be significantly colder than the mean forecasted temperature in a NWP model grid square. A temperature offset of 12K for Low Terrain and 16K for High Terrain is therefore added to the simulated thresholds.
t11 < threshold (static)	Snow surfaces (melting snow) have a theoretical upper temperature limit at 272K. Here, it is used that the **t11** feature must not exceed 270K.
r37 < threshold (static)	Snow surfaces reflect poorly in AVHRR channel 3b. Here, the **r37** reflectance must not exceed 10%.
r06 > threshold (dynamic)	The same simulated threshold as used for cloud screening is used here.
qr37r06 < threshold (static)	As a complement to the previous two tests, the quota between the **r37** and **r06** features must be low (here, lower than 0.20).
t37-t12 < threshold (static)	The different reflecting properties between snow and clouds at shortwave IR wavelengths clearly affects the **t37-t12** feature. The threshold is here set to 8K.
t11-t12 < threshold (dynamic)	The IR split window temperature difference test later used for thin Cirrus detection is used here but with inverse conditions.
t11-t12 > threshold (dynamic)	The expected cloud free IR split window temperature difference may even be reversed in sign for a very cold surface (here snow or ice). A difference of -0.8K is here allowed.

scale. Such gradients are normally caused by well-defined cloud edges, by clouds at the sub-pixel scale or by semi-transparent clouds over a strongly inhomogeneous surface.

The test components are applied in a ranked order so that all tests producing the cloud filled output are executed prior to the tests giving the output cloud contaminated. If a test is positive but with pixel values close to a threshold, the testing continues with further tests meaning that the result may be altered if another test is more unambiguous. This last circumstance also affects the results of the quality information in the processing flags (see section 3.2.4.1).

Simulated thresholds are applied directly or after modification by incorporating appropriate threshold offsets (discussed in section 3.2.3) for the features **r06, r09, t37-t11, t11-tsur, t37-t12** and **t11-t12**. For the remaining features, static thresholds are applied.

Table 3-7: Basic threshold test components for cloud screening.

Component name (*output*)	**Used image features**	**Function**
Cold Cloud *(cloud filled) or (cloud contaminated)*	**T11-tsur** **Tsur**	Screens all clouds sufficiently colder than the surface but only if the surface is not too cold.
Cold Bright Cloud *(cloud filled)*	**T11-tsur** **Tsur** **R06**	Same as above but also requires the reflectance to exceed a threshold.
Bright Cloud *(cloud filled)*	**R06** **T37-t12**	Screens all sufficiently bright clouds, requiring high reflectance in both AVHRR channels 1 and 3b.
Reflecting Cloud *(cloud filled)*	**Pseudo06** **T37-t12**	Identifies any reflecting cloud near the night/day terminator. Requires reflection also in AVHRR channel 3b (separation from snow/ice).
Cold Water Cloud *(cloud filled)*	**T11-t37** **T11**	Screens sufficiently cold water clouds at night due to their colder appearance in AVHRR channel 3b.
Water Cloud *(cloud filled)*	**T11-t37**	Same as above but without temperature restriction.
Thin Cirrus primary *(cloud contaminated)*	**T37-t12**	Screens thin Cirrus clouds at night through their warmer appearance at shorter infrared wavelengths (semi-transparency sign).
Thin Cirrus secondary *(cloud contaminated)*	**T11-t12**	Same as above but using a smaller spectral interval and applied at daytime/twilight.
Thin Cold Cirrus *(cloud contaminated)*	**t11-t12** **t11**	Same as above but requiring clouds to be sufficiently cold.
Texture IR combined *(cloud contaminated)*	**t11_text** **t37t12_text**	Pixels with high spatial variations in IR identified as clouds. Difference of infrared channels are used in addition to reduce influence from thermal fronts at sea.
Texture VIS *(cloud contaminated)*	**r06_text**	Pixels with high spatial variations in VIS identified as clouds.
Texture IR/VIS *(cloud contaminated)*	**t11_text** **r06_text**	Pixels with high spatial variations in both VIS and IR identified as clouds. High texture in both VIS and IR required for avoiding thermal fronts.
Sunglint *(cloud free)*	**r06** **qr37r06**	Sunglints are separated from clouds when the **r37**/**r06** quota exceeds the value 0.7 and **r06** exceeds 10%.

Notice that despite the use of a pre-screening of snow surfaces, some threshold test components (the **Bright Cloud** test and the **Reflecting Cloud** test) include also tests for avoiding snow covered areas to be misinterpreted as clouds. This extra security is required since the previously described snow scheme is only capable of identifying pure snow areas and not the more common case with pixels consisting of both snow surfaces and vegetation (forests). Prototyping has shown that it is still possible to separate these mixed snow-vegetation signatures from clouds by applying the mentioned tests.

3.2.2.1 The daytime sub-schemes

The daytime processing sequence for the Sea sub-scheme is given by the following steps (executed in the given order):

1. **Cold Cloud** test with large temperature offset (opaque and cold clouds)
2. **Cold Bright Cloud** test
3. **Bright Cloud** test
4. **Cold Cloud** test with minimum temperature offset (low or thin clouds)
5. **Cold Water Cloud** test
6. **Thin Cirrus secondary** test
7. **Texture VIS** test
8. **Texture IR combined** test

For the Sunglint category, processing steps 1, 3, 7 and 8 have been excluded. Instead the **sunglint** test in is performed as processing step 1. This test is generally successful for moderate to strong sunglint but not for weak sunglint. However, weak sunglint is most often correctly separated from clouds by the use of processing step 4 above. The texture tests in steps 7 and 8 above have also been replaced by the **Texture IR/VIS** test which contributes to the identification of very low and warm clouds at the pixel or sub-pixel scale. It must though be noted that the applied texture thresholds must be very low (~0.3K) while the applied texture thresholds otherwise are of the order 0.5-1.0K for IR channels and 0.5% for VIS channels. This circumstance makes this texture test rather sensitive, especially in sunglint cases with largely varying local surface wind fields.

The corresponding day-time sub-scheme for Land is very similar to the Sea sub-scheme but the texture component tests are excluded since the inhomogeneous land surface appearance implies a very limited contribution to the cloud separability. For the remaining components some minor differences in the applied threshold offsets may be seen. The minimum temperature offset for the **Cold Cloud** test is 7K for sea surfaces and 8K for land surfaces. Furthermore, the offset for the **t37t12** feature in the **Bright Cloud** test is 4K over sea and 15K over land. This difference is due to noticed stronger bi-directional effects for the land surface (especially for non-vegetated desert type areas) and the risk for possible sunglint contamination from very small lakes. Notice that a screening for sunglints is not made for pixels of the Land categories but exclusively for Coast and Sea pixels. A small difference between the sea and land offsets is also seen for the **t11t12** feature in the **Thin Cirrus secondary** test. The offset over sea is 0.5K while it is 0.0 over land.

The daytime sub-scheme for High Terrain generally follows the principles for Low Terrain but the processing steps 1, 2 and 4 have been excluded or replaced by a modified version of processing step 3. The temperature offset for the **Cold Cloud** test have been increased from 8K to 12K in order to minimise the risk of misinterpreting cold mountain tops as clouds. In addition, the coupling of the IR and VIS tests were found essential for the same purpose and also for avoiding the misinterpretation of snow-covered mountain tops.

The sub-schemes for the Coast category tries to incorporate the methodology of all previously mentioned sub-schemes. Notice here that a sunglint test is included , though not visible in Figure 3-3. The basic idea is to use the same kind of tests but only chose the threshold values among the other possible categories that minimise the possible errors due to inherent navigation problems. For example, when using the **Cold Cloud** test the Land offset value 8K is prioritised and more safe to use compared to the corresponding Sea offset value 7K. In addition, all texture tests are avoided due to the obvious risk for high texture values due to radiance gradients along coast lines.

3.2.2.2 The night-time sub-schemes

The night-time processing sequence for the Sea sub-scheme is given by the following steps (executed in the given order):

1. **Cold Cloud** test with maximum temperature offset (opaque and cold clouds)
2. **Cold Water Cloud** test
3. **Water Cloud** test
4. **Thin Cirrus primary** test
5. **Texture IR combined** test
6. **Cold Cloud** test with minimum temperature offset (remaining low or thin clouds)

The corresponding processing sequence for the Land sub-scheme for Low Terrain in the case when no temperature inversions are present is exactly identical with the exception that the texture test is omitted. The threshold offset values are the same as for the daytime case except there is no longer any land/sea difference for the **t37t12** feature. This offset is now set to 2K for both land and sea areas.

The corresponding Land sub-scheme for High Terrain is different from the Low Terrain and the Sea schemes and is described as follows:

1. **Water Cloud** test with extra security
2. **Cold Water Cloud** test
3. **Cold Cloud** test with maximum temperature offset (opaque clouds)
4. "Normal" **Water Cloud** test
5. **Thin Cirrus primary** test

The main idea here is to use a more restricted **Water Cloud** test to account for the increased problems with a noisier AVHRR channel 3b appearance in the colder mountain regions. A security offset of 1K is added to the **t37t12** threshold. In addition, cloud pixels detected with

the "normal" **Water Cloud** test will now be given lower quality (see section 3.2.4.1). Notice also that the **Cold Cloud** test is performed with a maximum temperature offset aiming only for detection of cold and opaque mid- or high level clouds.

The effect of temperature inversions being present means that the previous methodology for High Terrain is also applied for Low Terrain. In addition, some extra security measures are added when applying the **Cold Water Cloud** test and the **Cold Cloud** tests. These are prevented from being used when the strength of the temperature inversion (**t950-tsur**) is more than 5K. In addition, the used **t11-tsur** threshold offset value has been increased from 8K to 10K.

As for daytime, the Coast sub-schemes try to utilise both the Land and the Sea sub-scheme components but with careful use of the corresponding thresholds. In practice, it generally means that the land sub-scheme tests and threshold offset values are given higher preference. Notice also that the Coast scheme is further sub-divided according to land elevation. This last feature was found necessary when processing in areas where steep terrain meets the ocean (e.g., at the coasts of Norway and on islands of Jan Mayen and Svalbard).

3.2.2.3 The twilight sub-schemes

The twilight sub-schemes are more complicated and extensive due to the fact that both illuminated and dark conditions in satellite imagery must be tackled simultaneously (most critical at the day/night terminator). Thus, the sub-schemes contain typical daytime as well as typical night-time test components and, in addition, some tests have been modified.

The processing steps for the twilight sub-scheme for Sea areas are the following:

1. **Cold Cloud** test with large temperature offset (opaque and cold clouds)
2. **Reflecting Cloud** test
3. **Cold Water Cloud** test
4. **Water Cloud** test
5. **Cold Cloud** test with minimum temperature offset (thin or low clouds)
6. **Thin Cirrus** secondary test
7. **Texture IR** combined test
8. **Thin Cirrus** primary test

The most remarkable change compared to the daytime schemes is the replacement of the **Bright Cloud** and the **Cold Bright Cloud** tests with the **Reflecting Cloud** test. Here, the main idea has been to avoid using the bi-directional reflectances for very high solar zenith angles and instead use the nominally calibrated reflectances (not compensating for the solar zenith angle), here denoted **pseudo06**. The reasons are mainly that the bi-directional reflectance is poorly determined at very high solar zenith angles. If still aiming at using the information in the VIS and short-wave IR channels here, this step was found necessary. By doing so, it is possible to detect a reflected contribution from clouds and snow surfaces and also to separate these two categories even for pixels situated at or very close to the day/night terminator. This ability to utilise all information given by the VIS and short-wave IR channels

has been considered as essential for the CMa performance under these problematic conditions.

It can be noticed that only processing steps 2 and 6 represent typical daytime threshold test. All other tests are typical night-time tests or general-purpose tests (e.g., the **Cold Cloud** test). However, it must be remembered that the sub-scheme also contains the initial snow test which is basically a daytime test.

The sunglint sub-scheme is basically the same scheme as used in the daytime case. Thus, the shift from the **r06** feature to the **pseudo06** feature has not been applied here. Consequently, for precaution reasons the applied sunglint tests are only made for solar zenith angles below 88º.

The Land sub-scheme for Low Terrain and without Inversion is practically the same as the Sea scheme but all texture tests have been excluded. In general (common for all twilight sub-schemes), the used threshold offset values are composed as the mean of corresponding day and night values. However, in some cases the night-time values are preferred (e.g., it is well-known that surface temperatures at dawn often are at their minimum daily values). Another exception is valid for non-vegetated land surfaces where the daytime offset value of 15K for the **t37-t12** feature is used.

In the case of Inversion, the Land processing sequence looks as follows:
1. **Reflecting Clouds** test
2. **Thin Cold Cirrus** test
3. **Cold Cloud** test
4. **Water Cloud** test
5. **Thin Cirrus secondary** test
6. **Thin Cirrus primary** test

The **Cold Cloud** tests are not performed for strong inversions (stronger than 5K) in a similar way as for the previously described night schemes. At the same time, the used threshold offset for the test have been increased to 10K.

The corresponding Land sub-scheme for High Terrain is different from the Low Terrain and the Sea schemes and is described as follows:

1. **Cold Bright Cloud** test
2. **Cold Water Cloud** test
3. **Cold Cloud** test with maximum temperature offset (opaque clouds)
4. **Cold Cloud** test with minimum temperature offset (low or thin clouds)
5. **Water Cloud** test
6. **Thin Cirrus secondary** test
7. **Thin Cirrus primary** test

Notice here that the **pseudo06** feature is not used. One reason is that illumination of mountain sides may distort results near the day/night terminator. As in the night case, the **Water Cloud** test is used more carefully to account for the increased problems with a noisier AVHRR

channel 3b appearance in cold mountain regions. Thus, cloud pixels detected with the **Water Cloud** test will be given lower quality (see also section 3.2.4.1).

Finally, the Coast sub-schemes tries also here to utilise both the Land and the Sea sub-scheme components but with careful use of the corresponding thresholds. In practice, it generally means that the land sub-scheme tests and threshold offset values are given higher preference. Notice again that the Coast scheme is also sub-divided according to land elevation.

3.2.3 Derivation of thresholds

3.2.3.1 Basic methodology

A substantial part of the prototyping work has naturally been focused on the definition of appropriate thresholds for the algorithm. Before going into details here it is important to know about the basic thresholding concept that has been applied. The thresholds for the CMa scheme have been defined according to the following classical assumption:

> ***FOV containing clouds or being contaminated by clouds can be identified by comparing measured radiances to the radiances which would have been measured in cloud free but otherwise similar conditions. Any deviation from these radiances would indicate the presence of clouds.***

The consequences of this approach for prototyping and for the derivation of appropriate thresholds have been the following:

- Cloud free radiances in VIS, shortwave IR and IR have been simulated by use of RTM models.
- Output from the HIRLAM NWP model has been used to estimate the present state of the atmosphere and the thermal conditions at the surface in the RTM simulations.
- Surface characteristics necessary for simulations in VIS have been defined by use of land cover information.
- The final definition of applicable thresholds has been made in tuning activities utilising an interactive training target database.
- Tabulated sea surface emissivity characteristics neccessary for IR simulations have been used (Masuda et al., 1988).

3.2.3.2 RTM simulations and the training data set

The RTM simulations have been performed by use of the RTTOV model (Eyre, 1991) for IR simulations and the 6S model (Tanré et al., 1990) for simulating conditions in VIS and shortwave IR. Since RTM simulations are expensive in CPU time no RTM simulations are performed in "real-time" (i.e., in the Pre-processing stage). In IR, a large and globally representative dataset with vertical profiles from radiosonde measurements (TIGR – see Smith et al., 1993) has been utilised to create a reference database with simulated IR radiances as functions of the most essential parameters according to atmospheric state and viewing geometry. In VIS, the U.S. standard atmosphere updated with the actual water vapour ontent as given by NWP data has been chosen for the corresponding radiance simulations. The thresholds prepared in the Pre-processing stage are defined from lookup tables which were compiled based on the contents of the simulated reference database.

More information on the used RTM models can be found in Appendix A.8.

For the tuning and validation of the derived tresholds an Interactive Training Target data set consisting of nearly four thousand training targets has been utilised. Each training target file consists of pixel radiances from a carefully selected target area in a satellite image representative for a specific cloud or surface type. In addition, all necessary auxiliary information valid for this target and its geographical position are attached (e.g., NWP model profiles, land cover and elevation information, solar illumination and satellite viewing conditions). More details on the Interactive Training Target database can be found in Appendix A.5.

3.2.3.3 Composition of IR thresholds

The basic methodology for composing IR thresholds from the RTM simulations is described by the following development steps given in chronological order:

1. Based on the TIGR database, RTM simulations for all possible cloud free atmospheric situations, illumination conditions and viewing angles (or rather, a representative subset of them) were computed.
2. The large volume of simulation results was divided into a sub-structure (radiance bins) which was organised by use of the most important atmospheric environment variables. The intention here was to use exactly the same environment variables later for regulating the selection of thresholds in the CMa scheme.
3. For each radiance bin, exclusively determined from a certain combination of environment variable values, the mean and standard deviation of the radiance simulation results were computed.
4. Thresholds were defined as the radiance value at the distance of two standard deviations away from the mean radiance value plus an additional temperature dependant noise factor. The final results here were collected in lookup tables for further use in the **Pre-processing stage** (section 3.2.1.1).
5. The chosen values in the lookup-table thresholds values may finally be modified by use of specific threshold offset values in the **On-line processing stage** (section 3.2.1.2). The threshold offset values have resulted from tuning activities or from other considerations.

A fundamental question is how to define the appropriate environment variables for development step 2 above. Some of them were selected for quite obvious reasons, e.g., the particular image feature, the current satellite number, the local solar zenith angle, the local satellite zenith angle and the local satellite-solar azimuth angle difference. Other parameters more directly related to the simulation of atmospheric absorption and surface behaviour effects were not that obvious to choose.

It was clear that the total moisture content (total precipitable water) in a vertical column must be included due to the importance of atmospheric water vapour absorption and the varying amounts of water vapour in the troposphere. However, since the resulting amount of absorbed radiation energy also depends on the actual radiation energy input into the atmosphere at the lower boundary, a special study on the possible additional importance of the surface temperature was made.

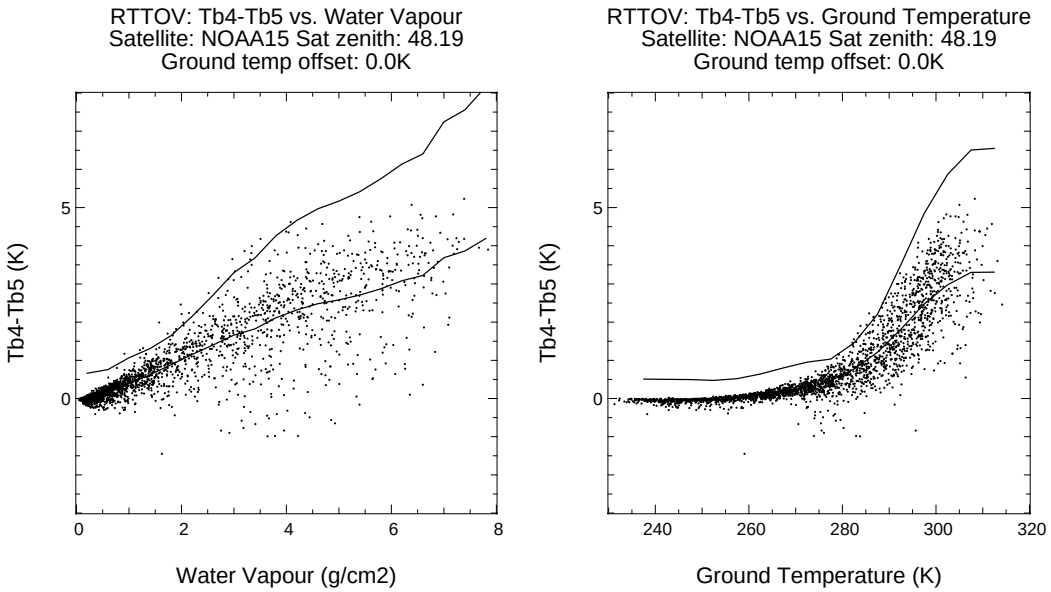

Figure 3-4: Simulations of the brightness temperature difference (feature t11-t12) plotted against the moisture content (total precipitable water – left) and the surface temperature (right). The lower curve in each figure represents the mean value and the upper curve the sum of the mean plus two standard deviations and an additional noise factor.

Figure 3-4 shows some results from the simulation of the **t11-t12** feature based on the TIGR profile database. Calculations are made exclusively for AVHRR/3 on NOAA-15 at a satellite viewing angle of 48°. From these results, it is quite clear that the distribution around the mean value for the surface temperature plot (right in Figure 3-4) is not as wide as for low temperatures (below 280K) as the corresponding distribution for the total moisture content (left in Figure 3-4). This indicates that the large spread around the mean in the total moisture case may to a large extent be explained by the additional dependence on the surface temperature. It is not likely that possible variations in the vertical temperature and humidity profiles are responsible for these large deviations, in particular when considering that the spread around the mean in the surface temperature case is so remarkably decreased.

Consequently, it was decided to use both the forecasted surface temperature and the total precipitable water as essential additional environmental variables. The two variables show a natural correlation (i.e., an increase in atmospheric and surface temperatures means also normally an increase in the total moisture content). However, it must be recognised that a large diurnal variation of the surface temperature is not necessarily accompanied by a corresponding variation in atmospheric humidity. This motivates the choice of these parameters as two complementing environment variables despite their partial correlation.

No other possible environmental parameters influencing atmospheric effects have been utilised here. The reason is that other effects are generally small (e.g. due to varying concentrations of other absorbing gases) or difficult to assess with present knowledge and observations (e.g. aerosol concentration). Regarding surface effects, some compensation for varying emissivity over ocean at large viewing angles has been utilised.

The need for the last development step (step 5) is motivated by the fact that there must be a possibility to compensate for possible errors in the used RTM simulations and in the input information (e.g., NWP model output). One must remember that the estimated cloud free radiances are rather first guess estimations, not the truth. This fact is particularly important when using features like e.g. **t11-tsur.** A threshold offset parameter must here be added to the pre-calculated threshold determining how close to the forecasted surface temperature we may go considering the typical errors inherent in NWP model forecasts or effects due to the different scale of NWP model grids and individual pixels. These offset values can later easily be reconfigured if considerable improvements of NWP models occur.

3.2.3.4 Composition of VIS thresholds

The basic methodology for composing VIS thresholds from the 6S RTM simulations is described by the following development steps given in chronological order:

1. The combination of scattering in the atmosphere-surface system was calculated excluding any absorption by atmospheric gasses. Included here were aerosol and Rayleigh scattering and the BRDF according to the model of Roujean et al. (1992).
2. The atmospheric transmittance due to gaseous absorption was calculated for the U.S. standard atmosphere with varying water vapour content
3. Two tables (one for each of the above steps) were created. The scattering component (surface BRDF, aerosol and rayleigh scattering) was described as a function of solar zenith, viewing and relative azimuth angles, and atmospheric transmittances due to gaseous absorption, as a function of viewing angles.
4. Thresholds were composed as the tabulated surface reflectivity multiplied by the tabulated transmittances.
5. Finally thresholds were modified by offset values deduced from tuning activities.

De-coupling the scattering and absorption components of the surface-atmosphere system was chosen to keep the amount of input threshold tables manageable. Compared to the errors introduced by the uncertainty in the description of the surface BRDF[1] and the aerosol optical depth, the errors introduced by this de-coupling, and which for most cases do not exceed a few percent, can be neglected.

3.2.3.5 Thresholds and threshold offsets for IR channels

The lookup tables for all IR and short-wave IR image features (**t11-tsur**, **t11-12**, **t11-t37** and **t37-t12)** were organised according to the previously mentioned environment variables. Linear regression was applied to describe the dependence on the total precipitable water and the surface temperature. The moisture information was sub-divided into a number of moisture content intervals and for each interval a separate linear regression curve was

1 The actual state of the surface within the FOV is unknown. Over sea the actual local surface wind speed is not known, and less is the sea surface state. Over land the current state of the art land cover description is very coarse and inaccurate .

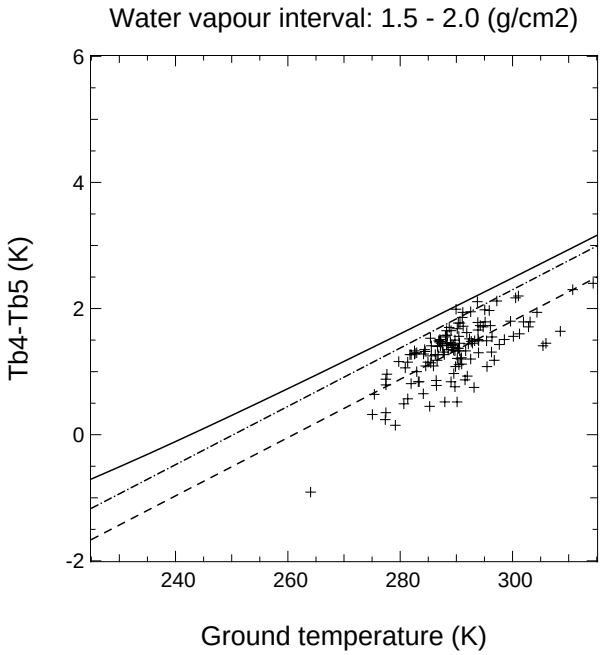

Figure 3-5: Simulated values of feature t11-t12 as a function of surface temperature for total moisture interval 1.5-2.0 gcm^{-2}. Dashed line linear regression curve, dash dotted line regression curve plus two standard deviations and solid line regression curve plus two standard deviations and an additional temperature dependent noise factor.

calculated. Figure 3-5 illustrates such a regression curve for the NOAA-15 **t11-t12** feature and for a total moisture content interval of 1.5-2.0 gcm^{-2}. The solid line in Figure 3-5 gives finally

the tabulated threshold. By this methodology, each regression curve will have a larger slope when shifting to a moisture content interval with higher moisture contents. Different sets of regression curves were further derived for varying satellite viewing angles in the secant interval 1.00-3.00 with a secant resolution of 0.25.

In order to test the validity of the tabulated thresholds and the need for use of threshold offsets, training targets available in the Interactive Training Target database (described in Appendix A.5) were grouped into cloudy and cloud-free categories. Their corresponding IR radiances were then compared to the tabulated thresholds in order to optimise the separation of the two groups.

One example of the use of the targets in the target database is shown in Figure 3-6. This figure shows how the simulations of the threshold values have been able to compensate for the varying surface emissivities as a function of the satellite viewing angle.

The feature **t11-tsur** (or, for other schemes, similar features using climatological temperatures instead of forecasted) is fundamental for all cloud screening applications. It was quite obvious that a threshold offset significantly higher than zero would be necessary for the **t11-tsur** feature. After years of tuning, the corresponding threshold offset in SCANDIA was set to -8K. However, this offset is not directly comparable, since for SCANDIA no additional distribution measure and no noise factor was accounted for. Thus, slightly smaller offset values should be expected here.

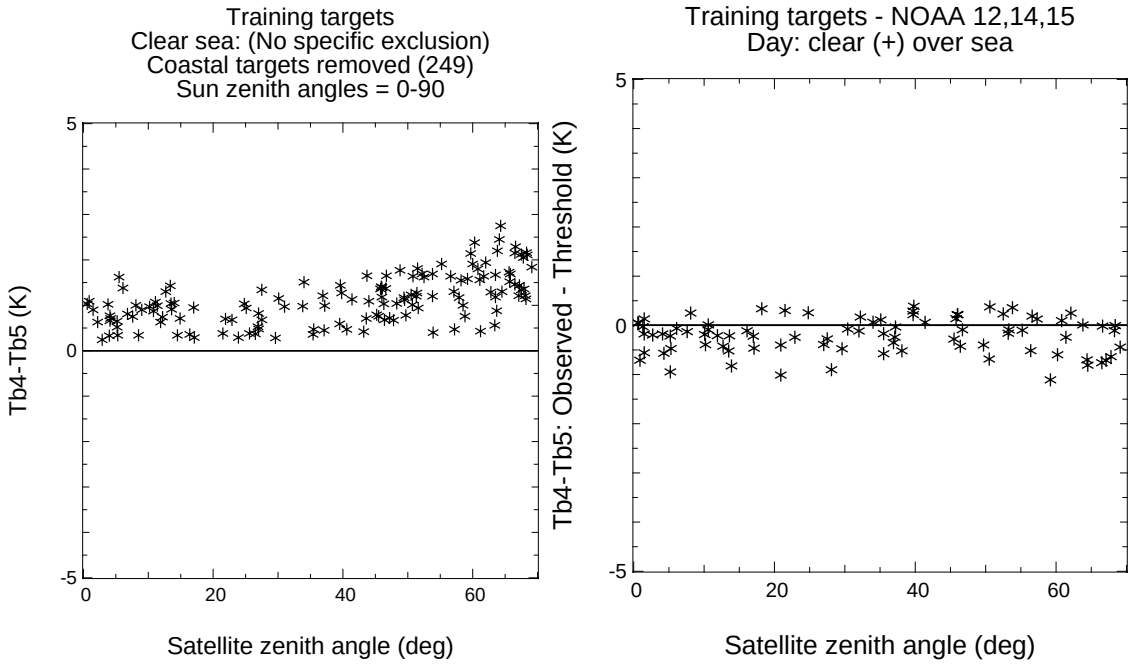

Figure 3-6: Observed t11-t12 feature values (left) for cloud free ocean targets compared to the difference between the observed and simulated threshold (right).

Figure 3-7 shows results for clear and cloudy ocean targets, indicating that the offset value could be as small as or even smaller than -5K (horizontal line) to achieve almost 100% separability. However, the corresponding results for land surfaces (Figure 3-8) are more ambiguous and a considerable overlap between the two categories is visible. An increased offset value seems necessary for not misclassifying cloud free pixels, but this would also increase the risk of misclassifying cloudy targets as cloud free. Here it seems obvious that the separability will be limited, unless other image features can compensate for this loss of separability.

We may conclude that there are two possible explanations for the necessary threshold offsets indicated in Figure 3-7 and Figure 3-8: The HIRLAM surface temperature forecasts appear to have a weak warm bias or, alternatively, the HIRLAM atmosphere is too moist. It must also be mentioned that the modelled surface temperature is only a rough estimate of the skin temperature. Errors due to deficiencies in the RTM models used are not very likely. Increasing deviations from true conditions are indicated for land surfaces, especially in cold situations. This is due to the increased temperature inhomogeneities within a grid square in cold conditions with a stable stratification. However, one must also remember that the likelihood for clouds to have temperatures equal to or even warmer than the surface is high over land during the cold season. Thus, in these situations the basic assumption for cloud detection as stated in section 3.2.3.1 is generally violated.

The finally chosen threshold offset values here are -7K over ocean, -8K over land, -10K over land in situations with temperature inversions and -12K over mountain areas. These threshold offsets were chosen with a rather large security marginal. Further tuning will show if these values can be decreased as far as e.g. indicated in Figure 3-7.

Concerning the treatment of temperature inversions near the surface, a previous study (VSci-1 in Appendix A.1.2) recommended the comparison of the 950 hPa level temperature to the forecasted surface temperature when identifying surface inversions. We have adopted this recommendation and introduced a more careful thresholding procedure when inversion conditions are found. In addition, if the inversion strength (temperature difference) is larger than 5K some threholding tests are even omitted.

For the **t11-t12** feature, the indicated threshold offset as deduced from target studies were small or negligible. However, it was found that an offset of -0.5K must be applied over land both during day and twilight (see Figure 3-9). The reason is probably due to deficiencies in the forecasted surface temperatures and/or total moisture contents.

3.2.3.6 Thresholds and threshold offsets for VIS channels

Simulations of the **r06** feature for the sea surface are compared with target observations (cloudy and cloud free) over sea in Figure 3-10. For the cloud free targets there is some overestimation of reflectances for all viewing angles. Furthermore, this overestimation seems to increase significantly at very large viewing angles (near the swath edge). Cloudy reflectances appear to be well separated from cloud free for low and moderate viewing angles, but for large viewing angles a significant fraction of the cloudy targets appear to have a similar or even a darker appearance compared to the simulated sea surface. The conditions near the swath edge seem not to be well simulated, i.e., the used BRDF model have some deficiencies in the description of bi-directional effects at very large viewing angles over ocean. A closer examination of results has shown, that the observed deviations occurred primarily at very high solar zenith angles and near conditions for sunglint occurrence. Highly varying sunglint effects in combination with appearing shadows are possible sources of error which might have contributed to the deviating results. In addition, the wind speed is a sensitive parameter for the description sunglints. A fixed wind speed of 7 m/s was used for the simulations. It is possible that sunglints have been overestimated which also could explain why cloud reflectances here appear darker than the simulated sea surface.

A threshold offset value of –5% was chosen over sea. The zero offset over land has not been thoroughly validated. However, over land the separability is normally much better than in sunglint areas. We simulated the surface by assuming forest and a constant aerosol content.

No thresholds or threshold offsets for the **r09** feature has been defined. The use of this feature is pending and is treated as optional. A future use will depend on the results of further validation and tuning activities. The idea is that **r09** could possibly replace **r06** over sea, due to its lower sensitivity to aerosols. However, so far the improved performance over **r06** has only been marginal. Another possible use is as a complementary feature in the snow detection scheme.

The sunglint problem (as handled by the **sunglint** component in Table 3-7) is discussed further in the next section.

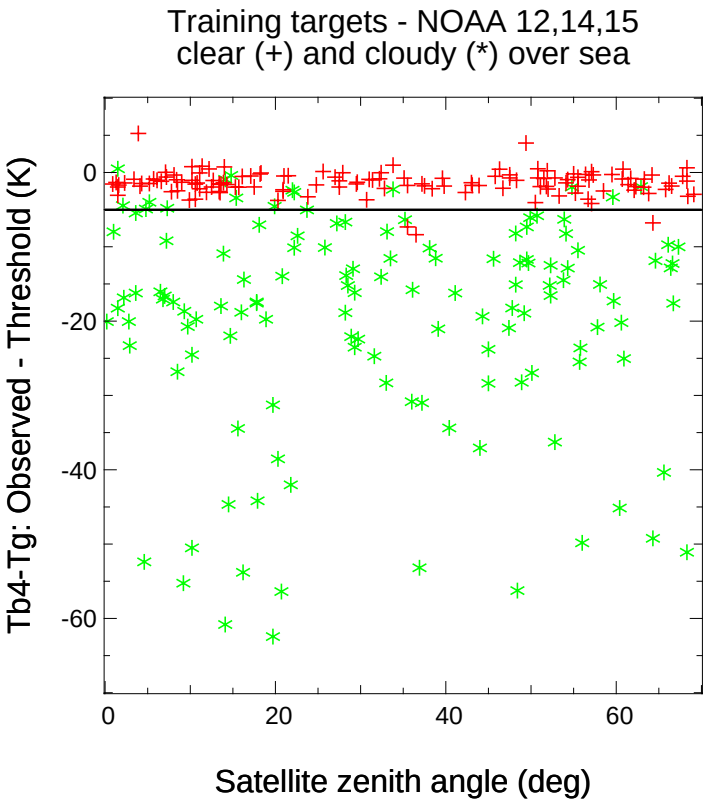

Figure 3-7: Distribution of clear and cloudy training targets over ocean areas after subtracting suggested t11-tsur thresholds from the measured temperature differences.

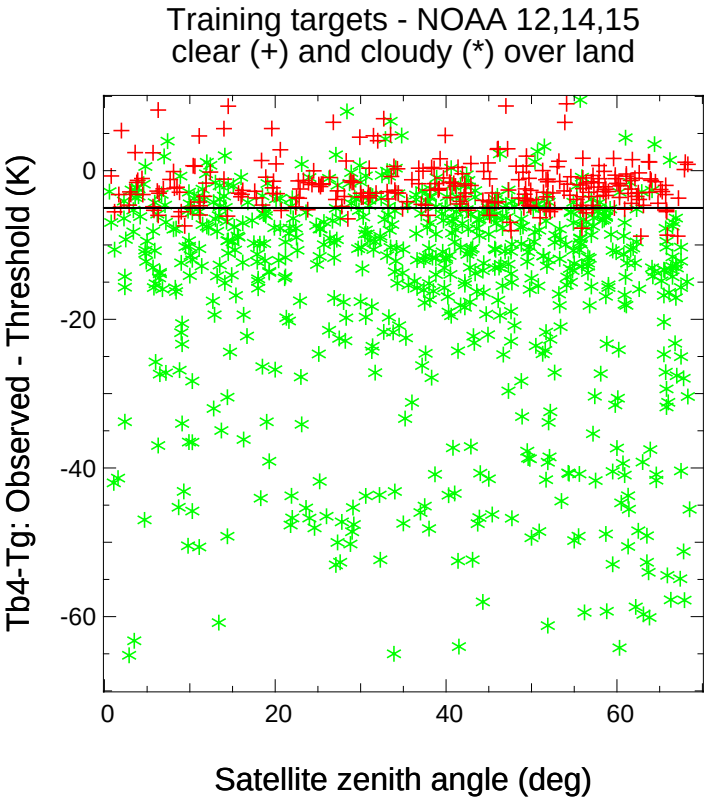

Figure 3-8: Distribution of clear and cloudy training targets over land areas after subtracting suggested t11-tsur thresholds from the measured temperature differences.

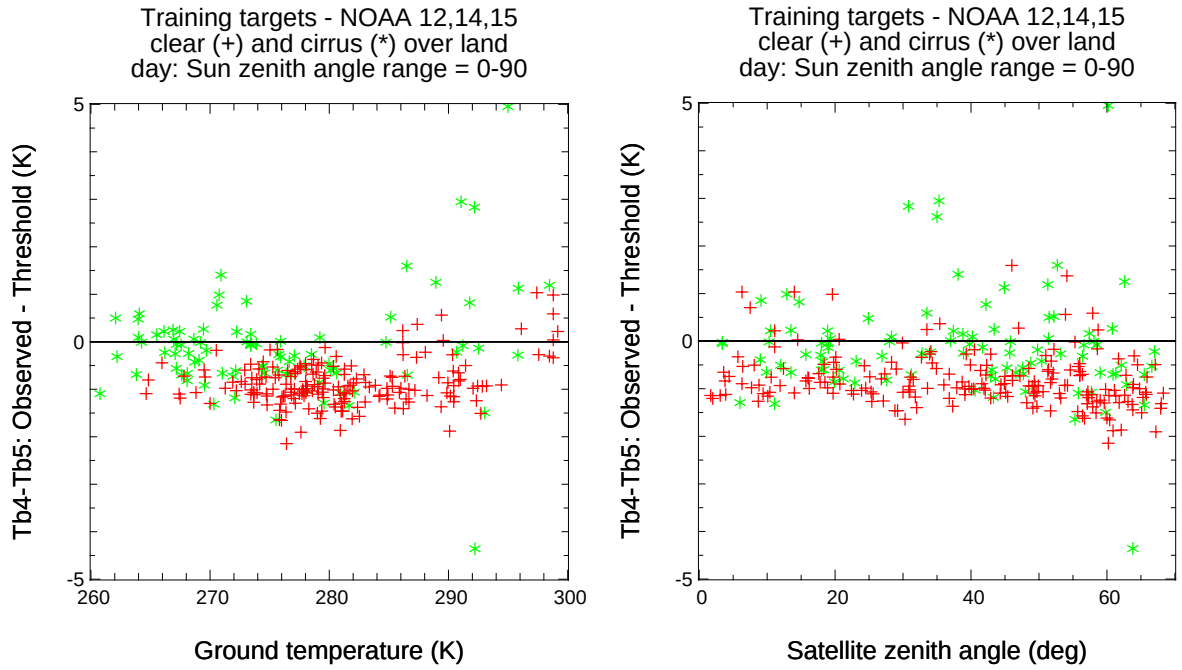

Figure 3-9: Simulated versus observed t11-t12 feature values for cloud free and cloudy (Cirrus) targets over land. Results are shown as function of ground temperature (left) and satellite zenith angle (right).

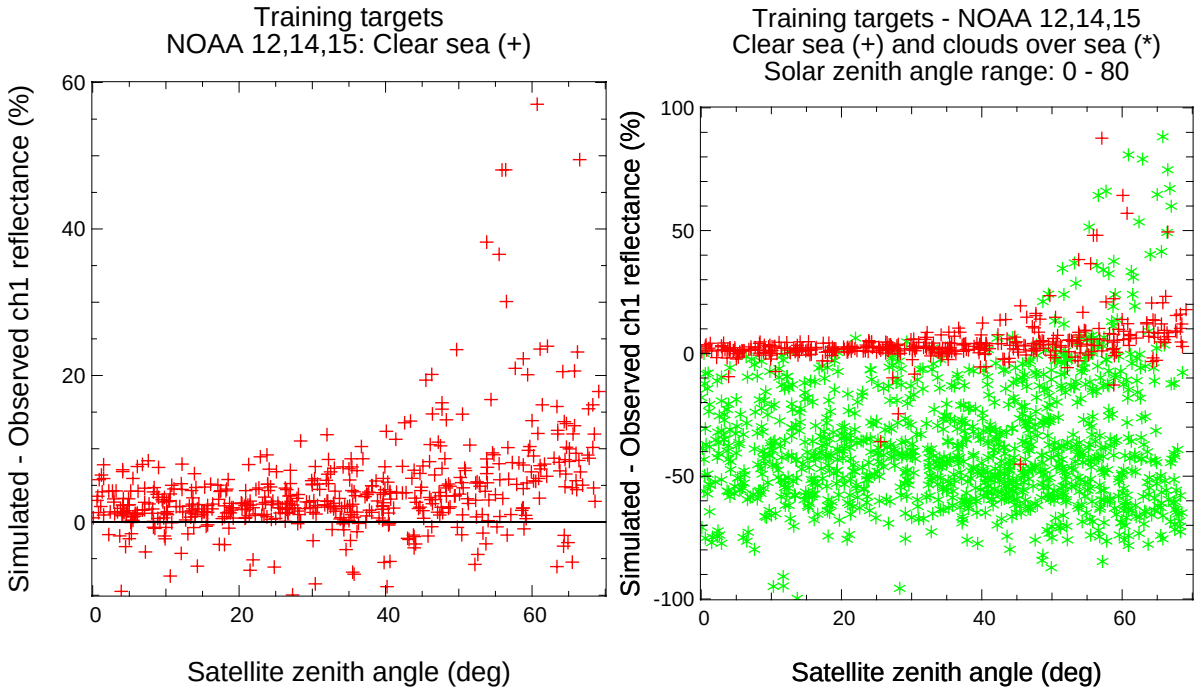

Figure 3-10: Simulated ocean surface reflectances versus observed AVHRR channel 1 reflectances for cloud free targets (left) and for cloudy and cloud free targets (right) as a function of satellite zenith angle.

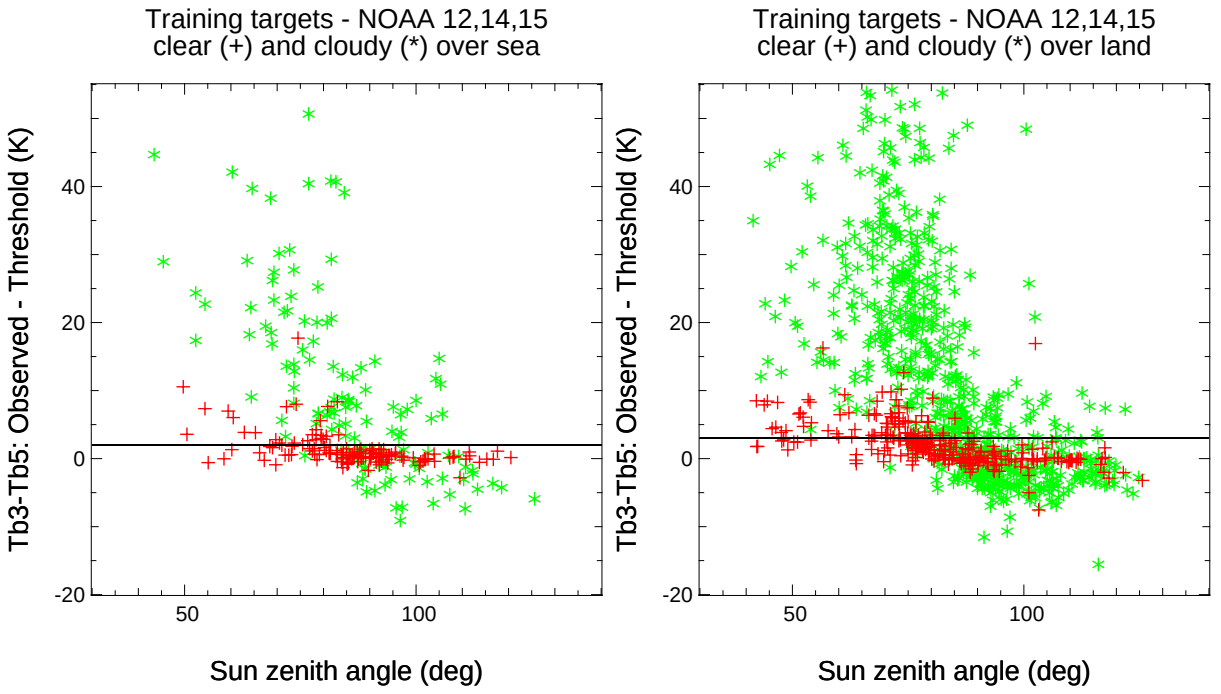

Figure 3-11: Difference between observed t37-t12 feature values and the simulated threshold for cloudy and cloud free targets over sea (left) and land (right).

3.2.3.7 Thresholds and threshold offsets for shortwave IR channels

The short-wave IR channel (AVHRR channel 3b - in future combined with channel 3a) is involved in several of the crucial cloud component tests throughout the day. It is used in the **t37-t12** feature at night for identifying semi-transparent clouds, in the **t11-t37** feature at night for detection of water clouds and in the **t37-t12** feature during day and twilight for identifying reflecting clouds. Channel 3b is also used in the **r37** feature for snow detection, in the **qr37r06** feature for sunglint detection and in the **t37t12_text** feature for detection of fractional clouds. Notice that the channel 3b reflectance (**r37**) is not used in the active cloud tests (except for the **sunglint** test) due to the problem to accurately estimate this quantity for semi-transparent clouds.

Figure 3-11 shows results for the t37- t12 feature over sea and over land comparing cloudy and cloud free targets throughout the day. The goal for the night-time test is to separate semi-transparent clouds (being more transparent, i.e., warmer, in AVHRR channel 3b) and it is here found that an offset of 2K is required (solid line in Figure 3-11) for achieving optimal thresholding efficiency. The daytime goal for this feature is to separate all clouds, since the reflection from water clouds in AVHRR channel 3 will make also these clouds appear warmer in this channel. However, also land and sea surfaces may reflect considerably in AVHRR channel 3b, especially when being close to specular reflection conditions which over sea leads to sunglint. Since the used RTM simulations (RTTOV simulations) only consider emitted radiation and not reflected, it is likely that the observed deviation from the night-time threshold as seen in Figure 3-11 is caused by this deficiency. The way to compensate for this in the CMa algorithm has been to increase the threshold offset to 4K during day over sea and to 15K over land. Although this seems insufficient for sea surfaces according to Figure 3-11,

one must remember that the sunglint component does not use the t37- t12 feature (see also the discussion on sunglints below). At twilight conditions, a combination of both the night and daytime versions is used (as described in section 3.2.2).

The **t11-t37** feature is used during night for detecting water clouds (being colder in **t37** than in **t11**) as described in section 3.2.2.2. In this case, the simulated threshold appears to be quite effective and therefore no additional threshold offset is applied. However, since the AVHRR channel 3b is quite sensitive to noise for low temperatures, an additional offset of 1K is used in high terrain and in the case of temperature inversions.

As described in section 3.2.2.1, a special sunglint test procedure is applied when the computed probability for sunglint exceeds a configurable constant value. The used **sunglint** test component uses a combination of the **qr37r06** and the **r06** features. Studies of sunglint targets compared with cloudy targets showed that it was possible to separate the two classes by utilising a constant threshold value in the **qr37r06** feature (Figure 3-12 left).

We have here adapted exactly the same threshold as being used in the Pathfinder project since it was found to give a very good separability of the two classes in the target database.

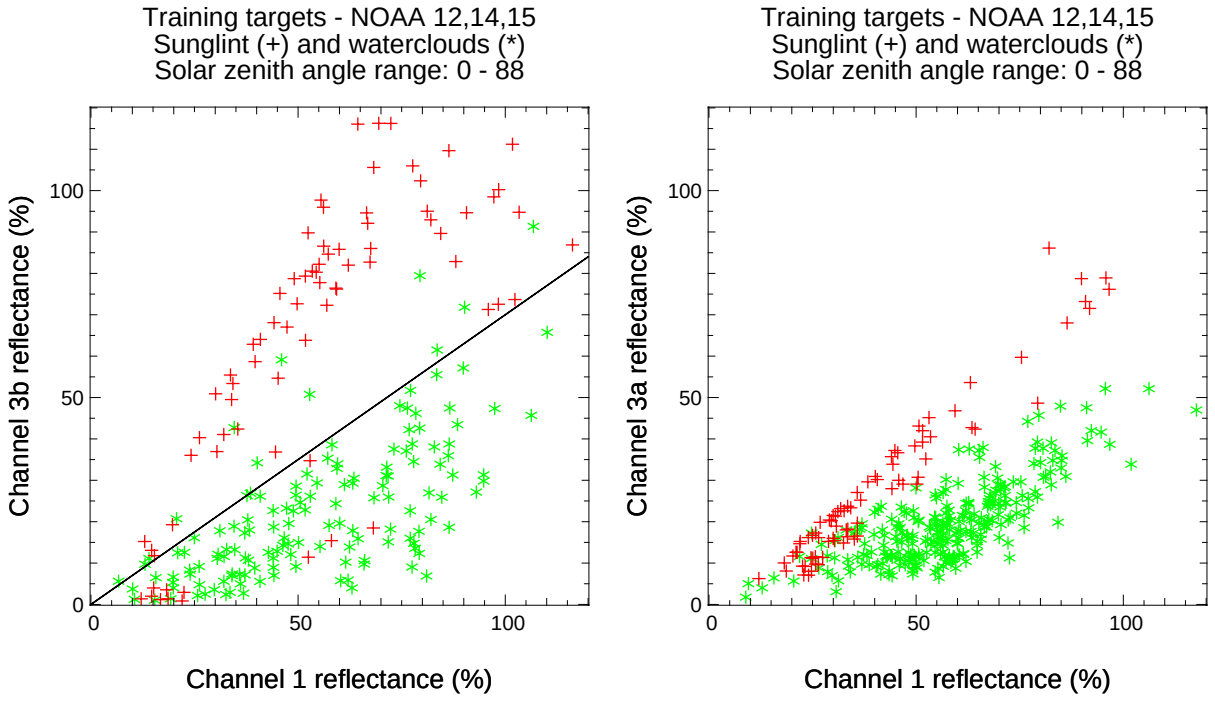

Figure 3-12: Left: AVHRR channel 3b reflectances plotted versus channel 1 reflectances for sunglint and water cloud targets. Solid line shows the Pathfinder thresholding algorithm for sunglint separation. Right: Corresponding plot but for AVHRR channel 3a reflectances for NOAA-15 targets.

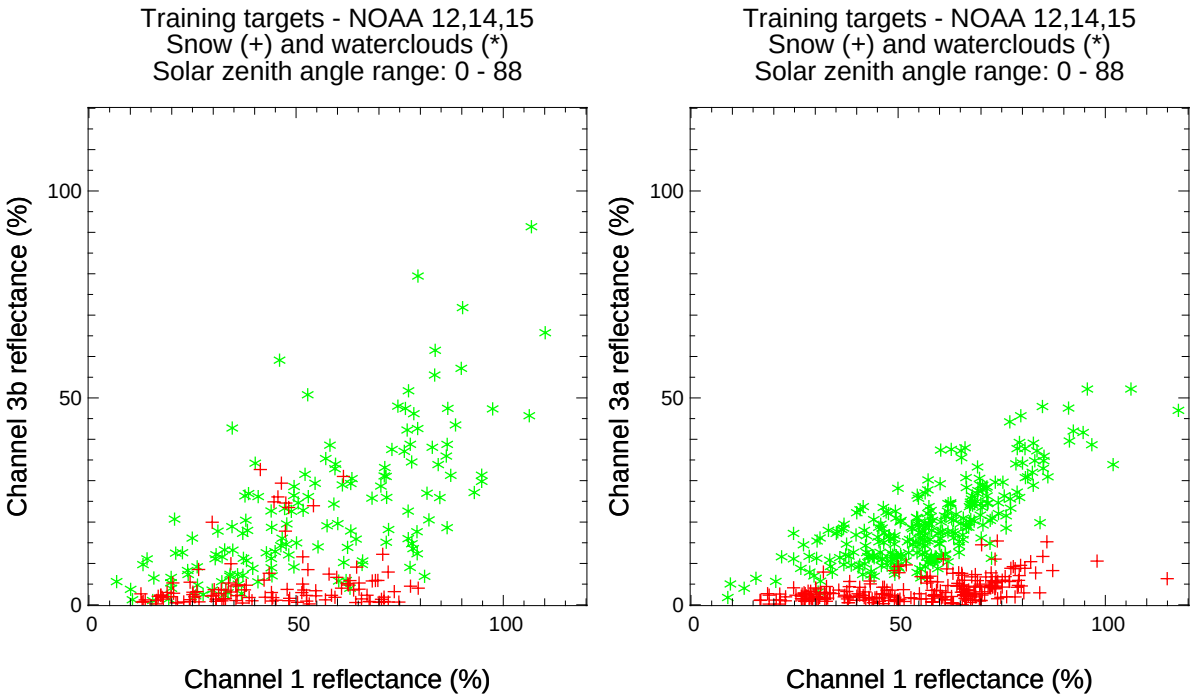

Figure 3-13: Left: AVHRR channel 3b reflectances plotted versus channel 1 reflectances for water cloud and snow targets: Right: Corresponding plot but for AVHRR channel 3a reflectances for NOAA-15 targets.

Studies of data from the AVHRR/3 channel 3a test data period (March 9th to April 20th 1999) gave some indications on the potential use of this channel when replacing channel 3b daytime on future NOAA satellites. The results of these studies were reported in VSci-2 (Appendix A.1.2). A circumstance causing some concern was that the above described sunglint discrimination method using channel 3b of AVHRR/2 appeared to yield better results than attempts to use AVHRR/3 channel 3a for the same purpose (as could be seen in Figure 3-12 right). Channel 3a appeared to give satisfying separabilities only in cases of strong sunglints.

However, it was evident that the use of channel 3a for snow and water cloud discrimination was much more effective than the use of channel 3b. Figure 3-13 illustrates this very clearly. This means that in cases when no sunglints occur and if surface temperatures are not too cold (thus risking to spoil thin Cirrus identification by use of the **t11-t12** feature over snow covered surfaces), cloud identification will be greatly improved compared to using AVHRR/2 data.

A general conclusion from the AVHRR channel 3a studies is that the simultaneous availability of both channels 3a and 3b should give the best overall performance if also wanting a proper handling of the sunglint discrimination problem. In this respect, it is very unfortunate that this opportunity will be realised only on MSG/SEVIRI and not on future NOAA/EPS satellites.

At the present stage, no prototype version including the handling of AVHRR/3 channel 3a data (feature **r16**) exists. Some classifications tests were made on data from the test period in

1999 and are reported in VSci-2. However, since the material from the test period is only representative of a small part of one season (with restricted solar zenith angles, satellite-sun azimuth differences and atmospheric variability), the finalisation of prototyping will be postponed until after having access to continuous channel 3a data stream from coming NOAA satellites.

3.2.4 Derivation of processing, threshold test and aerosol flags

3.2.4.1 Processing flags

Table 3-2, Table 3-3 and Table 3-4 in section 3.1.4.3 describe what is called ***Processing flags*** as an additional output for the algorithm. Most of these flags (i.e., the ones given in Table 3-2and Table 3-3) carry information about the conditions under which the processing was executed according to illumination and environmental status parameters. They are easily determined from the auxiliary, NWP, geometrical and viewing information which is utilised as input parameters in the On-line processing stage. Generally, these flags carry all information necessary to describe the chosen path in the processing flow in Table 3-3 for a pixel. The purpose of these flags is that they will give the user a possibility to track if there are special circumstances that could eventually affect product quality. However, since any detailed information about quality must be gained from extensive validation efforts, we have chosen not to call these flags *quality flags* at this stage since a more thorough validation will not be carried out until after MTR. For the moment, it is enough to state that these flags have been arranged and chosen in a way that from previous experience and from experience during prototyping have seemed reasonable as indications of the most sensitive environmental parameters.

The two remaining processing flags in Table 3-4 are so far the only attempts to directly label quality properties for a processed pixel. The first one will indicate if a pixel category has been chosen during thresholding with a very small margin to the threshold in the decisive test. If thresholds have been derived in an optimal way this information would be of great value in applications where a high confidence in the results is required. However, if serious and fundamental separability problems exist, such information could be misleading. In those cases, a more reasonable output would be to label the pixel as unclassified. Further tuning and validation activities will hopefully result in a proper balance in the use of this quality flag compared to the use of the unclassified category (which is not used in the present prototype). Furthermore, reasonable values on the applied margins from thresholds for this quality evaluation remain to be firmly determined and tuned. The typical margins shown in Table 3-8 are used in the present prototype.

The second of the processing flags in Table 3-4 results as an additional output from the spatial smoothing post-processing in Figure 3-2. Here, isolated cloudy pixels resulting from tests based on the **t37-t12** and the **t11-t37** features may be removed from the result image in cold weather situations and labelled as having low quality. The reason is the well-known noise problem in AVHRR channel 3b seriously affecting cloud processing, especially in cold and dark winter conditions.

Table 3-8: Used threshold margins for quality flag in prototype

Image features	Threshold margin
R06, r09, r37	1%
Pseudo06	1%
t11, tsur, t11-tsur	1K
t11-t12, t11-t37, t37-t12	0.5K
Qr37r06	0.1
R06_text	0.05%
t11_text, t37t12_text	0.05K

3.2.4.2 Threshold test flags

A very important tool that has been used during prototyping is the threshold test flags which are available as a complementary product output. These contain information on the decisive threshold tests for each pixel unless being labelled as cloud free land or sea pixel. Since these flags are optional and not intended for the user they are not described in detail here. It is sufficient to mention that it is possible to identify both the basic threshold test component used and its accompanied image features (as given) using the information available from the processing flags and the threshold test flags, respectively.

3.2.4.3 The aerosol flag

The intention of this flag is to indicate cases with excessive aerosol contamination of the atmosphere, in order to provide warnings for aviation activities and to prevent further use of these pixels in surface analysis applications. Notice here that we are mainly discussing extreme cases with pronounced aerosol contamination since aerosols are generally very difficult to distinguish from the cloud free surface signature, especially over land surfaces.

Three different cases of aerosol contamination have been considered: volcanic plumes, dust clouds and fire smoke. Each of these cases has a specific appearance, slightly different from the others and from ordinary clouds. Volcanic plumes have been reported to show a slightly negative value of the **t11-t12** feature in contrast to most other cloud types and surface types (Prata, 1989). Dust clouds are very warm clouds observable at least over dark ocean areas with a discernible but quite low **r37** value. Smoke clouds from fires resemble very much the dust clouds but have slightly higher **r37** and **r06** values. Notice also that the aerosol flag includes a special category for description of actual fire centres. It is here utilised that the very large sub-pixel variation of ground temperatures gives rise to remarkably high negative values of the **t11-t12** feature and that even small sub-pixel fires almost saturates channel 3b.

The present formulation of the aerosol detection concerning volcanic plumes is based on the finding of Prata (1999), despite the fact that this method seems to have limited applicability in

general. According to LeGleau (1999, Meteo-France, personal communication), only at about one out of ten volcanic plume events a clear negative **t11-t12** value was discernable.

Concerning smoke and fires, the aerosol detection algorithms is inspired by the tests of the CERES algorithm development (as reported by Baum and Trepte (1999).

Due to the very limited number of test cases available so far, the final formulation of the algorithm will be postponed until the planned validation and tuning activities.

3.2.5 The use of NWP data and their impact on quality

The CMa makes use of the surface temperature, the 950 hPa temperature, and the total precipitable water. The pre-computed thresholds depend on the surface temperature and the total precipitable water, and in addition the surface temperature and the 950 hPa temperature are used in the on-line processing, mainly in the identification of low level inversions.

3.2.5.1 Impact on product quality of errors in the NWP output

The most critical parameter is the surface temperature. It is highly variable both spatially and temporally, and in the IR channels a large part of the received signal is stemming from the outgoing radiation originating from the surface. At the same time, under certain conditions (during dawn and dusk and during night when semitransparent cirrus overlay low or mid-level clouds) a cloud/cloud-free discrimination is ambiguous without the addition of the t11-tsur feature. In order to improve the detection in such situations an accurate estimation of the actual surface temperature is thus vital.

The best candidate at hand is the surface temperature as estimated by a short range NWP model forecast. The errors introduced to the Cloud Mask due to errors in the NWP model forecast are much less on average than if a static, or even climatological, surface temperature is chosen. This is so even though NWP models in general is known to occasionally (depending on season and weather situation) deviate substantially from the observed one (as given by Synop station reports).

Thus large errors in the predicted surface temperature is likely to severely degrade the output during twilight and during night-time. It is exactly for this reason that we have avoided the use of static temperature thresholds or climatology, almost always being far from reality.

3.2.5.2 Dependency on NWP model

The pre-computed thresholds derived using RTM simulations have been tuned/validated against interactively collected training/validation data (covering all seasons). In the algorithm we apply certain offsets to these dynamical thresholds partly to be on the safe side mainly taking into account inaccuracies and biases in the NWP model (HIRLAM).

The accuracy of the NWP model will naturally affect the algorithm performance. The more accurate the NWP model the more accurate the cloud mask. This is to a large extent a direct benefit of deriving the thresholds dynamically by the use of RTM simulations. Thus any future improvement in NWP modelling will only have a positive impact on the quality of the CMa.

Using data from other NWP models than HIRLAM with inaccuracies in surface temperature and total precipitable water comparable to that of HIRLAM will not call for any adaptation of

the algorithms. Since the training and validation data set cover a long period with data from all seasons also any seasonally dependent bias in the surface temperature is accounted for. This is supported by the fact that the offsets applied in the GOES prototype (developed by MF using ARPEGE output) and the AVHRR prototype (developed by SMHI using HIRLAM output) are nearly the same concerning the use of the t11-tsur feature.

3.3 Practical application

3.3.1 Implementation

The coding of the core CMa model is done using the C language. Python is used as the glue when implemented in the pre-operational scheme – e.g. for grabbing the right NWP model output, extracting the physiography data, and the production of derived image outputs.

Re-mapping to polar-stereographic map-projection is done outside the PGE and not considered here. Also the calculation of satellite and sun angles on region is done outside. Thus the starting point for the CMa is mapped angles on region, mapped physiography data on region and some NWP parameters (temperature at pressure levels – here only the 950 hPa is relevant) already post-processed.

System tests of the CMa was carried out on an Alpha Digital Personal Workstation (DPW) 433 MHz (one CPU) with 384 MB RAM, and on a regional area of size 1024 times 1024 pixels. The operative System is OSF1 Version 4.0, and we used the native compiler with the options "-O –Olimit 1500".

Testing was performed on different satellite scenes and different regional area. The pre-processing step required between 60.8 and 75.1 seconds CPU time, and consumed 64 MB memory. These results were achieved with a compression level of 1 for the HDF5 output files (minimum compression). Processing time was decreased by 2.5% if choosing no compression on the output files.

The on-line processing took between 18.8 and 26.9 seconds CPU time, and again 64 MB RAM was required. Again a little time was gained (between 1 and 2 seconds) if not compressing the output file.

3.3.2 Product demonstration

Results from the CMa prototype were demonstrated in connection to the SAFNWC Demonstration experiment taking place between November 8 and December 7 in 1999. During this experiment, the CMa product was produced in an operational mode for all received NOAA scenes at SMHI. The cloud mask was processed on various regional areas in a polar stereographic map-projection. All the areas had a size of 1024 rows and 1024 columns, with a pixel size of 1 km. The following six areas were covered: Scotland and Faroe islands, Great Britain and Ireland, Germany and Central Europe, North Western Mediterranean, Southern Scandinavia and Northern Scandinavia.

Cloud mask results were collected and displayed in near real-time mode at a specially designed SMHI SAF web site (at address http://www.smhi.se/saf/). Also some general information about the SMHI SAFNWC development work was made available at this site.

Figure 3-14 below shows an example of the CMa product and accompanying original AVHRR imagery in the same format as was utilised during the Demonstration Experiment.

The SMHI SAF website was frequently visited during the Demonstration Experiment. In summary, a total of 11601 requests were recorded meaning that on the average 314 daily requests were noticed. This web site has been kept open also after the end of the Demonstration Experiment showing results from an updated version of the CMa scheme. A continuation of the demonstration of the CMa prototype is expected at least until the end of MTR.

3.4 Validation

3.4.1 Validation method

The basic validation method used for the first validation of the CMa scheme has relied on the availability of co-located surface observations (Synop) and satellite information gathered in the MSMS database (described in Appendix A.6). A pilot study utilising this information for evaluation of SCANDIA results was performed (SMHI_1 in Appendix A.1.3). Information from the Interactive Training Target database has not been used here since this information cannot be considered as strictly independent (this database was used when deriving thresholds and thresholds offsets as described in section 3.2.3.2).

In addition to the use of MSMS, it must be mentioned that visual inspection of CMa imagery and corresponding AVHRR imagery has been another cornerstone in the evaluation and tuning of the algorithm performance. This method, however not completely objective, has been found very important over areas without available surface observations (e.g., over ocean areas).

3.4.2 Validation data sets

The Cloud Mask algorithm was run on one year (1999) of data of the MSMS database, making up a total of 64899 validation datasets. The result (including quality flag and threshold test flag) was appended to the database, before a statistical analysis was performed.

Except for the static auxiliary data and the total columnar precipitable water all necessary data are available in the MSMS. The physiography data (land use and DEM) and the threshold tables were ingested separately, and the precipitable water was derived from the vertical humidity profile (20 pressure levels) of the HIRLAM grid point stored in the MSMS.

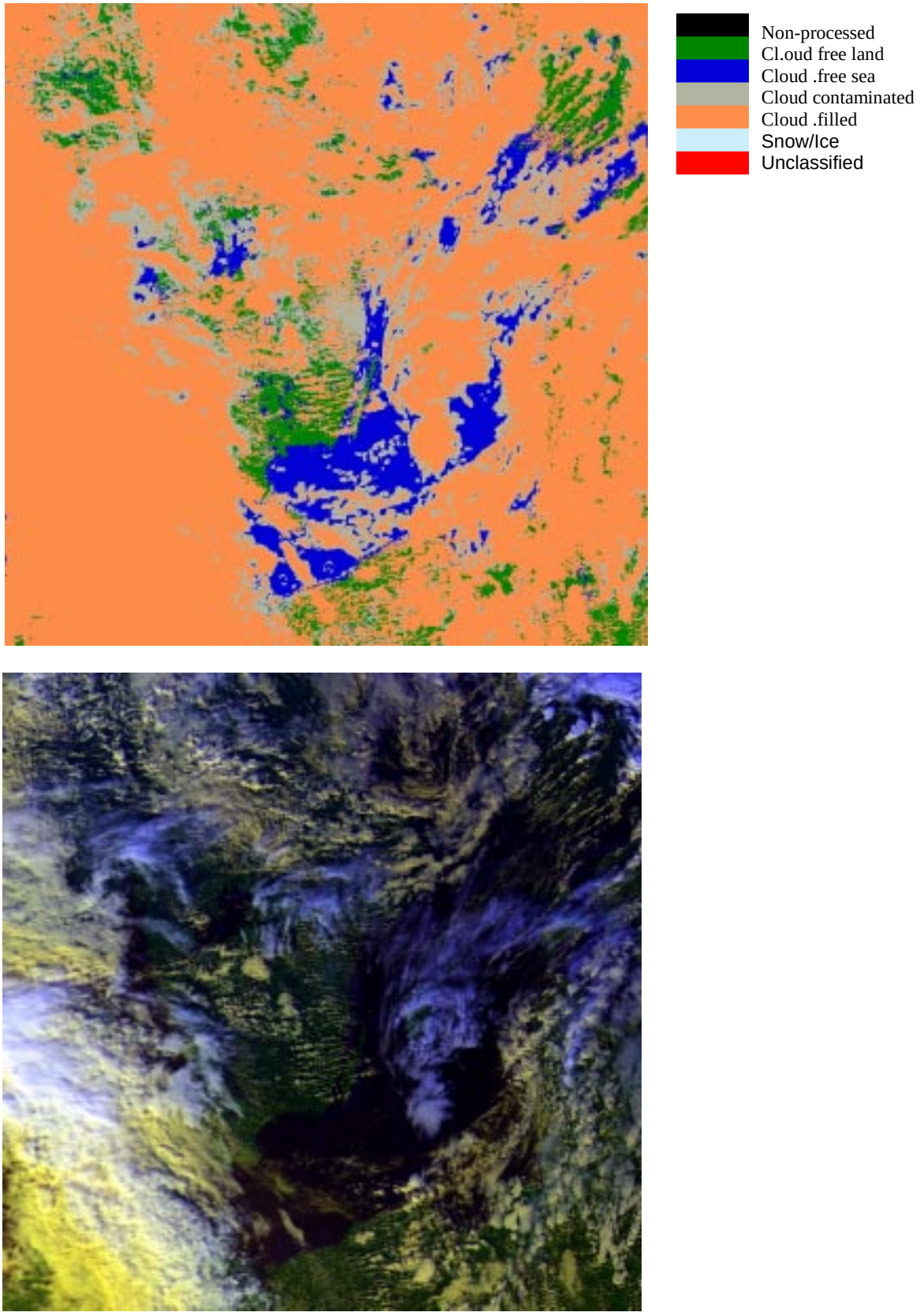

Figure 3-14: Demonstration of the CMa product (top) compared to RGB image (bottom) for NOAA-14 from September 29 1999 at 12:45 UTC.

The data from MSMS used as input to the Cloud Mask are not exactly comparable to the data ingested when running the prototype scheme on full scene data. The deviations are in the derivation of the precipitable water, and in the way HIRLAM data and the view angles are spread on the 32 by 32 pixel area.

When ran on full scene data the precipitable water is derived from the full resolution model data (31 levels in the current HIRLAM). In the MSMS, the closest HIRLAM profile (to the Synop station) is used over the entire 32 by 32 pixel area as compared to the bi-linear interpolation used in full scene processing. Similarly the same satellite and sun view angles (the centre values) are used over the entire area.

This is to say that the Cloud Mask results on the matchup data will not be identical to the results achieved if running the Cloud Mask on the same full AVHRR scene data. This slight degradation of the input data is, however, not considered a major constraint in this objective.

3.4.3 Results

The Cloud Mask cloud fraction, derived over the 32 by 32 pixel area, is compared to the cloud coverage reported from the observer at the Synop station. Due to the nature of the Synop reports also the satellite cloud coverage is given in octas.

We have derived a number of contigency tables and calculated various verification scores for all stations in the database, and divided the results mainly according to illumination and time of year. The contigency table for the comparison against all available Synop reports (after quality control) during the whole year of 1999 is shown in Table 3-9.

Table 3-9: Contingency table for all stations in MSMS during 1999

obs \ sat	0	1	2	3	4	5	6	7	8	*N*
0	**967**	378	260	173	145	113	112	155	369	*2672*
1	1435	**869**	575	429	372	281	320	429	1152	*5862*
2	571	524	**460**	346	316	266	314	380	1191	*4368*
3	295	334	292	**289**	304	267	374	439	1457	*4051*
4	114	164	180	201	**232**	229	287	378	1396	*3181*
5	92	137	168	223	224	**285**	372	521	2253	*4275*
6	67	117	165	224	298	355	**506**	734	3956	*6422*
7	85	173	241	280	395	511	862	**1356**	11940	*15843*
8	93	149	223	279	352	507	864	1412	**14336**	*18215*
N	*3719*	*2845*	*2564*	*2444*	*2638*	*2814*	*4011*	*5804*	*38050*	*64889*

In order to have objective means for validating the Cloud Mask we have calculated some standard measures of score commonly used in connection with verification of meteorological forecast models. These measures are the *Ranked Probability Score* (RPS), the *Probability Of Detection* (POD), the *False Alarm Rate* (FAR), and the *Critical Succes Index* (CSI).

The ranked probability score is a standard measure of the accuracy of a probabilistic forecast model where the predictant can be considered as ordinal. In this case (cloud fraction resolution in number eighths) it ranges from 0 for a completely accurate cloud coverage estimator (as derived from the Cloud Mask considered here to be the "forecast" model) to 8 for a completely erroneous estimator.

For the other measures we have defined two categories, *Cloudy* and *Not-Cloudy* requiring that more than 5/8 of the sky shall be obscured in order for the observation to be classified *Cloudy*, and less than 6/8 for the observation to be classified as *Not-Cloudy*.

For all stations in the year 1999 (Table 3-9) the POD is 88.84%, the FAR is 24.86%, the CSI is 0.69, and the RPS is 1.73.

Below, a summary of the statistics for a few selected stations is given. The data have been divided according to local time of the day, defined by the solar zenith angle (day: below 80 degrees; night: above 95 degrees; twilight between 80 and 95 degrees), and according to season of the year. Summer is here taken to be between May and September (both inclusive – giving five months) and winter to be between November and March (both inclusive – giving five months).

Maritime station 01400 – Ekofisk:

The station Ekofisk is situated on an oil rig in the North Sea, and therefore provide unique data for testing the performance of the ocean scheme. Table 3-10 shows the scores.

Table 3-10: Verification scores for the station 01400 (Ekofisk)

Score \ Subset	1999	Day	Night	Twilight	Winter	Summer
POD	94.74%	97.27%	91.30%	94.03%	91.98%	98.02%
FAR	32.3%	33.33%	33.18%	29.21%	31.20%	35.08%
CSI	0.65	0.65	0.63	0.68	0.65	0.64
RPS	1.87	1.95	1.77	1.81	1.70	2.07
N	910	439	266	205	290	444

According to the CSI score the data show no strong dependency on season or time of day. But the RPS indicates that the CMa performs slightly better during night and during winter time as compared to day and summer. If one reduce the problem of only validating how good the scheme is when it comes to detecting the nearly 100% cloudy cases, The picture is the

opposite. According to the POD the CMa perfoms best during day (high sun) and during summer time. Here it is important to remember that the Synop reports are known to be more reliable during daylight hours. Night and winter gives the lowest POD and twilight gives the lowest FAR.

Thus the results for Ekofisk seems to point at a CMa scheme that in general gives higher cloud coverage during day time than at night time, as compared to the cloud coverage determined from the ground.

Continental station 12300 – Gorzow:

The station Gorzow in Northern Poland represent a continental inland station. Table 3-11 shows the scores.

Table 3-11: Verification scores for the station 12300 (Gorzow)

Score \ Subset	1999	Day	Night	Twilight	Winter	Summer
POD	93.56%	96.87%	89.16%	92.27%	92.71%	95.82%
FAR	25.4%	35.97%	12.56%	11.98%	13.04%	35.91%
CSI	0.71	0.63	0.79	0.82	0.81	0.62
RPS	1.70	2.24	1.24	1.14	1.20	2.17
N	1241	602	319	320	420	584

From the RPS score the CMa is better during night, twilight and at winter, as compared to day and summer. Also the SCI is lower during summer and daytime. But the POD is highest at day and summer, but with the cost of a somewhat higher FAR.

The higher RPS during the light hours seems to be a result of a CMa that tends to overestimate the cloud coverage as compared to the Synop. The CMa is in better overall agreement with the Synop reports during nigh time where, however, the Synop report is likely to underestimate the cloud coverage.

Continental high latitude (Arctic) station 02836 – Sodankylä:

The matchup data for the station Sodankylä in Northern Finland provide means to verify the scheme in high latitude continental conditions. The scores are given in Table 3-12.

According to the RPS the CMa performs better during day and summer time conditions (observe that these are strongly correlated). Also the CSI is higher at day and summer conditions, as is he POD. The lowest scores are found at night and wintertime. Here the FAR is very low, but with the cost of a rather low POD.

Table 3-12: Verification scores for the station 02836 (Sodankylä)

Score \ Subset	1999	Day	Night	Twilight	Winter	Summer
POD	81.64%	97.28%	68.30%	69.53%	68.86%	93.35%
FAR	14.45%	19.32%	4.73%	11.01%	6.59%	20.97%
CSI	0.72	0.79	0.66	0.64	0.66	0.75
RPS	1.65	1.41	1.90	1.80	1.89	1.57
N	1340	607	351	382	465	619

The better daytime/summer time performance is what can be expected for high latitude conditions. The very cold (and snow covered) surface, and occasional very strong low level inversions posses evident problems during the winter season when the sun is never high enough (sun zenith angle below 80 degrees) to provide "day" conditions.

Coastal station 06190 – Rønne:

The station at Rønne on the island of Bornholm in the Baltic Sea provides the means to test the scheme in coastal conditions. The scores are presented in Table 3-13.

Table 3-13: Verification scores for the station 06190 (Rønne)

Score \ Subset	1999	Day	Night	Twilight	Winter	Summer
POD	97.22%	99.63%	93.68%	94.89%	95.02%	100.00%
FAR	43.35%	51.78%	27.64%	27.78%	22.90%	58.19%
CSI	0.56	0.48	0.69	0.70	0.74	0.42
RPS	2.46	3.04	1.49	1.62	1.46	3.24
N	1051	636	160	255	363	506

The RPS is somewhat higher at day and during summer than at night, twilight and winter conditions. Most of the explanation for this shall be found in the POD and FAR which are both rather high. The CMa day-coast scheme seems to have a clear bias, as compared to the Synop reports, in estimating the fractional cloud coverage.

3.4.4 Discussion

The better performance over open sea (Ekofisk), when comparing with ground observations, is a bit surprising. It is a common belief that cloud/clear separation is easier with a high sun than at twilight and nigh time conditions. And also the Synop reports should be more reliable during daylight. However, the dependencies on season and daytime is rather small as compared to over land and coastal regions, as represented by the three other stations for which results are shown here. The explanation for the overestimation, as compared to the night and twilight schemes could be many. It may be a result of a general feature of the Synop

cloudiness of less cloud during night than at daylight hours. But could also be explained by occurrence of sunglint being mis-classified as clouds. Even though the sunglint treatment was concluded to be rather good and close to optimal, from subjective validation on selected cases and during the demonstration period, it is not unlikely that sunglint may still affect verification scores.

As compared to the sea scheme, the coast scheme seems to be a bit better correlated with the Synop reports at night, twilight, and winter conditions. We cannot point at a reasonable possible reason for this feature. But at daylight and summer conditions the performance of the coast-scheme is poorer than the sea scheme, which is in agreement with the subjective validation. The coast scheme is implemented in order to try to treat the inherent difficulties with mis-navigation and large gradients in satellite radiances over the FOV. The coast scheme is bound to give poorer results, but we think it may be possible to make some improvements here.

Concluding the results of the coast and sea schemes it is encouraging that the twilight schemes are performing that well, and not deviating significantly from the day and night time schemes. The reasons for a higher RPS during daytime will be investigated further, but it is not necessarily due to a poorer CMa. It may well be a result of comparing two rather different kinds of observations (cloudiness as derived from the ground by an observer and an estimate derived from a 32 by 32 km satellite FOV).

The daytime-land scheme performs reasonable well in high latitudes, represented by Sodankylä, but according to the results for Gorzow less good in central Europe. This may be a result of the different climatic conditions, but could also be caused by the fact that Gorzow does not represent a true land station. Several pixels are actually treated as coast here.

The difficult winter conditions at high latitudes show up in the data for Sodankylä, where the nightime and twilight schemes has low POD. Here somewhat better are seen for Gorzow.

3.5 Adaptation of the MSG/SEVIRI CMa scheme to high latitude conditions

The NOAA/EPS CMa scheme is naturally focused on the conditions prevailing at high latitudes while the corresponding MSG/SEVIRI scheme is more oriented towards conditions at low- and mid-latitudes. In this section, a discussion on how some of the special features of the NOAA/EPS scheme could be considered for implementation in the MSG/SEVIRI scheme in order to get a further harmonisation of the two schemes in the future.

The following topics will be discussed:

- Treatment of conditions when surface temperatures are close to or colder than cloud temperatures – the surface temperature inversion problem
- Snow and ice discrimination
- Conditions at twilight and near the day/night terminator
- Consequences of very large viewing angles

3.5.1 The surface temperature inversion problem

The frequent occurrence of temperature inversions at the lower tropospheric boundary at high latitudes in the dark and cold winter season causes serious cloud detection problems. The basic pre-requisite for cloud detection (as expressed in section 3.2.3.1) is thus often violated and clouds risk to remain undetected unless other threshold tests (e.g., the **Water Cloud** test in *Table 3-7*are successful. It must however be pointed out that the problem is not unique for high latitudes. Major parts of central Europe will at least temporarily experience similar conditions during the months ranging from November to February.

If the surface inversion is strong and forecasted properly, the **Cold Cloud** test in Table 3-7 will loose its ability to detect low-level clouds. Only mid-level and high-level clouds may now be captured by the test. If the surface temperature forecast is too warm (a quite common feature of today's NWP models in situations with a cold surface and a low level inversion, including the used HIRLAM model), cold cloud free surfaces may be mistaken for clouds. Thus, it is important that any scheme using a similar test takes the following precaution measures when surface inversions are likely to occur:

- The **t11-tsur** threshold offset value should be increased to avoid misclassification of cold ground pixels as clouds
- A quality or processing flag must indicate that conditions for surface temperature inversion has been encountered

The recommended methodology relies on the availability of a high performance NWP model capable of reproducing surface inversion conditions, however not always with the correct strength. Several NWP models fulfil this task and it seems plausible to use model output from levels from 850-950 hPa for achieving an acceptable detection of inversions (as shown in VSci-1). Thus, the mentioned methodology is recommended over the use of climatological static thresholds which are believed to yield inadequate results. However, it is here essential to continuously monitor the performance of NWP models and, if possible, also apply corrections due to obvious model deficiencies (e.g., as discussed by de Valk et al., 2000).

If NWP model results continue to improve in the future, the task of identifying so called "Black Stratus clouds" (i.e., low-level clouds significantly warmer than the ground temperature) may eventually be addressed. Such clouds are often easily identified by the human eye in imagery but problems may occur for automatic interpretation schemes, especially if tests similar to the **Water Cloud** test fail (indicating clouds containing both water droplets and ice crystals). The latter case occurs frequently during winter in very cold situations in the inner parts of Scandinavia, northern Russia and over the Arctic area.

3.5.2 Snow and ice discrimination

A typical complication for cloud screening methods applied at high latitudes is the presence of snow and ice surfaces. These are not easily separated from clouds in VIS and IR imagery. In fact, there are situations other than the obvious night-time situation when this task appears impossible to carry out (also discussed in the next section).

The standard snow and cloud discrimination method applied to AVHRR imagery (including the NOAA/EPS CMa scheme) is to utilise the rapid decrease of snow reflectances when changing focus from the VIS region to the short-wave IR region. This behaviour is not seen for water clouds which continue to reflect considerably. Thus, the separation of snow surfaces and water clouds must rely on the analysis of short-wave IR reflectances, possibly by use of image features comparing reflectances in the VIS and short-wave IR regions (e.g., the **qr37r06** feature in Table 3-5 and Table 3-6). The use of the SEVIRI 1.6 μm channel is expected to greatly facilitate this separation (as indicated in VSci-2). Possibly, the simultaneous measurements in the 1.6 μm and 3.9 μm channels may be an additional advantage here for MSG/SEVIRI scheme compared to the NOAA AVHRR scheme. However, these circumstances cannot be fully revealed until having continuous access to AVHRR/3 channel 3a data on NOAA-L and onwards for the final incorporation of AVHRR channel 3a data into the CMa algorithm.

As regards the discrimination of Cirrus clouds and snow, the situation is not favourable. Thin Cirrus clouds superposed over snow covered surfaces are hardly likely to be separable from cloud-free snow covered surfaces unless the temperature difference between the clouds and the surface is large. However, the large viewing angles at high latitudes for SEVIRI data may here be an advantage compared to the situation when using NOAA AVHRR (see discussion in section 3.5.4).

Ice surfaces may to some extent be treated in the same way as snow surfaces since they are normally snow covered. However, frequent exceptions from this circumstance are seen in situations with newly frozen ice or old melting ice. Both these categories are difficult to separate from other surfaces and clouds. New ice is hardly distinguishable from open sea, but studies of ice targets in the target database have indicated that a negative **t11-t12** feature might be a typical feature here. The physical explanation of this behaviour is not fully understood and more studies are necessary to establish an explanation. However, this circumstance also means that new ice would have almost the same appearance as thin Cirrus clouds, which probably would spoil a proper identification anyhow.

3.5.3 Conditions at twilight, dawn and dusk

The most problematic conditions for cloud screening methods occur at the night and day terminator and in the closest area surrounding this zone. The reason is the very weak or, in many cases, the loss of the reflected solar component (due to shadows) in the VIS and short-wave IR channels in this area.

At high latitudes, these conditions will dominate in daytime images during the winter season. Thus, combined with the circumstance described in section 3.5.1, cloud screening results in the northern hemispheric winter at high latitudes are likely to be very limited in accuracy for both the NOAA/EPS and the MSG/SEVIRI scheme.

The strategy for the NOAA/EPS CMa prototyping has been to try to optimise the use of any small but detectable reflected solar component. This explains the preferred use of the **pseudo06** and **t37-t12** features instead of using the features **r06** and **r37** in the Twilight CMa algorithm branches. The latter features approach indefinite values when being close to 90º

solar zenith angle (generally caused by enhanced illumination of cloud sides and topographic obstacles) and cannot be used efficiently. The idea here is to utilise that non-zero **pseudo06** values at very high solar zenith angles are likely to emanate from clouds if at the same time a reflected component is measured in the **t37-t12** feature (a positive value). However, if no **t37-t12** difference is measured a snow surface is the most probable reflection source in **pseudo06**. As a complement to these twilight illumination tests, also a test assuming night-time conditions (i.e., a **Water Cloud** test) must be used in order to capture the case of low-level clouds being in shadow.

These two methods (twilight illumination plus shadow tests) have earlier been used (e.g., by Karlsson, 1996) with some success although results still show remaining weaknesses in the separation of clouds and snow surfaces. A careful tuning of these tests plus the additional use of the **t11-tsur** feature (possibly also use of independent information on snow and ice cover) may lead to further progress here. However, it is quite possible that a further study of the CMa algorithm performance in the planned validation activities may lead to a decision to use the unclassified category as the most appropriate CMa output in these special situations.

It is concluded that the mentioned problems will also hamper the performance of the MSG/SEVIRI scheme and that a careful investigation of possible remedies to these problems must be considered.

3.5.4 Conditions at very large viewing angles

High latitudes are by definition viewed at very large viewing angles from a geostationary satellite orbit. The increased path length through the atmosphere and through clouds compared to the nadir or near-nadir case means apparent increases in the atmospheric absorption and in cloud thicknesses (especially in the thin Cirrus case). The latter effect might be positive in the sense that thin Cirrus clouds (appearing significantly colder than in nadir view) are more easily detected over snow covered surfaces from a geostationary platform. However, the artificial geometrical displacement of high level compared to surface objects clouds due to the viewing geometry will instead impose a new complicating factor which is not easily corrected for.

The increased atmospheric absorption effect in IR has significant implications for the used thresholds in features like **t11-t12**, **t37-t12** and **t11-tsur**. The most important aspect here is the additional dependence on the surface temperature (previously illustrated in Figure 3-4). A common feature during the northern European autumn and spring seasons is the large diurnal temperature amplitude (often larger than 20K) of the surface. This will have significant impact on the definition of threshold values, especially for moderate to high total moisture contents. The impact of the combined effect of the apparent increase of total moisture content and the rapidly varying surface temperatures is suggested for further investigations for the MSG/SEVIRI scheme. In this respect, an additional study of the estimated error introduced by using total moisture contents integrated in vertical NWP model from single grid columns instead of a more correct use of information simulating the slanted path through several grid columns could also be proposed. It is obvious that the deviations here could be large in frontal regions.

Finally, it is worth mentioning that the general performance of any cloud detection scheme operating on geostationary satellite imagery at high latitudes will be seriously affected by the low horizontal pixel resolution. Each pixel will now have a high risk for containing a mixture of several cloud and surface types, leading to increased problems in using dedicated tests like the **Water Cloud** test and the **Thin Cirrus** tests. Thus, the frequency of fractional clouds (sub-pixel clouds) increases and complicates the cloud analysis and the detection of absolutely cloud free pixels.

4 Prototyping the Cloud Type product – CT

4.1 Overview

4.1.1 Objectives

This product will provide information on the type of cloud - the cloud class - within every satellite FOV. The classification will concentrate on separation of the following main cloud groups:

- sub pixel (or fractional) clouds
- semitransparent clouds
- high level clouds (HLC)
- medium level clouds (MLC)
- low level clouds including fog (LLC)

Information on cloud free areas contaminated by snow, sea-ice or aerosols, and non-processed areas (with no pixel information) will also be included in the product. Furthermore, the separation of convective from stratiform clouds as well as the distinction between pure water clouds and pure ice clouds will be considered during prototyping.

The CT product will also include an “unclassified” category among the output classes. This will reflect the fact that under certain conditions class separability is extremely low (e.g., near the day/night terminator).

The main objective of this product is to support detailed cloud analysis. It may be used as input to an objective meso-scale analysis, which in turn may feed a simple Nowcasting scheme, or as an image product for display at a forecaster’s desk. The CT product is also essential for the computation of radiative fluxes over sea (SAFOSI) and over land, for the generation of the Cloud Top Temperature and Height product (CTTH) and for the identification of precipitating clouds (PC).

These objectives are described in the URD, section 7.2.1.

4.1.2 Background

The development of the NOAA/EPS CT product has its background in the previous experience of the SMHI SCANDIA model (described earlier in section 3.1.2). SCANDIA produces cloud type information over the Nordic region in support of Nowcasting applications. Results are used directly from image displays at the forecaster’s desk or, alternatively, as input to a meso-scale cloud analysis scheme.

The goal of the SAFNWC CT prototyping has been to transfer the experience gained from SCANDIA and to further develop what was considered as deficiencies and weaknesses of SCANDIA. Among these can be mentioned the lacking compensation for atmospheric absorption at large viewing angles and for conditions with strong anisotropic reflection. In addition, improvements in the detection and in the separation of LLC and MLC in cold winter situations are aimed for. Improvements are also essential in the accompanying quality information since this information is crucial for a successful use in objective analysis and forecasting schemes.

4.1.3 SAF Product requirements

A condensed description of the prescribed SAFNWC Cloud Mask product is given in the following sub-sections referring to the SP (section 2.2.2) and the given descriptions and corresponding user requirements in the URD. This should be compared to the final definition of the product which is described in a later section (section 4.1.4).

4.1.3.1 Source

The CT product shall be derived from the complete AVHRR data set comprising of spectral channels at 0.6 μm, 0.9 μm, 1.6 μm, 3.7 μm, 10.8 μm and 11.9 μm. [TBC] (**UR-7.2.2.2.1**)

4.1.3.2 Product description

Twenty-one different categories will be considered (TBC during prototyping):

- land non contaminated by clouds/aerosol/snow
- sea non contaminated by clouds/aerosol/ice/snow
- land contaminated by snow
- sea contaminated by ice/snow
- very low clouds (2 optional classes: cumiliform and non-cumuliform)
- low clouds (2 optional classes: cumuliform and non-cumuliform)
- medium clouds (2 optional classes: cumuliform and non-cumuliform)
- high opaque clouds (2 optional classes: cumulonimbus and non-cumulonimbus)
- semi-transparent ice clouds (4 possible classes: 3 classes according to thickness plus cirrus above clouds)
- fractional clouds
- aerosol clouds (2 possible classes: volcanic and sand)
- unclassified
- non-processed.

The CTy product shall include the cloud type category as defined above, a quality flag and water cloud flag (water or ice clouds). (**UR 7.2.2.2.2**).

4.1.3.3 Quality control

The CTy product shall include a quality flag, which gives information on the conditions under which the product has been derived and informs on the availability of NWP outputs, the illumination conditions and the viewing geometry. (**UR-7.2.4.1**)

For unclassified and unprocessed pixels the quality flag shall give an information on the reason. (**UR-7.2.4.2**)

4.1.3.4 Product output content and format

The product output comprises of the pixel categories given in section 4.1.3.2 and the associated quality flag specified in section 4.1.3.3.

The format of the CT product is [TBD]. (**UR-7.2.2.2.3**)

4.1.3.5 Time constraints

The CTy product - for an area of 1024 x 1024 AVHRR IR pixels - shall be available within 5 minutes after the end of pre-processing of the EPS data (to generate level 1.b data), provided that the user installs the software on the target hardware, indicated by the SAF NWC Consortium. (**UR 7.2.2.2.4**).

4.1.3.6 Internal product dependency

The Cloud Type product is dependent on the Cloud Mask product.

4.1.3.7 Chosen method

The method will be based on a multispectral thresholdning scheme. (SP section 2.2.2.2.2)

4.1.3.8 Auxiliary and ancillary data

NWP – Temperature at several levels (TBD)

OTHER - Sun, satellite zenith and azimuth angles, Land/sea mask, Elevation map, Land cover map, Snow/sea ice map (TBC)

4.1.4 Prototype description

A short summary of the Cloud Type product in its present prototype stage is described in this section. The purpose is mainly to indicate the level of agreement between the specified product and the final prototype version. Deviations from the prescribed product definitions and relevant additional information on the product are briefly mentioned. Unless specifically commented later on in the text, the general product requirements listed previously in sections 2.4 and 2.5 have been followed. For clarity, the same ordering of sub-sections as in the previous section 4.1.3 is used. Further details on the prototype version are given later in section 4.2.

4.1.4.1 Source

All channels except channel 2 of the AVHRR/2 and the AVHRR/3 is used. Prototyping has shown that this channel has a marginal impact on the cloud type separability compared to the use of AVHRR channel 1. However, the prototype does not yet include a valid scheme for the 1.6 μm channel (channel 3A). Such a scheme will be added later in conjunction with the availability of operational data from NOAA-L.The mandatory channels are

- channel 1
- channel 3B (or 3A)
- channel 4
- channel 5

Thus when channel 2 data are missing the algorithm will not be affected, however if any of the other channels are missing the CTy cannot process.

In general, the use of image features in the cloud type algorithm is biased towards a heavier use of IR and shortwave IR features than of VIS features. The reason is that prototyping has shown that the information correlated to vertical variations in the atmosphere (i.e., temperature) is more important for cloud type separation than changes in reflection characteristics. However, this conclusion is not true for the derivation of cloud phase information (to be discussed later).

4.1.4.2 Product description

The prescribed product requirements have been followed. However, two additional cloud classes have been included: Very high stratiform clouds and Very high cumuliform clouds. The reason for adding them was that a further subdivision of the very high clouds was considered as able to give additional information to the user on the status of intense convection and precipitation processes. The two classes were defined as opaque clouds being colder than the mean of the 500 hPa temperature and the tropopause temperature. This change of the product output was unanimously agreed upon between SMHI and Meteo-France.

Thus, the complete output list of classification categories is:

- Unprocessed
- Cloud free land
- Cloud free sea
- Snow contaminated land
- Snow or Ice contaminated sea
- Very low clouds
- Low clouds
- Medium level clouds
- High opaque clouds
- Very high opaque clouds
- Very thin cirrus
- Thin cirrus
- Thick cirrus
- Cirrus superimposed on low clouds
- Fractional clouds
- Unclassified

As a complementary output to the classification categories, a separate cloud phase flag is to be defined according to Table 4-1. Even if such a flag is not implemented in the current prototype, it is worth mentioning that we intend to extend its definition slightly. Two bits will be used to describe four possible output categories. If the dominating cloud phase is not possible to retrieve a mixed phase category will be chosen. From the users point of view, the last category will be the most important due to its correlation to icing conditions (see discussion in section 4.2.3.2).

Table 4-1: Cloud phase categories

Category #	Category name
0	Non-processed (containing no data or corrupt data)
1	Dominating water phase
2	Dominating ice phase
3	Mixed phase

4.1.4.3 Quality control

The first 11 bits of the processing flags are the same as for the CMa product. In addition, there will be a bit to inform on the performance of the cumuliform-stratiform separation (optional according to the prescribed description of the product). This bit will be set to one if separation between cumuliform and stratiform clouds has been performed.

Like for the CMa the information in the processing flags is available for each individual pixel.

Table 4-2: Processing flag for Cumuliform-stratiform separation

Bit #	Meaning of the bit – 1/0
11	Separation made/Not made

4.1.4.4 Product output content and format

The AVHRR Cloud Type output consist of

- Main output (classification categories)
- Quality flags (TBD)
- Cloud particle phase flag (TBD)

The product output is given in the HDF5 format (see information and motivation in section 3.1.4.4 and in ICD).

4.1.4.5 Internal product dependency

The Cloud Type product depends on the output from the Cloud Mask product.

4.1.4.6 Chosen method

The prescribed method is used.

4.1.4.7 Auxiliary data

The auxiliary data used are:

- NWP surface temperature
- NWP temperature at the following vertical levels (hPa): 950,850,700,500, and tropopause
- Satellite zenith angle
- 1 km Land use data (including land/sea mask)
- 1 km Digital elevation map

4.2 Detailed algorithm description

4.2.1 Algorithm outline

As for the CMa product, the algorithm is executed in two separate processing stages: the ***Pre-processing stage*** and the ***On-line processing stage***.

The Pre-processing stage, the On-line processing stage, the general and the detailed structure of the cloud classification algorithm are described in the following sub-sections.

4.2.1.1 The Pre-processing stage

The processing tasks carried out in the Pre-processing stage are very similar to the corresponding tasks for the Pre-processing stage of the CMa product. Consequently, they are for practical reasons performed simultaneously within one unified module as indicated in Figure 3.1.

The differences between the CMa and CT pre-processing tasks result from the slightly different needs of auxiliary and ancillary data. Concerning the preparation of NWP data for CT, information from a few additional vertical levels is needed and the temperature at the tropopause level (being not a standard NWP model output parameter) must be calculated.

4.2.1.2 The On-line processing stage

The activities carried out in the On-line processing stage are described in Figure 4-1.

Prior to performing the cloud type classification, necessary satellite input imageries must be prepared. This preparation is illustrated at the top of Figure 4-1 and is identical to the corresponding preparation being made for the CMa product (see section 3.2.1.2).

When performing Cloud Type classification, the extraction of the cloud phase flag is treated as a separate optional function. A final post-processing step is applied where isolated pixels resulting primarily from noisy AVHRR channel 3b imagery are removed. It is also possible to extract statistical information based on the complete output data set.

4.2.1.3 General structure of the cloud type classification algorithm

The developed cloud type classification algorithm is based on the following approach:

- IR and short-wave IR imagery be used to separate opaque from semi-transparent or fractional clouds

- IR and short-wave IR imagery can be used to separate semi-transparent clouds from fractional clouds
- Opaque clouds may be vertically sub-divided by use of AVHRR 11 μm imagery compared to NWP temperature profile information
- Cumuliform opaque clouds may can be separated from Stratiform opaque clouds by use of texture features and IR imagery
- The cloud phase flag can be defined by use of VIS and short-wave IR imagery

Notice that the distinction between Opaque and Semi-transparent/fractional cloud types does not rely entirely on the detailed output of the CMa scheme. The main use of the CMa information is to identify Cloud free and Snow/Ice contaminated pixels to prohibit further processing of these pixels. This means in practice that the pixels contained in the CMa Cloud contaminated category will not be exactly identical to the sum of the CT semi-transparent and fractional cloud category pixels. The reason is that the structure of the CMa algorithm only permits a rough estimate of the sub-division of opaque and thin/fractional clouds. CMa produces output from algorithm components that may involve only a few threshold tests and they are applied with quite large security margins in order to prevent possible overestimation of the number of cloud free pixels. The identification of the opaque clouds (now interpreted as the cloud appearance in IR) is crucial for the further separation of cloud types in the vertical by use of estimated cloudtop brightness temperatures. For this reason, the CT scheme contains a slightly modified and more consistent sub-division of the cloud mask information as compared to the CMa scheme.

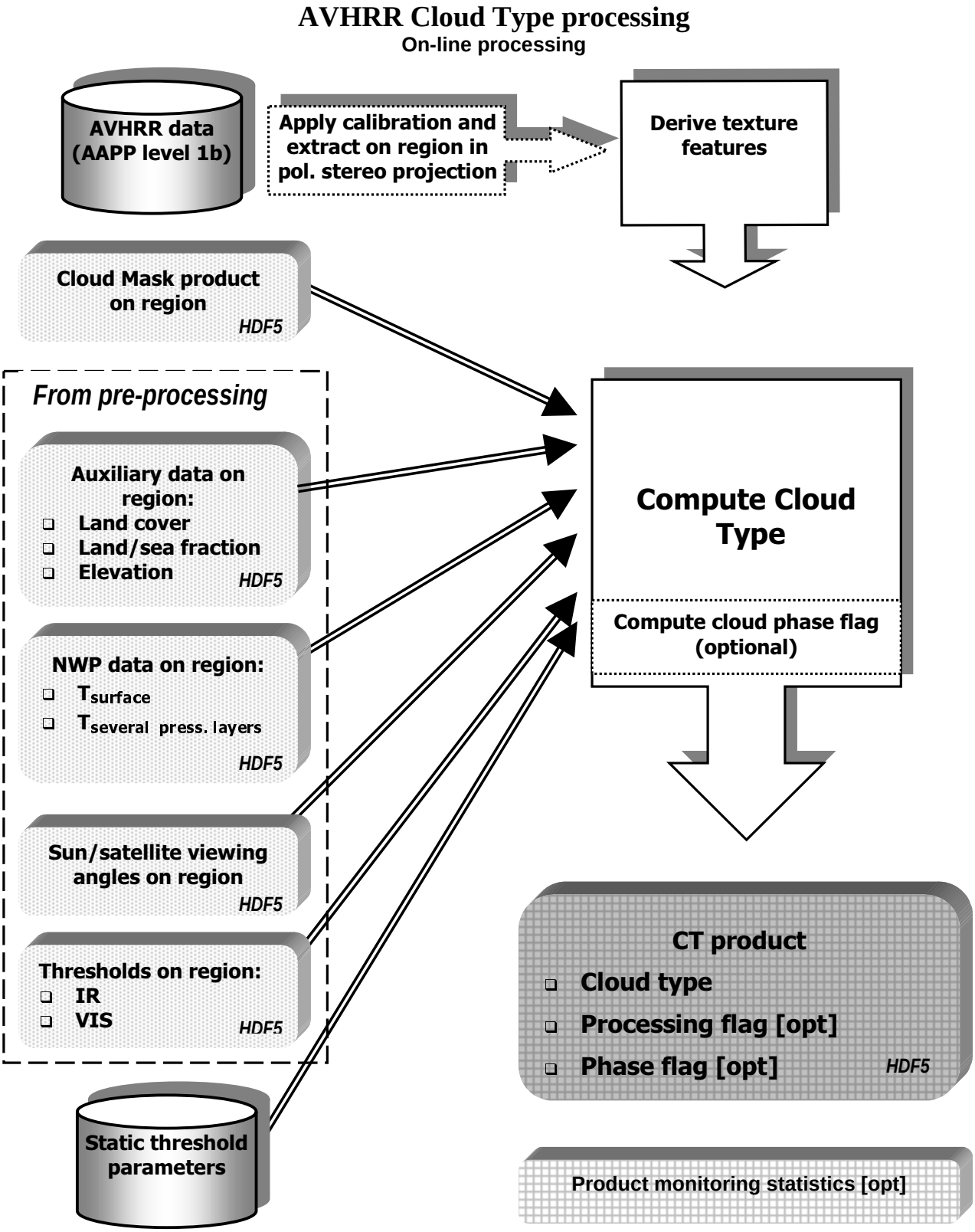

Figure 4-1: AVHRR Cloud Type processing

4.2.1.4 Detailed structure of the cloud type classification algorithm

The consequences of applying the general approach as outlined in the previous section are described in some more details in the following.

Separation of opaque clouds from semi-transparent and fractional clouds:

- At night, if the **t37-t12** feature exceeds a threshold (i.e., if **t37** is sufficiently warmer than **t12**), the cloud is considered as non-opaque (a semi-transparent or fractional ice cloud). This test will unfortunately not capture fractional water clouds (having a negative **t37-t12** value). These are identified by using that fractional water clouds will have a small **t11-tsur** difference and a high **t11_texture** in addition to the negative **t37-t12** value.
- During day and twilight, if the **t11-t12** feature exceeds a threshold (i.e., if **t11** is sufficiently warmer than **t12**), the cloud is considered as non-opaque (a semi-transparent or fractional ice or water cloud).

Separation of semi-transparent and fractional clouds:

- Fractional clouds are in the following assumed to consist of sub-pixel water clouds for separability reasons (sub-pixel Cirrus clouds are here assumed as being non-separable from overcast although semi-transparent Cirrus clouds).
- At night, all non-opaque cloud pixels are assumed to be semi-transparent Cirrus clouds (fractional water clouds are treated separately as described above).
- During day and twilight, fractional clouds are separated from semi-transparent (Cirrus) clouds requiring them to be relatively warm (small **t11-tsur** difference) but significantly reflecting as deduced from the **r06** feature.

Sub-division of opaque clouds into categories LLC, MLC and HLC:

- Assignment of the opaque clouds to the appropriate main cloud category is made by comparing the **t11** feature to the temperature of the pressure levels 700 hPa and 500 hPa. Thus if the t11 is lower than the temperature at 500 hPa the cloud is assigned to the high level cloud (HLC) category. Else if it is lower than the temperature at 700 hPa the cloud is assigned to the mid-level cloud (MLC) category, and if it is higher than the 700 hPa temperature it said to belong to the low level cloud (LLC) category.
- The LLC category is further sub-divided into an additional very low level (VLLC) cloud category by using the temperature of the 850 hPa pressure level.
- The HLC category is further sub-divided into an additional Very high level cloud category using the 500 hPa and the tropopause level temperatures.

In the presence of a low level inversion the assignment of pixels to the low level and very low level cloud categories may be ambiguous, and thus the classification calls for a special approach:

If no low level inversion is present a cloudy pixel will be assigned to the VLLC category if the t11 brightness temperature is above the temperature at the 850 hPa level. If the pixel is colder than at 850 hPa but warmer than at 700 hPa, and the terrain is *low* (here lower than 1000 meters), we assign the pixel to the LLC category. If the terrain is *high* (here above 1000 meters) also pixels having a t11 temperature below that at 850 hPa, but still above the temperature at 700 hPa, will be assigned the VLLC category.

If a low level inversion is present low clouds are always categorized as a VLLC, and no such pixel can be assigned to the LLC category.

Separation of cumuliform clouds from stratiform clouds (optional)

- For the low-level and mid-level cloud groups, the separation will based on the combined use of texture features **r06_text**, **t11_text** and **t37t12_text**.
- For high level clouds, clouds are labelled cumuliform if IR cloudtop brightness temperatures are close to the tropopause temperature and if having a low **t11_text** value.

Definition of the cloud phase flag

- For opaque clouds, water clouds are identified as clouds having a **r37** value exceeding a threshold. Ice clouds are here identified as clouds having a **r37** value below a second threshold being lower than the one used for water cloud identification. The mixed phase category will consequently be formed by the remaining cloud pixels not sufficiently reflecting to be denoted a water cloud but reflecting more than the ice cloud category.

- For semi-transparent and fractional clouds, the cloud phase flag will depend on the output results of the activities described above to separate the two cloud groups.

4.2.2 Derivation of thresholds

4.2.2.1 Thresholds for separation of opaque clouds from semi-transparent/fractional clouds

In analogy with the discussion of atmospheric absorption effects due to atmospheric water vapour, a similar dependence of the surface temperature as illustrated in Figure 3.4 could be expected for semi-transparent Cirrus clouds. This is also to a large extent verified when studying Cirrus targets in the target database in Figure 4-2. The large scatter here is most probably caused by thickness variations for Cirrus targets in the target database (in analogy with the variation caused by varying total moisture contents in Figure 3.4). The indicated non-linear relation to the surface temperature is caused by the dependency on the Planck function.

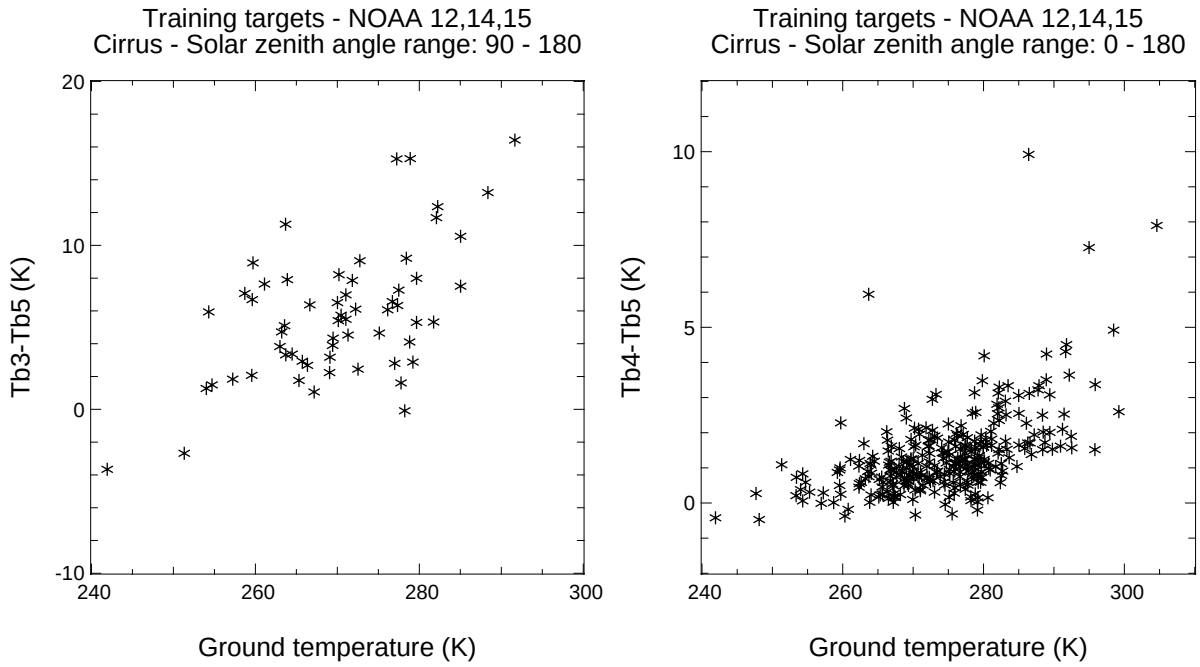

Figure 4-2. Features t37-t12 (left –only at night) and t11-t12 (right – all day) plotted as functions of surface temperature for Cirrus targets.

The dependency on the satellite viewing angle is analogous to the effect of changing the Cirrus thickness. For increasing viewing angles, the path length through the cloud layer (representing the apparent cloud thickness) increase by a factor of $cos\phi^{-1}$ where ϕ is the satellite zenith angle. This leads to a decrease in the transmission through the cloud, thus decreasing values of the **t37-t12** and **t11-t12** features. However, it is generally not possible to find a simple analytical formulation of this effect without making very restrictive assumptions about the optical properties of Cirrus clouds (i.e., the distribution, shape and concentration of ice crystals) and the true geometrical depth. We have therefore followed an empirical approach based on studies of the Cirrus targets in the target database.

The present prototype only includes a threshold dependence on the satellite viewing angle (a surface temperature dependence will be considered later). Principally, semi-transparent clouds are separated from opaque clouds by comparing the **t37-t12** and **t11-t12** features to the simulated thresholds related to the cloud free case (same as used in the **Thin Cirrus** test for CMa). Pixels having a difference exceeding this threshold are labelled semi-transparent. For the further sub-division of the Cirrus clouds into the CT Cirrus categories, a satellite viewing angle dependence is introduced (notice that this dependence is implicitly included in the basic test separating opaque and semi-transparent clouds). For nadir conditions the required feature differences are at maximum. However, these differences are then linearly decreased for increasing viewing angles.

4.2.2.2 Thresholds for separation of semi-transparent and fractional clouds

We have chosen to use observed small differences in reflection characteristics between semi-transparent Cirrus clouds and fractional water clouds for their separation. The existence of such a difference is indicated from the target studies as shown in Figure 4-3. Notice here that all water clouds are included in this figure. This means that the separability of fractional water clouds probably is not as evident as shown in the figure (indicated by the existence of some water clouds in the same reflectivity region as the Cirrus clouds).

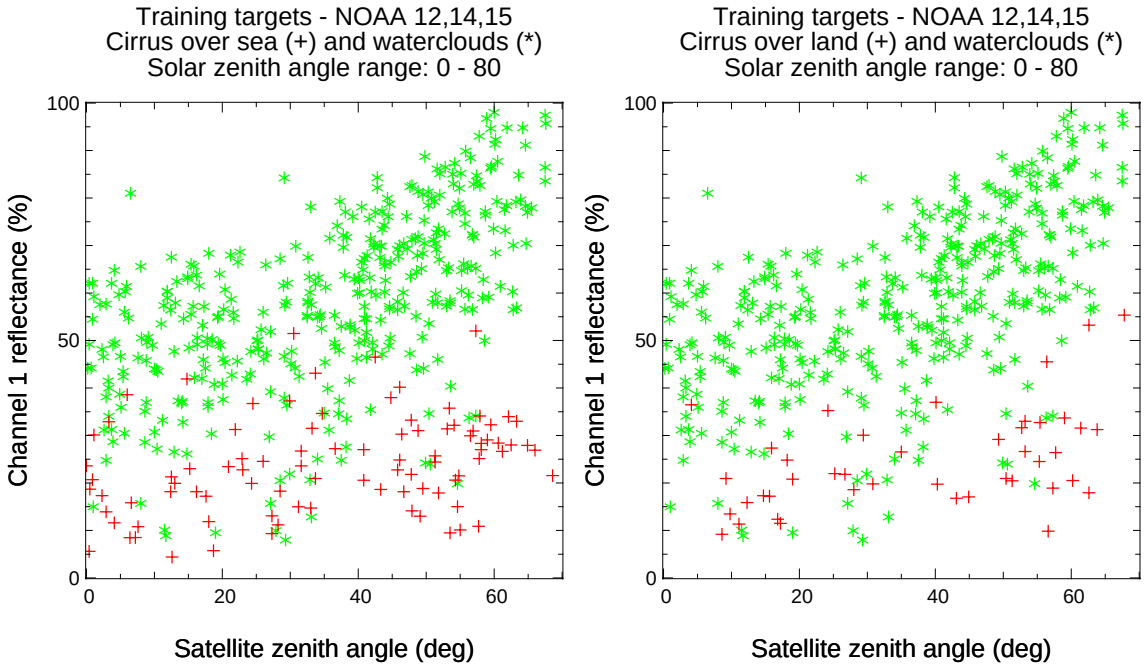

Figure 4-3: Feature r06 for Cirrus targets and water cloud targets over sea (left) and land (right) plotted as functions of satellite zenith angle.

The applied threshold is implemented as a linearly varying function of satellite viewing angle. In the prototype we have used a reflectivity range from 25% at nadir to 40% at the swath edge over sea. Over land, a slightly steeper slope of this function has been applied.

4.2.2.3 Thresholds for vertical sub-division of opaque clouds into categories

A straight-forward method, comparing **t11** temperatures to the 700 hPa, 500 hPa, 850 hPa and the mean of the 500 hPa and tropopause pressure levels, has been applied for the sub-division of the opaque clouds.

When near-surface thermal inversions are identified (via the imported processing flag from CMa), the separation of low level clouds from medium level clouds is not made by comparing to the 700 hPa temperature. Instead, the comparison is made against the forecasted surface temperature (a low level cloud would then be warmer than the surface). For this test to be more effective, it should also in the future utilise cloud phase information as extracted from the cloud phase flag.

4.2.2.4 Thresholds for separation of cumuliform clouds from stratiform clouds

Tests for this separation (optional) have not been defined in the present prototype.

4.2.3 Derivation of processing and cloud phase flags

4.2.3.1 Processing flags

The CT algorithm outputs the same processing flags as the CMa algorithm except for an addition flag indicating if the separation of the cumuliform and stratiform cloud classes (optional) has been made.

4.2.3.2 The cloud phase flag

The implementation of a cloud phase flag has not been made in the present prototype.

Radiative transfer modelling may also eventually be used in the definition of this flag. Water/ice phase distinction using only one of the two AVHRR/3 channels 3a or 3b are rather ambiguous, so this information is likely to only serve as a rough guideline.

4.2.4 The use of NWP data and their impact on quality

The CTy makes use of the surface temperature and the total precipitable water, and the temperature at the vertical levels; 950 hPa, 850 hPa, 700 hPa, 500 hPa, and the tropopause.

The temperature at the surface and at 950 and 700 hPa are used for the detection of low level and lifted inversion, determining the sequence of tests. In addition to the definition of inversions the surface temperature is used for the detection of semi-transparent and fractional clouds, and in presence of an inversion also in the discrimination between low and mid-level clouds.

The temperatures at 850 hPa, 700 hPa, 500 hPa, and at the tropopause are used to classify clouds into the very high, high, mid-level, low and very low level classes.

The total precipitable water is used indirectly for the derivation of thresholds like for the CMa (section 3.2.5.). The most pronounced impact is in the detection of fractional cloudiness and semi-transparent cirrus, where the features t11-t12 and t37-t12 are used.

4.2.4.1 Impact on product quality of errors in the NWP output

Since the CTy algorithm builds on the input from the CMa, any errors in NWP data causing errors in the Cloud Mask will obviously also effect the Cloud Type. Except for this dependency the CTy is less sensitive to the surface temperature being the most critical parameter for the CMa. The biggest impact is rather to be found from any general erroneous resolution of the actual vertical temperature profile in the lowest part of the atmosphere, causing the discrimination of mid-level and low and very level clouds to fail.

4.2.4.2 Dependency on NWP model

See section 3.2.5.

4.3 Practical application

4.3.1 Implementation

The coding of the core CTy model is done using the C language. Python is used only as the glue when implemented in the pre-operational scheme – e.g. for grabbing the right NWP model output, extracting the physiography data, and the production of derived image outputs.

As for the CMa (see section 3.3.1) the starting point for the CTy is mapped angles on region, mapped physiography data on region and some NWP parameters (temperature at pressure levels) already post-processed. In addition the CTy pre-processing makes use of the results of the CMa pre-processing, as concerns cloud free thresholds and NWP data (surface temperature and 950hPa temperature).

System tests of the CTy was carried out on the same hardware and operative system as specified in section 3.3.1. Also the same optimization flags were used.

On different regional areas of size 1024 times 1024 pixels and different satellite scenes, the pre-processing step required between 6.3 and 6.6 seconds CPU time, and consumed 41 MB memory. These results were achieved with a compression level of 1 for the HDF5 output files (minimum compression). CPU time consumption was not decreased significantly if choosing no compression on the output files.

The on-line processing took between 19.9 and 22.1 seconds CPU time, and 66 MB RAM was required. 0.5 to 1 seconds CPU time was saved if not compressing the output file. It shall be noticed here that this on-line processing did not make use of the already derived texture features from the CMa processing step. In the final integrated AVHRR/AMSU software package this will of course be the case. Since the derivation of the texture is the single most expensive task, concerning CPU time, in the on-line processing the figures given above will be reduced significantly.

4.3.2 Product demonstration

This product was not included among the demonstrated products in the SAFNWC Demonstrating Experiment.

Figure 4-4 shows an example of the visualisation of the product output from the present prototype. The intention is that product examples from the present CT prototype version shall be demonstrated at the SMHI SAF website (at address http://www.smhi.se/saf/) during MTR.

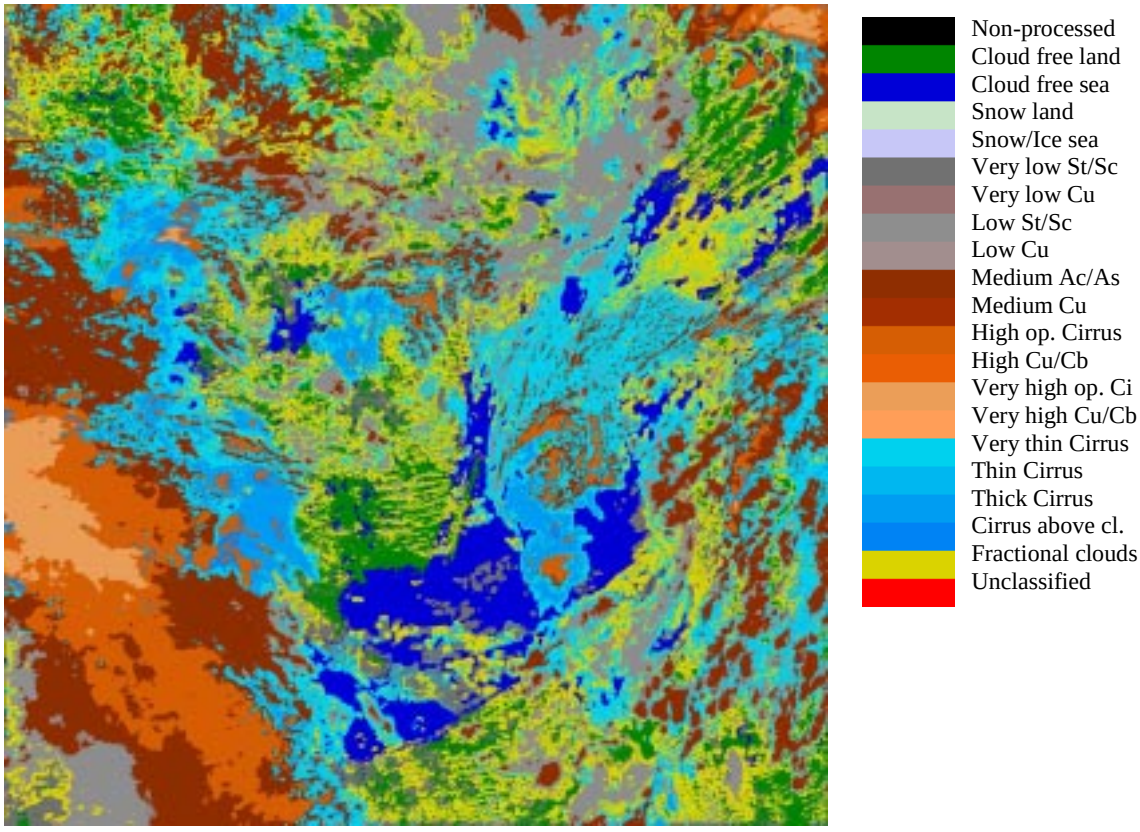

Figure 4-4: CT product example over southern Scandinavia 29 September 12:45 UTC 1999 NOAA-14.

4.4 Validation

No validation efforts have yet been made due to time constraints. Validation will be done using the large dataset of interactively gathered training targets.

4.5 Adaptation of the MSG/SEVIRI CT scheme to high latitude conditions

In principle, the same problems and circumstances as discussed in the previous section 3.5 are valid also for the NOAA/EPS and MSG/SEVIRI CT algorithms. However, the following two aspects are of particular importance to the task of identifying the correct cloud type:

- Treatment of conditions when surface temperatures are close to or colder than cloud temperatures – the surface temperature inversion problem
- Consequences of very large viewing angles

4.5.1 The surface temperature inversion problem

Besides the serious consequences for basic cloud detection (as discussed in section 3.5), the existence of strong thermal inversions near the surface introduce problems for the separation of very low clouds from low clouds and medium level clouds. Thus, even if cloud detection is successful (through threshold tests of the type **Water Cloud** in Table 1.7), very low clouds will risk to be mis-classified as higher level clouds. The reason is that Stratus clouds and fog being trapped in a strong near surface inversion are normally much colder at cloud top level

than the closest upper levels. It is quite common that these clouds are even colder than the 700 hPa level which might then lead to the serious mis-classification of fog and Stratus as medium level clouds (a defect often seen in SCANDIA classifications during the winter season).

There is no simple remedy for this problem since it emanates from the fact that there are several possible solutions to the problem of matching the cloud top temperature to a vertical temperature profile. However, one can take measures that minimise these errors as demonstrated above in section 4.2.2.3. The idea is here to abandon the normal assumption of one unique solution to the temperature matching problem when near-surface inversions occur. In those cases, the solution closest to the surface should be chosen prior to higher level solutions.

Experience has shown that this simple assumption gives a correct classification in a large majority of cases. The risk that higher level clouds (who now would risk to be mis-classified as lower level clouds) could co-exist with fog and Stratus cloudiness in these situations seems rather low. Such a situation would alter the thermal radiation balance near the surface drastically thus leading to cloud clearing of the near-surface clouds. This effect is often observed in cases when medium level clouds are advected over areas with near-surface clouds.

4.5.2 Conditions at very large viewing angles

Increasing viewing angles means that thin clouds artificially look less thin as a consequence of the increased path length through semi-transparent cloud layers. Consequently, there is an obvious risk that the MSG/SEVIRI CT algorithm will have an overrepresentation of the opaque cloud types at the cost of the semi-transparent and fractional cloud types unless some compensating efforts are introduced. It is here proposed to consider the introduction of viewing angle dependent thresholds for the separation of the semi-transparent and opaque clouds as described in section 4.2.2.1. This would at least reduce the distribution error even if a complete correction will never be accomplished.

A second aspect influencing results when operating the CT algorithm at increasing viewing angles is the obvious effect of a decreasing pixel resolution. The horizontal resolution of the SEVIRI pixels changes rapidly from about 4-5 km over central Europe to more than 10 km in northern Scandinavia. This will have serious consequences for the capability of texture tests (local variance tests) to successfully separate stratiform and cumuliform cloud types. A rapidly decreasing separability with latitude will thus be encountered at high latitudes.

It is likely that a complete harmonisation of the MSG/SEVIRI and NOAA/EPS schemes related to this latter effect will never be possible due to the quite different pixel resolutions. A typical cloud field with small convective clouds (Cumulus humilis, Cumulus mediocris and Cumulus congestus) will quite easily be separated from stratiform clouds (e.g. Stratocumulus and Stratus) in AVHRR imagery since the cloud elements are generally resolved. This will hardly be the case in SEVIRI imagery at high latitudes and the stratiform-cumuliform separation task is therefore likely to fail. This effect is easily seen when inspecting and comparing NOAA AVHRR imagery and current Meteosat imagery at high latitudes.

4.6 Remaining work

The following tasks remain to be completed from prototyping:

- Definition of the cloud phase flag
- Definition of the separation of cumuliform and stratiform cloud types (optional)
- Basic validation of prototyping results

5 Prototyping the Cloud Top Height/Temperature product – CTTH

5.1 Overview

5.1.1 Objectives

The CTTH product shall contain information on the cloud top temperature and height for all pixels identified as cloudy in the satellite scene with the highest possible spatial and temporal resolution.

The main use of this product is in the analysis and early warning of thunderstorm development. Other applications include the height assignment of tropospheric winds derived from cloud tracking and the cloud top height analysis for aviation forecast activities. The product may also serve as input to mesoscale models or to other SAF NWC products (e.g. the Rapid Developing Thunderstorms product).

These objectives are described in the URD, section 7.3.1.

5.1.2 Background

Many NMSs of EUMETSAT member states (including SMHI) use still today the uncorrected brightness temperature information from AVHRR IR imagery as a rough estimation of cloud top temperatures. For the optically thick clouds this estimation is in most cases acceptable. However, for pixels containing semi-transparent or fractional clouds (often representing a large fraction of cloudy pixels) this information is definitely misleading, yielding sometimes to quite a large underestimation of true cloud top temperatures and heights.

The intention of the SAFNWC CTTH product has been to create a product that as far as possible (considering both computational accuracy and CPU efficiency aspects) compensates for the semi-transparency effect and the effect of an absorbing atmosphere between the cloud top and the satellite sensor.

The semi-transparency correction is a theoretically challenging task due to a fundamental lack of information in the basic imagery in order to achieve an accurate determination of the essential parameter; cloud emissivity. Thus, simplifications have to be introduced and auxiliary data describing the prevailing vertical temperature and humidity profiles have to be utilised. Previous experience on the use of both window channels (described by Inoue, 1985) and sounding channels (described by Menzel et al., 1983) has been considered during the product development.

5.1.3 SAFNWC Product requirements

A condensed description of the prescribed SAFNWC Cloud Top Height/Temperature product is given in the following sub-sections referring to the SP (section 2.2.3) and the given descriptions and corresponding user requirements in the URD. This should be compared to the final definition of the product which is described in a later section (section 5.1.4).

5.1.3.1 Source

- The CTTH product shall be derived using the AVHRR channels at 10.8 μm and 11.9 μm. [TBC] (**UR-7.3.2.2.1**)

5.1.3.2 Product description

The output will provide information on the temperature and height (in meters or hPa) of opaque, and depending on the validation results, possibly also semi-transparent and sub-pixel cloud tops.

- The CTTH product shall be available both in meters and in hPa. (**UR-7.3.2.2.4**)

- The accuracy of the CTTH product, expressed in meters, shall be less than 100 m for low clouds and within 10% for all other clouds, including semi-transparent and fractional clouds. (**UR-7.3.2.2.2**)

5.1.3.3 Quality control

- The CTTH product shall include a quality flag. The exact content of this quality flag is TBD. It shall in any case contain an indication on the method that has been applied to retrieve the CTTH product, and the expected accuracy. (**UR-7.3.4.1**)

- The CTTH product shall be objectively verified by either comparison with ground based lidar systems or with data from special experimental campaigns. (**UR-7.3.4.2**)

- In addition to the objective validation, the CTTH product shall be subjectively verified (off line) by analysing the temporal and spatial coherency of the product, as well as the consistency with the meteorological situation. (**UR-7.3.4.3**)

5.1.3.4 Product output content and format

The Cloud Top Height/Temperature product output comprises of the pixel categories given in section 5.1.3.2.

The format of the CTTH product is [TBD]. (**UR-7.3.2.2.3**)

5.1.3.5 Time constraints

- The CTTH product - for an area of 1024 x 1024 AVHRR IR pixels - shall be available within 5 minutes after the end of pre-processing of the EPS data (to generate level 1.b data), provided that the user installs the software on the target hardware, indicated by the SAF NWC Consortium. (**UR-7.3.2.2.5**)

5.1.3.6 Internal product dependency

The product requires the AVHRR Cloud Type product as input information.

5.1.3.7 Chosen method

For opaque clouds, brightness temperatures will be compared directly to NWP model profile information including some corrections for water vapour absorption above cloud layers.

For semi-transparent clouds, an IR window technique will be used based on the study of IR histogram plots of the AVHRR 10.8 μm and 12.0 μm channel brightness temperatures. The plots are fitted to a non-linear curve describing the relation between the effective emissivity (or transmissivity) and the measured brightness temperature differences. Extrapolation of this non-linear curve will yield the corresponding opaque and true cloud top temperature.

The method is described in SP section 2.2.3.3.

5.1.3.8 Ancillary and auxiliary data

Ancillary and auxiliary data needed are:

- NWP temperature at several vertical pressure levels (TBD).
- NWP relative humidity at several vertical pressure levels (TBD).
- Sun zenith, satellite view zenith, and sun-satellite view relative azimuth difference angle
- 1km Land use data (including land/sea mask)
- 1km Digital elevation map

5.1.4 Prototype description

A short summary of the Cloud Top Height/Temperature product in its present prototype stage is given in this section. The purpose is mainly to indicate the level of agreement between the specified product and the final prototype version. Deviations from the prescribed product definitions and relevant additional information on the product are briefly mentioned. Unless specifically commented later on in the text, the general product requirements listed previously in sections 2.4 and 2.5 have been followed. For clarity, the same ordering of sub-sections as in the previous section 5.1.3 is used. Further details on the prototype version are given later in section 5.2.Notice that for this product, some prototyping work still remains to be completed. The algorithm for opaque clouds is being implemented, but the optional algorithm for semi-transparent clouds is not developed yet. Consequently, the following description is preliminary and future changes can be expected.

5.1.4.1 Source

For the retrieval on opaque clouds the AVHRR channel at 11 μm (channel 4) is used.

Since the CTTH requires the Cloud Type as input the mandatory channels are

- channel 1
- channel 3B (or 3A)
- channel 4
- channel 5

Thus only when all channel are available or when only channel 2 data are missing the algorithm will not be affected. If any of the other channels are missing the CTTH cannot process.

5.1.4.2 Product description

The current prototype only provides cloud top temperature and height information for opaque clouds. For those pixels the product output is then:

Main output

- Cloud Top Height in meters
- Cloud Top Temperature in K
- Cloud Top Pressure in hPa

The remaining pixels will be labelled cloud-free or semi-transparent.

5.1.4.3 Quality control

The processing flags include information on the cloudiness (opaque or not), the type of semi-transparency correction applied (if any), and whether or not RTTOV was applied to simulate TOA radiances. The full table describing the processing flags of the present prototype version is given in Table 5-1 Table 5-2 Table 5-3, Table 5-4 and Table 5-5.

Table 5-1: Processing flags for Cloudiness status

Bit #	Meaning of the bit – 1/0
0	Non-processed (corrupt data or cloudfree) / processed
1	Cloudy / cloudfree
2	Opaque cloud / semi-transparent cloud

Table 5-2: Processing flags for missing data

Bit #	Meaning of the bit – 1/0
4	One or more AVHRR channels missing / No channels missing
6	NWP data missing / Not missing

Table 5-3: Processing flags for RTM simulations

Bit #	Meaning of the bit – 1/0
3	RTTOV simulations available / Not available
7	RTTOV simulations applied / Not applied

Table 5-4: Miscellaneous processing flags

Bit #	Meaning of the bit – 1/0
5	Thermal inversion detected / Not detected
8	Window technique applied / Not applied

Table 5-5: Processing flags for quality estimation

Bit #	Meaning of the bit – 1/0
9	Quality estimation available / Not available
10	Low confidence / High confidence (or undefined if bit 9 not set)

The bits 11-15 are spare for yet not defined retrievals for semi-transparency correction.

Like for the other products the information in the processing flags is available for each individual pixel.

5.1.4.4 Product output content and format

The AVHRR CTTH output consist of the main output and the processing flags as described above.

The product output is given in the HDF5 format (see information and motivation in section 3.1.4.4).

5.1.4.5 Time constraints

Due to the preliminary status of the product, no information on the achieved processing time can be given at this stage.

5.1.4.6 Internal product dependency

The CTTH product depends on the output from the Cloud Type product.

5.1.4.7 Chosen method

The present prototype only includes the envisaged method (section 5.1.3.7) applied to opaque clouds. Atmospheric corrections are accomplished by use of RTM calculations.

5.1.4.8 Auxiliary data

The auxiliary data used are:

- NWP temperature profiles in 20 pressure levels including the surface temperature
- NWP humidity profiles in 20 pressure levels
- Satellite zenith angle
- 1 km Land use data (including land/sea mask)
- 1 km Digital elevation map

5.2 Detailed algorithm description

5.2.1 Algorithm outline

As already has been mentioned above, the present prototype includes a method which is only applicable to the opaque clouds as identified by the CT product.

As for the CMa and CT products, the CTTH algorithm is executed in two separate processing stages: the ***Pre-processing stage*** and the ***On-line processing stage***.

The Pre-processing stage, the On-line processing stage and the detailed structure of the algorithm are described in the following sub-sections.

5.2.1.1 The Pre-processing stage

The processing carried out in the Pre-processing stage is described in Figure 5-1.

Processing is carried out in segments that (however configurable) in principle corresponds to the used grid resolution of the NWP model. For these segments, a rough description determining the dominating surface type (land or sea), the land elevation and the satellite viewing geometry is extracted from ancillary and auxiliary data.

Cloud free top of atmosphere radiances and cloudy radiances from a large number of vertical layers (at present, 20 layers**)** are calculated from IR RTM calculations by use of the RTTOV model. The retrieval of the CTTH information is greatly obstructed in cases where temperature inversions are present. Therefore a special thermal inversion identification is performed and this information is carried throughout the processing chain and is also a part of the processing flags. The used forecast length is restricted to be between 6 and 18 hours (with a preference for the shorter forecast lengths). The lower limit motivated by the requirement that the model integration results should be free from spin-up deficiencies and the higher limit motivated by the wish to avoid too large phase errors in forecasts

5.2.1.2 The On-line processing stage

IR radiances (AVHRR channel 4) for pixels containing opaque clouds as identified by the CTy product are compared to the simulated cloud-free and cloudy radiances. The pressure level for which the best matching of simulated and measured radiances occur is identified, and the temperature, pressure and height of the top of the opaque cloud is found from the vertical atmospheric profile data using linear interpolation.

Notice here that the described method indirectly compensates for the water vapour absorption above the cloud layer by utilisation of NWP modelled moisture fields and the current satellite viewing geometry via the pre-calculated radiances.

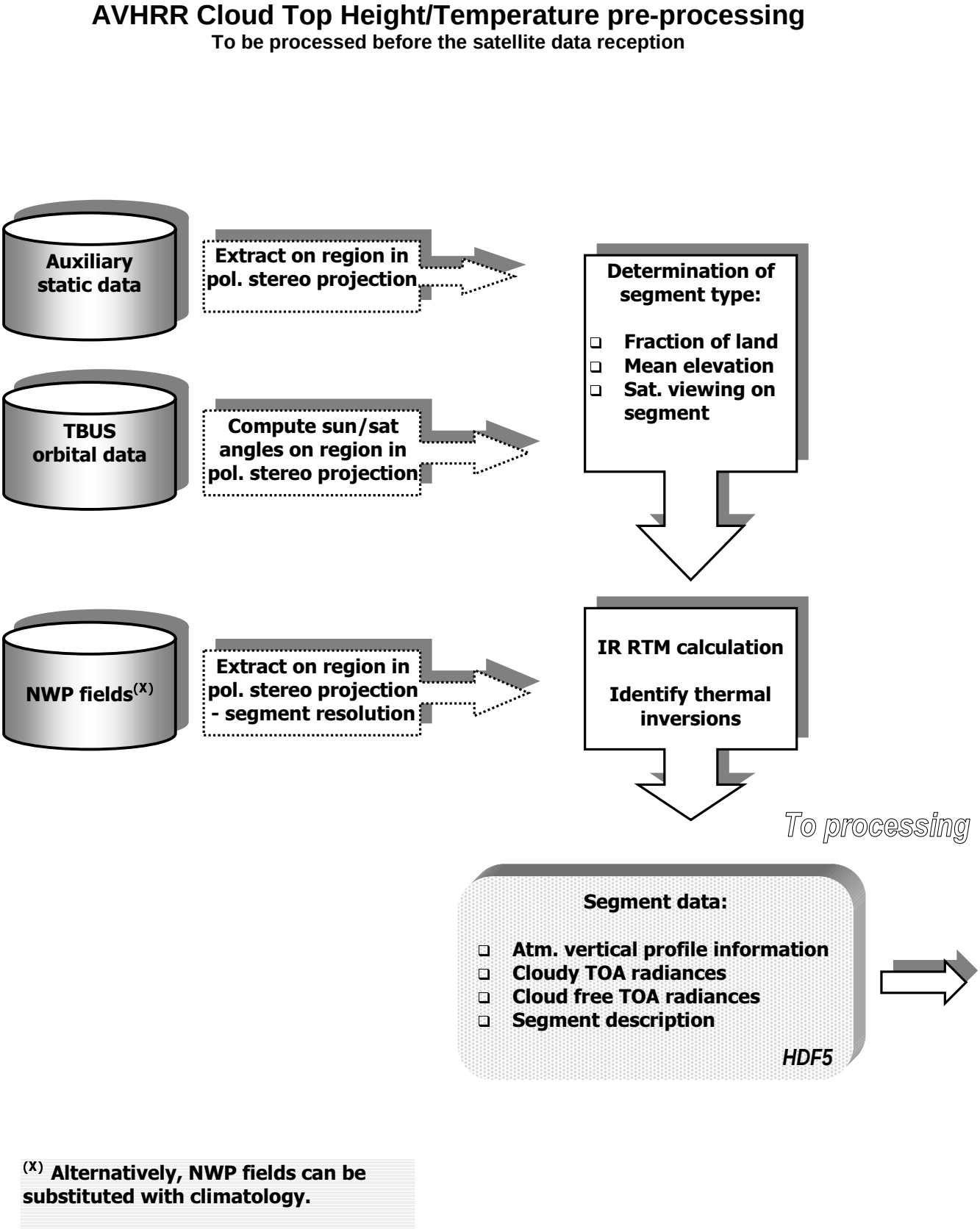

Figure 5-1: AVHRR Cloud Top Temperature and Height pre-processing

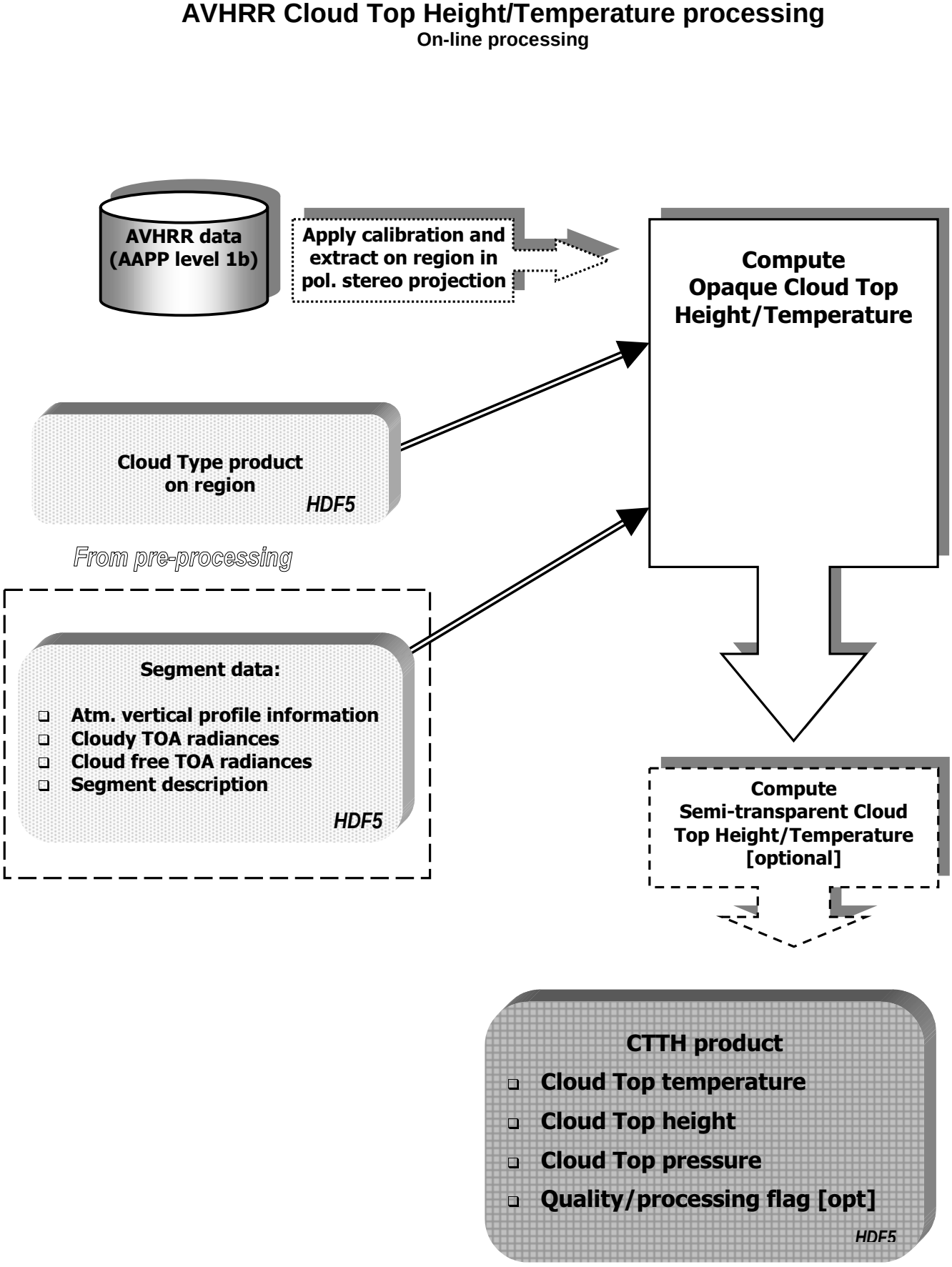

Figure 5-2: AVHRR Cloud Top Temperature and Height On-line processing.

5.2.2 Results from prototyping and validation

Since prototyping still is in an early coding phase no product results or comparisons with observations can be shown in this report.

5.2.3 The use of NWP data and their impact on quality

The CTTH takes as input the Cloud Type, and as such it depends indirectly on the parameters already discussed in section 3.2.5 and 4.2.4. More directly the algorithm use the vertical profile of temperature and humidity given by 20 pressure levels plus the surface given by the NWP model. This profile data is at first used to derive cloudy and cloudfree IR radiances, the cloudfree radiances used only for the semi-transparent retrieval.

5.2.3.1 Impact on product quality of errors in the NWP output

For the retrieval on opaque clouds errors in the resolution of the temperature profile at cloud level will be the main cause for errors in the CTTH output. The temperature and humidity profiles are used as input to the RTM simulations in order to correct for atmospheric absorption above the cloud, but since the abundance of water vapour is found beneath the cloud layer any errors in the profile above will normally only have marginal negative impact. The t11 is close to the physical cloud top temperature. Thus for opaque cloudiness the errors will mainly be in the height and pressure estimates.

For the CTTH retrieval in semi-transparent cloudiness the simulated cloudfree radiances become crucial and for reasons already given in section 3.2.5 the surface temperature is very important here. Thus the surface temperature is among the most critical NWP parameters for giving accurate retrievals. Other than the surface temperature it is important to have a correct description of the temperature and humidity in the lowest part of the atmosphere.

In addition the CTTH retrieval, especially in semi-transparent and fractional cloudiness, is particularly vulnerable to any errors in the Cloud Type (may be stemming from errors in the Cloud Mask) which might be caused by errors in the NWP model (as discussed in section 4.2.4.).

5.2.3.2 Dependency on NWP model

See section 3.2.5.

5.3 Practical application

5.3.1 Implementation

The coding of the core CTTH scheme is done using the C language. In the pre-operational implementation Python will be used as the glue for grabbing the right NWP model output, extracting the physiography data, and in the production of derived image outputs.

As the algorithm implementation is not ready yet, no exact details on processing requirements are given here. The most demanding tasks will be done in the pre-processing stage, where RTM simulations are carried out on a reduced AVHRR resolution (the segments – segment size to be configured by the user). In the on-line processing the algorithm for opaque

cloudiness is basically a task of making table look-ups, and therefore expected to require very litlle CPU time.

5.3.2 Product demonstration

This product was not included in the SAFNWC Demonstration experiment. The plan is to demonstrate product examples from the present CTTH prototype version at the SMHI SAF web site (at address http://www.smhi.se/saf/) during MTR.

At this stage, it is possible to illustrate how an image output from the CTTH product will appear when based on the input from previously processed CMa and CTy products. We have used the same case as previously shown in sections 3.3 and 4.4.

5.4 Remaining work

The prototype algorithm for opaque clouds will be implemented during spring 2000.

As already mentioned in section 5.1.2, the retrieval of the cloud top temperature and height for semi-transparent clouds, is not a simple task. The window-technique (Inoue, 1985) was suggested, as it is the only established approach using AVHRR data only. However, no semi-transparency correction scheme has been developed for the CTTH product, and no such scheme can be guaranteed, before the end of the project. There are several reasons and explanations for this:

- As the main use of the CTTH product, according to user requirements (**UR-7.3.1** in URD) is in the analysis and early of thunderstorm development, the algorithm for opaque clouds has naturally been given highest priority.
- Despite the finding of Inoue (1985) it is well known that the method is questionable when applied in reality, where multi layer and fractional/sub-pixel cloudiness are rather the rule than the exception. In addition the performance has shown serious problems in general and also when comparing with methods using sounding channels (see e.g., Putsay et al., 1999).

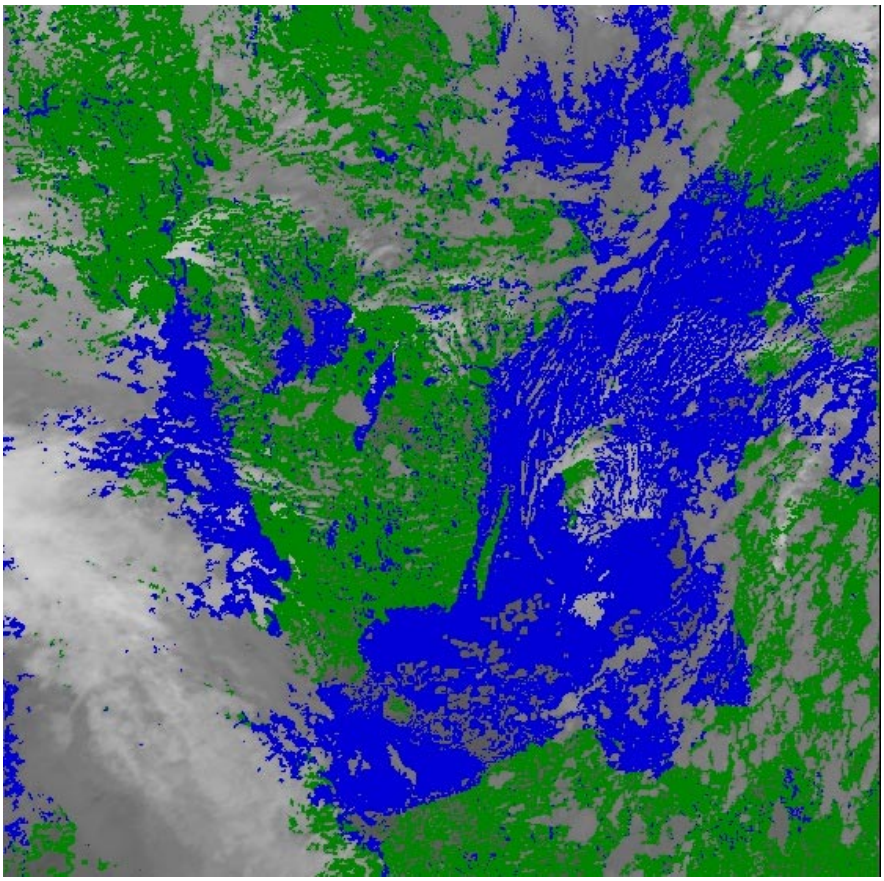

Figure 5-3. Demonstration of the CTTH product. Cloud top temperatures are given for the opaque clouds in grey shades, September 29, 1999 at 12:45 UTC, NOAA-14.

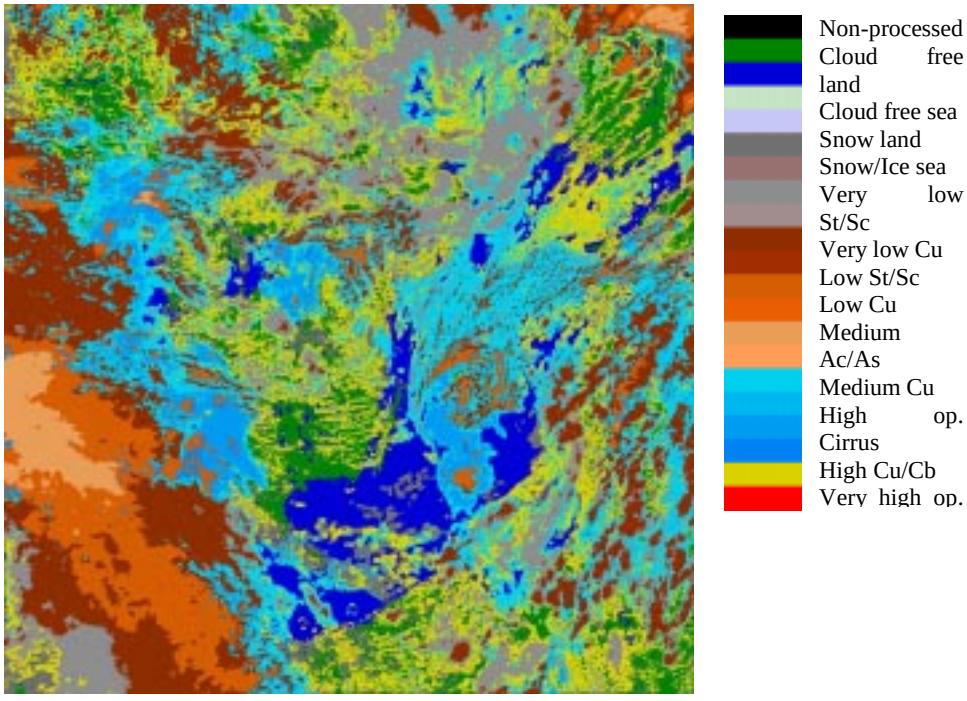

Figure 5-4. Cloud Type product example from the same occasion as above (Figure 5-3). Copy from Figure 4-4

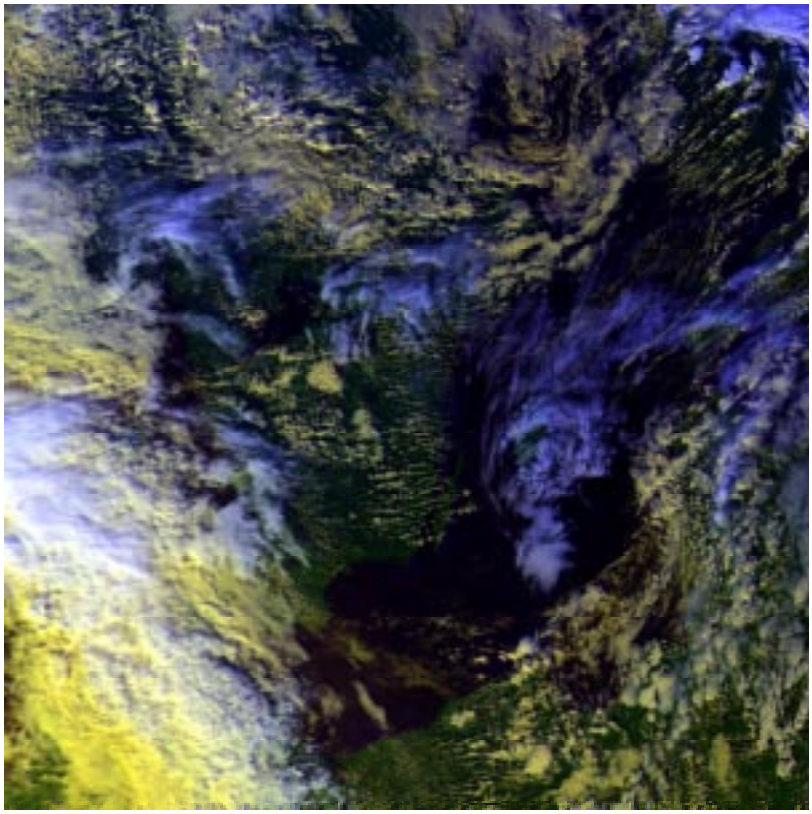

Figure 5-5. RGB image (channel 1,2 and 4) from the same occasion as above (Figure 5-3). Copy from Figure 3.14.

Therefore, concerning this remaining development for the semi-transparent correction, the strategy is to put a limited effort of three man months between June and October 2000 to try to develop and implement the window-technique. The validation will naturally be limited to a few case studies and make use of radiosoundings. The conclusions from the validation will show whether reasonable quality requirements are met, and decision whether or not to incorporate this scheme in the final CTTH product will be done.

6 Prototyping the SEVIRI Precipitating Clouds product – PC-1

6.1 Overview

6.1.1 Objectives

The Precipitating Clouds product provides information within every satellite pixel on the presence of precipitation and, in addition, indicates precipitation intensities, although only in very general terms.

The estimates will be given in precipitation likelihood in three different intensity classes. When considering IR/VIS channels, only strongly convective features have distinct spectral signatures. In mid – and northern latitudes a large fraction of the precipitation falls from stratiform clouds, were the coupling between brightness temperature and precipitation rate is not strong. For those stratiform cases it is not always straightforward to delineate precipitating from possibly precipitating areas and the spatial extend of precipitation is typically overestimated by VIS/IR methods. It is however possible to identify many cloudy areas with very low precipitation likelihood. The statistical scheme was developed and tuned using Weather Radar data composites as the precipitation ground truth. During the development phase the only radar data available was data of the BALTRAD Weather Radar network. This data has been regularly archived since April 1999. Since no GOES data with coincident radar data was available, prototyping was performed solely using AVHRR data.

Original plans to complement the spectral information from satellite channels with large scale forcing parameters from NWP models, have been dropped due to severe criticism from the user community at the SAF Nowcasting Workshop in Madrid, December 1998. The criticism was reflected in UR-7.4.2.1.6. The only NWP parameter now entering the PC module is the forecasted surface temperature.

The Precipitating Clouds product will provide information within every satellite FOV on the presence of precipitation and, in addition, indicate precipitation intensities, although only in very general terms, giving separate probabilities for intensive and weak to moderate precipitation.

6.1.2 Background

A precipitation product based on AVHRR data has been available at SMHI for several years as one output from the SCANDIA cloud classification scheme. It consists of a different colour coding of the cloud type output, delineating possibly precipitating cloud classes from non-precipitating clouds. Development and archiving of BALTRAD radar composites made it recently possible to refine the methodology and put it on a statistically more solid basis, even on pixel resolution. With these verification tools it was possible to also investigate the coupling of microphysical parameters (effective radius and pure spectral features indicating the microphysical state of a cloud top) to precipitation.

6.1.3 SAFNWC Product requirements

A condensed description of requirements and development plans for the SAFNWC Precipitating Cloud-1 product is given in the following sub-sections referring to the SAFNWC SP (section 3.1) and the descriptions and corresponding user requirements in the SAFNWC URD. The description of the actual product is given in section 6.1.3.8.

6.1.3.1 Source

- The PC product shall be derived using the window channels VIS 0.6, VIS0.8, NIR1.6, IR3.9, IR10.8, IR12.0. The use of the channels IR8.7, WV6.2 and WV7.3 is [TBC]. (UR-7.4.2.1.1)

6.1.3.2 Chosen method

Statistical scheme making use of IR/VIS spectral features and forcing parameters derived from NWP data (SP, section 2.2.1.2.2).

6.1.3.3 Product content and format

- The PC product shall consist of a numerical value for the precipitation probability for the pixels identified as cloudy by the CMa and CTy products within three precipitation intensity classes: no precipitation (R<0.1 mm/h), light precipitation and heavy precipitation. The threshold value for separating light from heavy precipitation is [TBD]. **UR-7.4.2.1.2**
- The following probability classes shall be used: 0-10%, 10-20%, 20-40%, 40-60%, 60-80% and >80% [TBC]. (**UR-7.4.2.1.5**)
- The format of the PC product is [TBD]. (**UR-7.4.2.2.3**)
- The PC product shall be extracted in satellite projection. (**UR-7.4.2.1.3**)

6.1.3.4 Quality control

- No separate quality flag shall be included in the PC product. Provision of the probability of precipitation in each of the intensity classes will give an indication of the uncertainty of the estimate. (**UR-7.4.4.1**)
- The PC product shall be routinely verified by comparison with radar measurements from local radar networks. (**UR-7.4.4.2**)

6.1.3.5 Coverage and resolution

Coverage defined by the SEVIRI North format, covering most of Europe and adjacent oceanic areas. The product will be extracted in full SEVIRI pixel resolution using the satellite projection.

6.1.3.6 Time constraints

- It shall be possible to extract the PC product every 15 minutes. (**UR-7.4.2.1.7**)

6.1.3.7 Internal product dependency

The SEVIRI PC product must have access to the SEVIRI CTy and CTTH products.

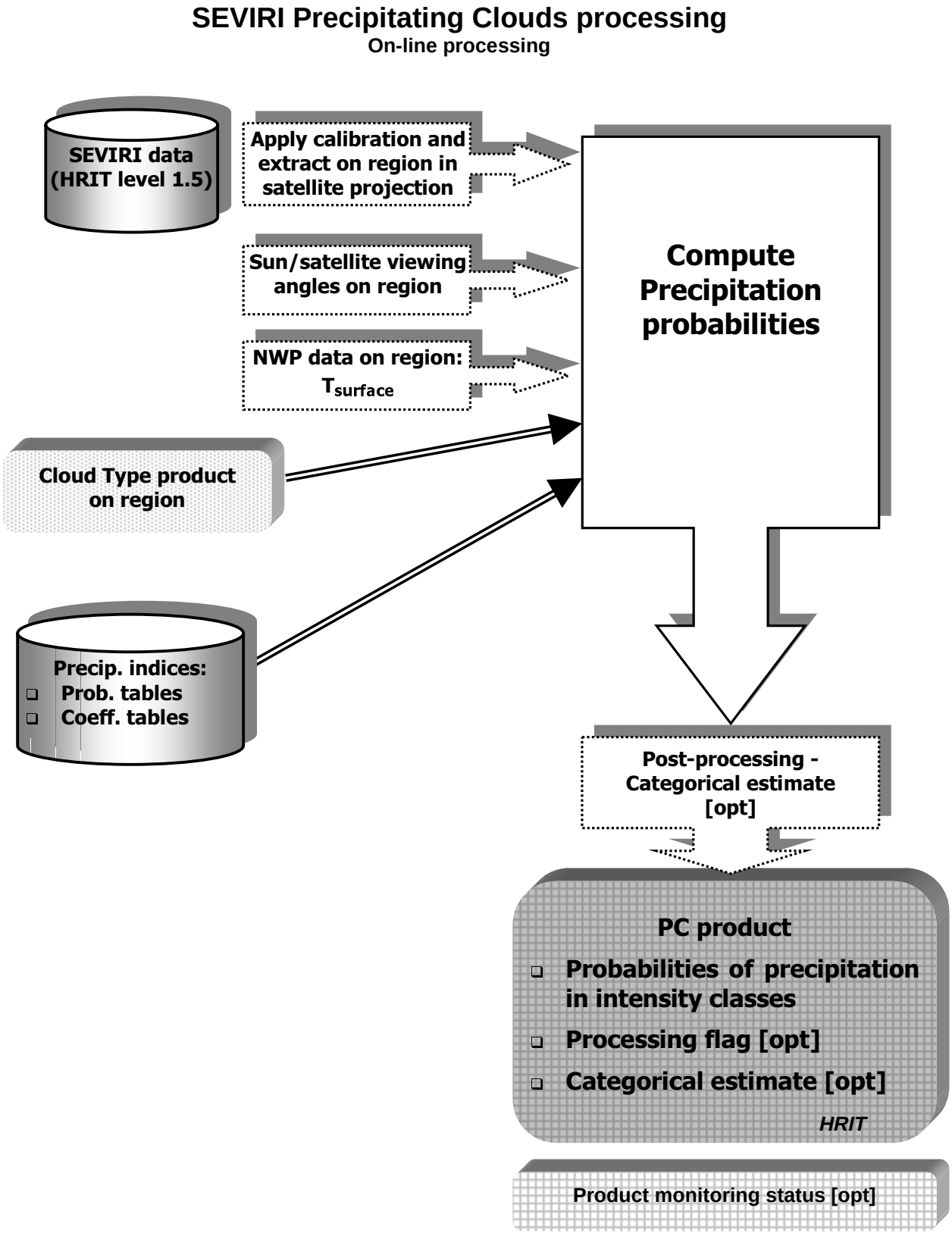

Figure 6-1: SEVIRI Precipitating Clouds On-line processing

6.1.3.8 Auxiliary and ancillary data

- The dependence of the PC product on so called forcing parameters derived from NWP data shall be minimal, i.e. the forcing parameters shall not dominate the final PC product. (**UR-7.4.2.1.6)**

6.1.4 Prototype description

A summary of the Precipitating Clouds product in its present prototype stage is described in the following sub-sections. The same sub-division as in section 6.1.3 is used. If there are no deviations from the prescribed product definitions or any additional information on the product, only a reference to the corresponding sub-section in 6.1.3 is given.

More details on the developed product are given later in section 6.2. An overview of the data flow is given Figure 6-1.

6.1.4.1 Source

Input to the PC module are the following SEVIRI spectral channels: 0.6μm, (1.6μm), 3.8μm, 11μm, 12μm. The mandatory channels for the current version of the PC product are : 0.6μm, 3.8μm, 11μm and 12μm.

The 0.8μm channel is not used since it is highly correlated with the 0.6μm channel in cloudy areas and does not seem to contribute additional information on precipitation.

The usefulness of further IR channels of SEVIRI, including 8.7μm and the WV channels could not be investigated, since we did not have access to collocated GOES and Radar data.

The current prototype does also not yet make use of the 1.6μm channel, since we did not have a large enough data sample of collocated radar and 1.6μm data to derive meaningful statistical estimates. Case studies from a special period in April 1999 suggest however, that the 1.6μm channel can be used in a very similar way as the reflectivity derived from 3.8μm data.

6.1.4.2 Chosen method

A statistical scheme making use of both IR and VIS features is employed. In contrast to original plans outlined in the science plan, any dependence on large scale forcing parameters from NWP data is not incorporated. Despite believing that such information could considerably enhance the performance of the product, it would be difficult to assure that the product would not be dominated by NWP information.

A precipitation index combining information from selected channels (depending on illumination conditions) is constructed and precipitation likelihood is assigned according to collocations with radar data from a large reference data set.

6.1.4.3 Product content and format

The PC product output consist of a numerical value for the likelihood of precipitation within the following three precipitation intensity classes:

Table 6-1: Intensity thresholds for SEVIRI precipitation classes

Class	Type of precipitation	Minimum rain rate, mm/h	Maximum rain rate, mm/h
0	No precipitation	0.0	0.1
1	Light/moderate precipitation	>0.1	5.0
2	Intensive precipitation	>5.0	∞

Results from prototyping suggest to chose a finer resolution of probability classes than given in the user requirements. Because the precipitating area is generally overestimated by IR/VIS methods, high precipitation probabilities are seldom reached. About half of the precipitation events of the VIS/IR algorithm are in areas which are assigned a precipitation likelihood between 5%-25%. We have therefore chosen to use a finer grading of probability intervals:

Table 6-2: Probability intervals

100-95% assigned to	100%
>95-85% assigned to	90%
>85-75% assigned to	80%
>75-65% assigned to	70%
>65-55% assigned to	60%
>55-45% assigned to	50%
>45-35% assigned to	40%
>35-25% assigned to	30%
>25-15% assigned to	20%
>15- 5% assigned to	10%
> 5- 0% assigned to	0%

6.1.4.4 Quality control

Even though there is no quality flag as such since the quality is given implicitly in the probability estimates, the generation of the product depends on availability and quality of the input components. A processing flag similar to the processing flag of the CT product is given in Table 6-3. It describes the quality of the input and the processing performed for each pixel.

Table 6-3: PC (SEVIRI) processing flag

Bit #	Meaning of the bit – 1/0
0	Processed/non-processed
1	AVHRR channels missing/not missing
2	CT used/not used
3	AVHRR solar channels used/not used
4	AVHRR land/no land
5	High terrain/no high terrain
6	NWP data missing/not missing
7	AVHRR cloudtype low quality/no low quality

6.1.4.5 Coverage and resolution

As specified in 6.1.3.5.

6.1.4.6 Time constraints

As specified in 6.1.3.6. See section 6.3.1.

6.1.4.7 Internal product dependency

The PC product depends on availability of the CT product only (no dependence on CTT/H).

6.1.4.8 Auxiliary data used are:

- NWP surface temperature
- Sun and satellite angles
- Coefficient tables for the calculation of a Precipitation index (static)
- Probability tables relating the precipitation index to probability (static)

6.2 Detailed algorithm description

6.2.1 Algorithm outline

The PC retrieval builds on the CT product. Pixels belonging to classes for which an a priory likelihood of precipitation of less than 5% can be assumed, are set to 100% likelihood for no precipitation. The association of cloud types with an a priori precipitation estimate is given in section 6.4. For pixels where the cloud type is indicating possible precipitation, a Precipitation Index (PI) is calculated, which simultaneously takes into account those spectral features which show the highest correlation with precipitation as measured by radar. The development leading to the current formulation of the algorithm is summarised in section6.2.2. The daytime algorithm is of the form:

$$PI_{day} = a(T_{surf}) - T11 + b * \ln(R0.6/R3.8) \qquad (6.1)$$

where PI is the precipitation index, T_{surf} is the NWP surface temperature, T11 is the 11μm brightness temperature, R0.6 and R3.8 solar reflectances of the 0.6μm and 3.8μm channel respectively. The derivation of the channel 3.8μm reflectance with help of the 11μm brightness temperature for removal of the thermal component is given in Appendix 9. The coefficients *a* and *b* are derived by tuning the performance of the PI to radar precipitation estimates. The coefficient a represents the surface temperature minus a temperature dependent offset. In the current version of the prototype the coefficient a is a constant set to 280K.

The night-time algorithm can not make use of information from visible channels relating to the microphysics of the cloud. The only improvement possible here compared to taking into account the 11μm channel brightness temperature only, is to correct for semitransparency to a certain extent:

$$PI_{night} = a(T_{surf}) - T11 + b * (T11 - T12) \qquad (6.2)$$

where T12 is the 12μm channel brightness temperature.

Table 6-4: A priori association of cloud classes with precipitation (for some of the associations it seems necessary to confirm by collocation with radar data that the precipitation likelihood is below 5%).

Cloud class	Considered as possibly precipitating
1: Cloud free land	No
2: Cloud free sea	No
3: Snow contaminated land	No
4: Snow or ice contaminated sea	No
5: Very low cloud – stratiform	No
6: Very low cloud– cumuliform	No
7: Low cloud – stratiform	No (to be checked)
8: Low cloud – cumuliform	No (to be checked)
9: Medium level cloud – stratiform	Yes
10: Medium level cloud – cumuliform	Yes
11: High opaque cloud – stratiform	Yes
12: High opaque cloud – cumuliform	Yes
13: Very high opaque cloud – stratiform	Yes
14: Very high opaque cloud - cumuliform	Yes
15: Very thin cirrus	No
16: Thin cirrus	No (to be checked)
17: Thick cirrus	YES
18: Cirrus superimposed on low /medium cloud	YES
19: Fractional clouds	No
20: Unclassified	No

The probability value of precipitation in the classes specified in Table 6-2 is then taken from lookup tables relating the PI to radar derived precipitation rates (see section 6.2.2 for further details).

The probability tables were created by deriving histograms of the distribution of the Precipitation Index. From the histograms we derived the likelihood for which a given PI belongs to a certain precipitation class under the constraint that for each PI the total probability has to be 100%.

6.2.2 Derivation and tuning of the precipitation index

When employing methods to derive precipitation from VIS/IR for nowcasting applications, one is faced with the difficulty that there is no direct coupling between the physical process causing precipitation and the remotely sensed parameters at the cloud top. For deep convection such coupling exists to a certain extend, as is used for example in the GPI (Arkin, 1979) for climatological studies. Even in the case of deep convection the area of precipitation is often overestimated since thick cirrus shields associated with the convective system show very similar spectral features as the active part of the convection. When not considering the lifetime cycle of the convective cell, this poses an enhanced uncertainty in nowcasting applications.

The problem is even enhanced when trying to determine the area extend of stratiform rain. The microphysical state of a cloud top can to a certain extend be correlated with rain, since a certain minimum particle radius must be present in order to provide nuclei for precipitation.

Encouraged by work of Rosenfield and Gutman (1994) as well as Ba and Gruber (1997), we spend considerable resources in developing an effective radius retrieval. An additional reason for trying to describe the microphysical state by a derived quantity was to eliminate any dependence from viewing geometry and illumination. The retrieval is based on a set of radiative transfer calculations for about 1000 clouds composed of spherical water and/or ice droplets using the adding and doubling model MOMO (Fischer and Grassl, 1991). We developed a retrieval algorithm for the effective radius by inverting the radiative transfer calculations using a neural backpropagation network. Best results were achieved when training the network on R0.6/R3.7, R0.6 and the full viewing geometry. The effective radius retrieval is described in more detail in Appendix 10.

Having the effective radius available, we had to conclude however, that the R0.6/R3.8 feature itself performed slightly superior as indicator of microphysical state (further details given in sections 6.2.2.2 and 6.2.2.3). Constraints with respect to development time prohibited further investigations into the causes of this unexpected result. One possible cause to be investigated would be that the model clouds assumed in the investigations might not be representative of the size/phase distributions of the investigated dataset. Another possible cause might be that a closer coupling between effective radius and precipitation might only exist for certain cloud types, which might not have been predominant in the investigated dataset. Candidate cloud types for a closer coupling would be warm stratus as well as strong convection. It might thus be beneficial to go into more detail and investigate the relationship between retrieved effective radius and precipitation for different cloud types and cloud top temperatures. On the other hand the calculation of the effective radius for a large number of pixels is rather time consuming (a neural net with 5 input nodes and 10 nodes in a hidden layer had to be chosen to arrive at good results). By directly using the R0.6/R3.8 feature we can also safely meet operational time constraints for SEVIRI processing, which might not have been the case when having to compute the effective radius.

As a first guess for the precipitation retrieval, we tested deriving precipitation probabilities for the 11μm brightness temperature. A first refinement was to derive different probability tables for the 11μm brightness temperature depending on thresholds set for other spectral features. After that a number of indices were tested and tuned which combined information from different image features in an additive way.

6.2.2.1 Development environment and data sets

The correlation of radar rain rates to VIS/IR spectral features varies greatly from case to case. Thus a large data set has to be input to any stable statistical algorithm. Since 10 March 1999, we are archiving AVHRR overpaths of NOAA15 processed by AAPP. Since 1 April 1999 BALTRAD radar composites are being archived, which cover most of Scandinavia including Denmark and a few sites in northern Germany. BALTRAD images are archived every 15 minutes, so the maximum time difference to a satellite overpath is 7.5 minutes. More details on the BALTRAD composites are given in Appendix 7. For the development, a subset of the archived data was retrieved from the period April to September 1999. The subset covers 110 overpaths for which the radar report precipitation and for which at least for parts of the scene the sun stands more than 10 degrees above the horizon. To be able to manage the data amount while retaining a representative sampling of different cases, the AVHRR images were processed in reduced resolution taking into account only every fifth pixel in every fifth row.

The resulting data set contains slightly over 2.2 million collocated pixels, of which about 300000 contained precipitation echoes.

The PC product had to be developed in parallel to the CT product. This made a few simplifications in the development of the current prototype algorithm necessary, which we hope to be able to adjust for before the end of year 2000 (see section 6.5). The prototypes for the other cloud products have not yet been adjusted to run from AAPP output. For this reason and because of time constraints, it was not possible yet to run input cloud products on the validation data set. This made it necessary to perform the assessment of spectral features on a very coarse ad hoc cloudmask instead of the real cloud type product. A pixel was assigned to be cloudy if the 11μm brightness temperature was lower than the 280K and the 0.6μm reflectivity was greater than 10%. For the purpose of the PC product the most severe defect caused by this very rough classification were misclassifications of snow covered mountain areas in spring as possibly precipitating clouds.

6.2.2.2 Correlation of spectral features with precipitation

For a first assessment of candidate input features to the algorithm, correlations between radar echoes and spectral features were investigated. The overall strength of correlations varies considerably from case to case, as does the performance of individual features. For the worst case the correlation of radar reflectivity and PI was around 0.1, whereas for several good cases a correlation of more than 0.6 was reached. In Table 6-5 the mean correlation over cases is given.

*Table 6-5: Mean correlation of features to radar reflectivity factors and to rain rate. T denotes brightness temperature, R denotes reflectance and PI the precipitation indices for day respective night conditions: PI_{day}=280–T11+10*ln(R0.6/R3.8); PI_{day}=280–T11+5*(T11-T12)*

Feature	Mean correlation - To dbz	Mean Correlation - To rain rate
R0.6	0.22	0.12
R0.8	0.22	0.13
T3.8	-0.33	-0.16
T11	-0.37	-0.19
T3.8-T11	0.02	0.03
R3.8	-0.10	-0.10
Effective radius	0.29	0.14
R0.6/R3.8	0.33	0.16
PI-day	0.40	0.20
PI-night	0.35	0.18

6.2.2.3 Selection of features and tuning

Based on results of Table 6-5, the most promising features were further investigated for algorithm development. The lower panel of Figure 6-2 shows histograms of the 280-T11 feature for different precipitation intensity classes as provided by radar. Estimates are valid for cloudy areas (cloudy if T11 < 280 and R0.6μm > 10%). The upper panel gives the respective probability of the precipitation classes. Figure 6-3 and Figure 6-4 give the same information for the effective radius and a feature related to R0.6/R3.8. As can be expected for the effective radius, the histograms for classes containing precipitation peak for large values

of the effective radius. Non precipitating cases show unfortunately no dependence on the effective radius, which puts limits to the usefulness of this feature for precipitation retrieval.

Features related to R0.6/R3.8 show histogram peaks for raining classes at larger values, when R3.8 is comparatively low due to the presence of large and/or frozen particles. The non-precipitating class is peaking at lower values, but there is however a considerable overlap.

For single features the 280-T11 feature shows clearly the best performance. We investigated whether thresholding the T11 feature with features related to microphysics would improve the discrimination of precipitation. For the effective radius we applied a threshold of 22 to separate the data set into two distributions, for R0.6/R3.8 we chose 7.4 as a separator (corresponds to a feature value of 20 in Figure 6-4). We then calculated the precipitation likelihood using the 280-T11 feature for each subset. Overall the performance increased slightly when applying the thresholding on microphysical constraints. There was no clear advantage of thresholding using the effective radius over using the R0.6/R3.8 feature. We thus decided to drop the effective radius from further development, also taking into account computing time constraints. The performance of incorporating the R0.6/R3.8 feature can be improved when using an additive way of combining it with temperature information. Best results were achieved for applying a logarithm on R0.6/R3.8 to account for its steep histogram with long tails. Multiplication with 10 yielded best results, although the sensitivity to scaling factor was minor.

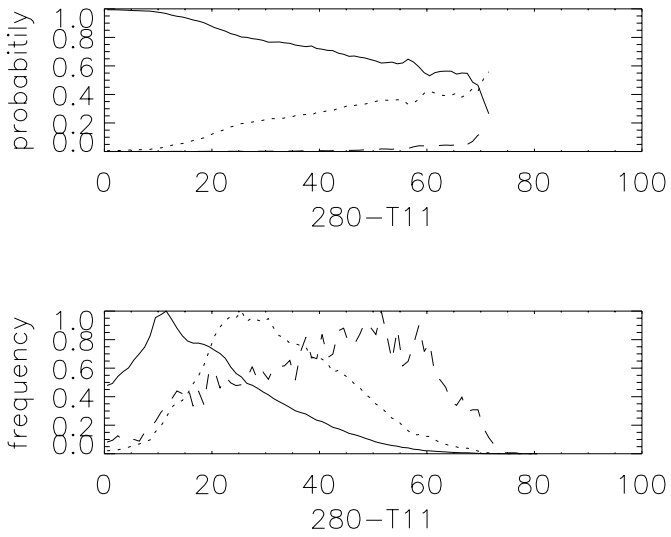

Figure 6-2: 280-T11μm feature. Lower panel: normalised histogram for different precipitation classes (solid line: no precipitation, dotted: light to moderate precipitation, dashed: heavy precipitation. Upper panel: same as above but for probability.

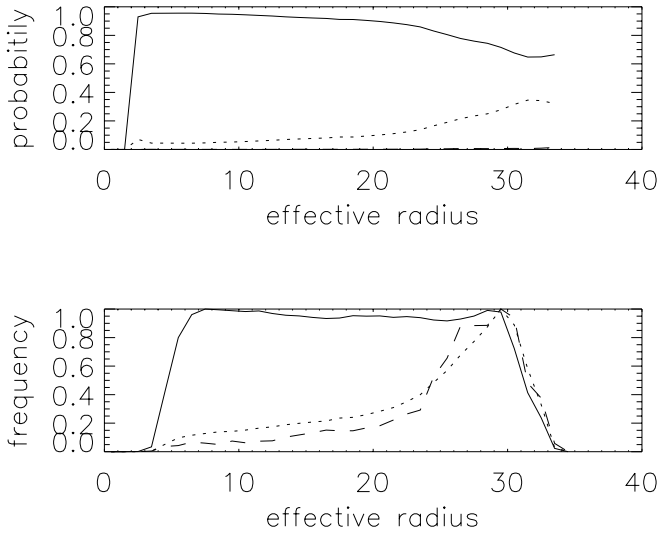

Figure 6-3: Same as Figure 6-2, but for the effective radius feature.

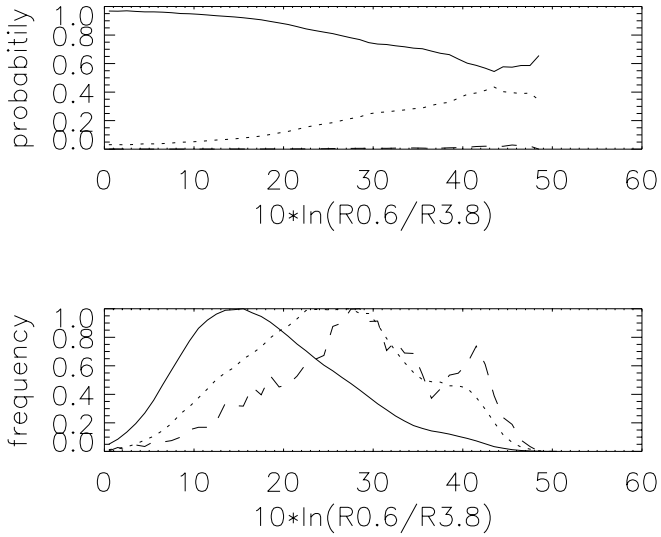

*Figure 6-4: Same as Figure 6-2, but for the feature 10*ln(R0.6μm/R3.8μm). Applying logarithm and scaling results in an approximate overlapping of histogram maxima with the maxima of the 280-T11μm feature.*

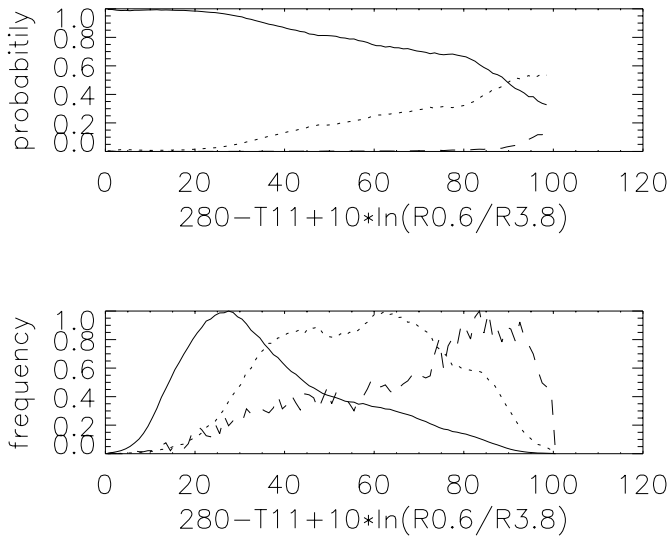

*Figure 6-5: Same as Figure 6-2, but for PI_{day}=280-T11+ 10*ln(R0.6μm/R3.8μm).*

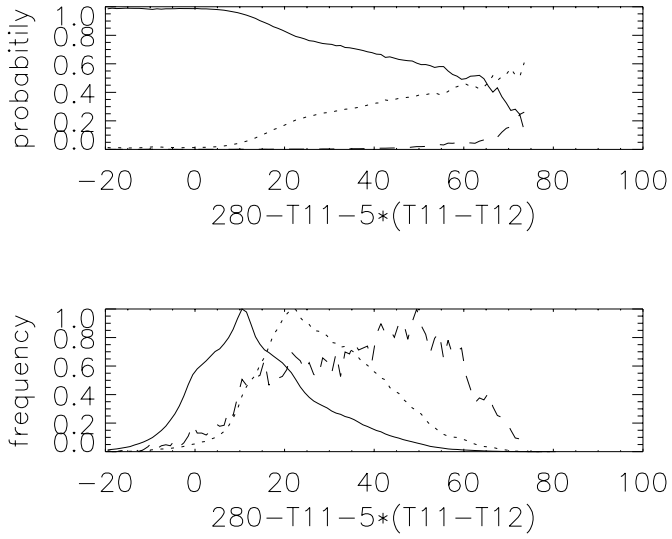

Figure 6-6: Same as Figure 6-2, but for PI_{night}=280-T11-5(T11-T12).*

The performance of different precipitation indices can be evaluated in Table 6-6. It gives the cumulative frequencies of rain and no rain indicated by radar in different classes of intensity. Only the best performing candidate for each combination of features is displayed. In general, a better description of higher precipitation probabilities seems to cause slightly more rain cases to be classified as not raining.

To improve the detection of precipitation at night-time when no solar channels are available, the usefulness of the T11-T12 feature was investigated. The idea was that the precipitation likelihood should be smaller for semitransparent clouds. For some cases this feature shows a week negative correlation to precipitation, even though this correlation does not show up when considering the whole data set. As compared to the use of the T11 feature only, more

cases are assigned to higher precipitation likelihood when incorporating the T11-T12 feature. On the other hand the definition of the no precipitation class degrades. For the time being we would suggest to use the T11-T12 feature at night time, but if the likelihood tables were specified separately for different cloud classes, this might be subject to discussion again.

A marked improvement of the accuracy of the method is to be expected if the probability distributions were derived for different groups of cloud types and were made dependent on the ground temperature (proxy for the atmospheric conditions) as well. Due to time constraints and parallel development of PC and CT product, this could not yet be attempted.

Table 6-6: Cumulative frequency of the occurrence of rain and no rain for different thresholds of rain probability. Note that the probabilities are derived on pixel level.

Cumulative frequencies ↘	280 – T11		280–T11; threshold reff <> 22		280 - T11 +10*ln(R0.6/R3.8)		280 – T11 –5*(T11-T12)	
Probability of rain	Rain	No rain	Rain	No rain	Rain	No rain	Rain	No rain
<5%	4.6%	36.4%	5.8%	41.3%	5.5%	38.6%	6.9%	43.9%
<15%	21.9%	63.2%	21.6%	63.8%	24.9%	66.5%	21.1%	65.0%
<25%	60.7%	86.5%	57.2%	84.8%	53.6%	84.7%	51.2%	83.7%
<35%	88.9%	97.3%	87.0%	96.0%	88.0%	97.7%	82.8%	95.8%
<45%	99.6%	99.9%	97.5%	99.6%	93.6%	99.1%	97.4%	99.5%

6.2.3 The use of NWP data and their impact on quality

The PC makes use of the surface temperature. It is used in the calculation of the precipitation index PI, mainly to account for seasonal differences in relating the 11μm brightness temperature to precipitation likelihood

6.2.3.1 Impact on product quality of errors in the NWP output

The PC product is building on the CTy product. Since possibly precipitating clouds exhibit destinct spectral features, they will be identified by the CTy product irrespective on how NWP data is used in the creation of the CMa and CTy products. The main influence of NWP data quality will thus be directly through errors in the forecasted surface temperature. However, the PI varies only smoothly with surface temperature, so that likelihood shifts due to model errors are only expected between adjacent likelihood classes and often will have no effect at all.

6.2.3.2 Dependency on NWP model

The variation of PI with surface temperature goes rather smoothly, thus eventual model biases will only have a minor effect on resulting likelihood. Otherwise the discussion in section 3.2.5 also applies to the PC product.

6.3 Practical application

6.3.1 Implementation

The code is written in the C language. A performance test was done on the same hardware as specified in section 3.3.1. The following set-up was used:

- Processing of a 1024*1024 pixel region.
- Incorporation of NWP surface temperature and CT product.

Processing required 39MB memory and 21.3 seconds at a CPU utilisation level of 42%.

6.3.2 Product demonstration

The following cases were processed using the development database software and not the prototype described above. The prototype described above only became available recently and has not been adapted yet to ingest AAPP output. For the current input data available (winter cases) the development data set used for tuning proved not to be representative.

The three cases below are typical examples of the algorithm performance. In Figure 6.7 an example of a fairly good algorithm performance is given. Despite overestimating the northward extend of both the precipitation areas over northern Scandinavia and over Denmark/southern Sweden, there is otherwise reasonable good agreement in location and extent of the precipitating area between the radar and satellite products. Note that the areas of highest precipitation intensity as given by radar do not necessarily correspond to the areas of highest derived precipitation likelihood from VIS/IR. This can be explained by the relative insensitivity of the precipitation index to rain rate for light to moderate precipitation since no direct physical coupling of cloud top properties and rain rate exists.

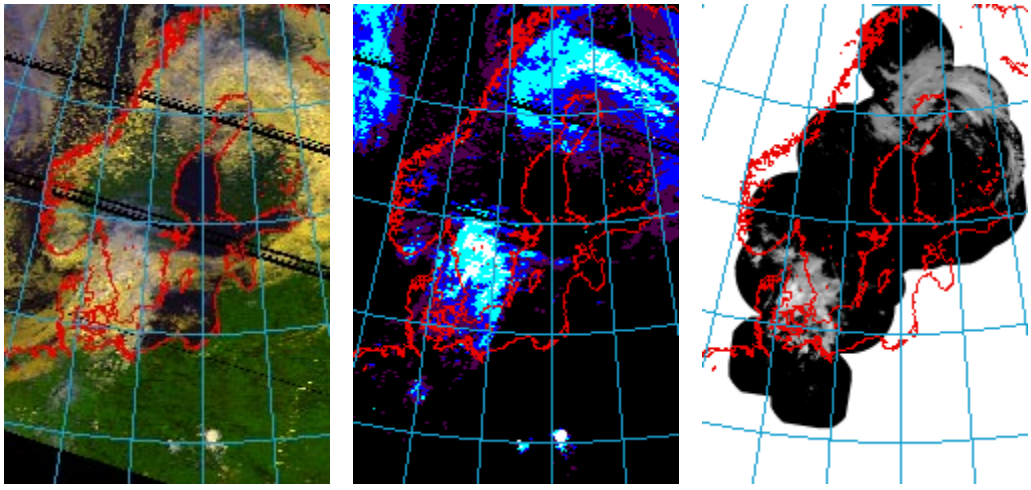

Figure 6-7: AVHRR NOAA15 overpath 30 May 1999, 07:02UTC.Left AVHRR RGB composite (0.6μm,0.9μm,11μm) Middle: total precipitation probability for day time algorithm (magenta 10%, dark blue 20%, cyan 30%, white40% and above). Right: BALTRAD radar composite for 7:00UTC.

More isolated precipitation events are represented in Figure 6-8. General features are well captured, but again the area extend is overestimated. Figure 6-9 is a bad example and clearly demonstrates the limits of the methodology of just using VIS/IR information to estimate precipitation. The area extend of the frontal precipitation is largely overestimated, and the highest retrieved likelihood values are actually found behind the frontal precipitation. This case was one of few example cases were the night-time algorithm employing semi-transparency correction with the T11-T12 feature performed slightly superior to the day time algorithm.

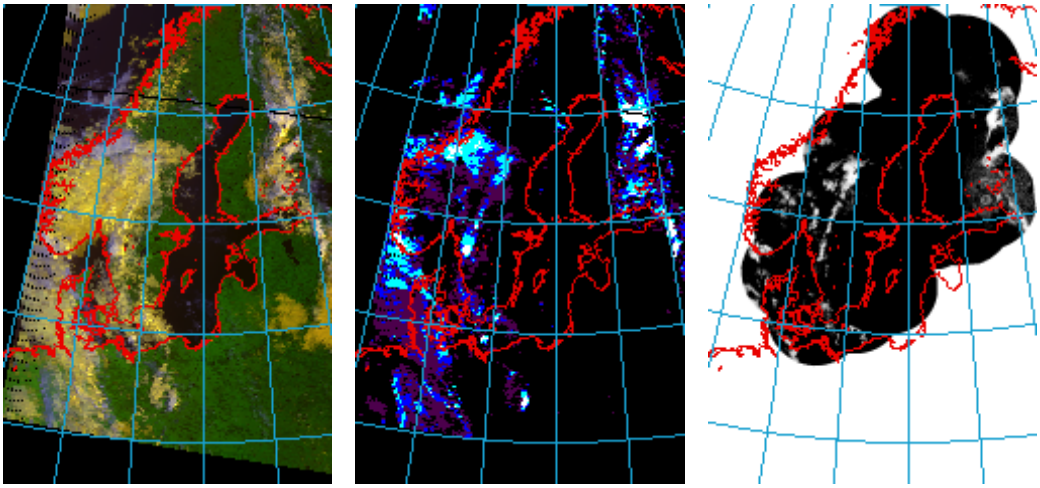

Figure 6-8: AVHRR NOAA15 overpath 28 June 1999, 06:21UTC.Left AVHRR RGB composite (0.6μm,0.9μm,11μm) Middle: total precipitation probability for day time algorithm (magenta 10%, dark blue 20%, cyan 30%, white40% and above). Right: BALTRAD radar composite for 6:15UTC.

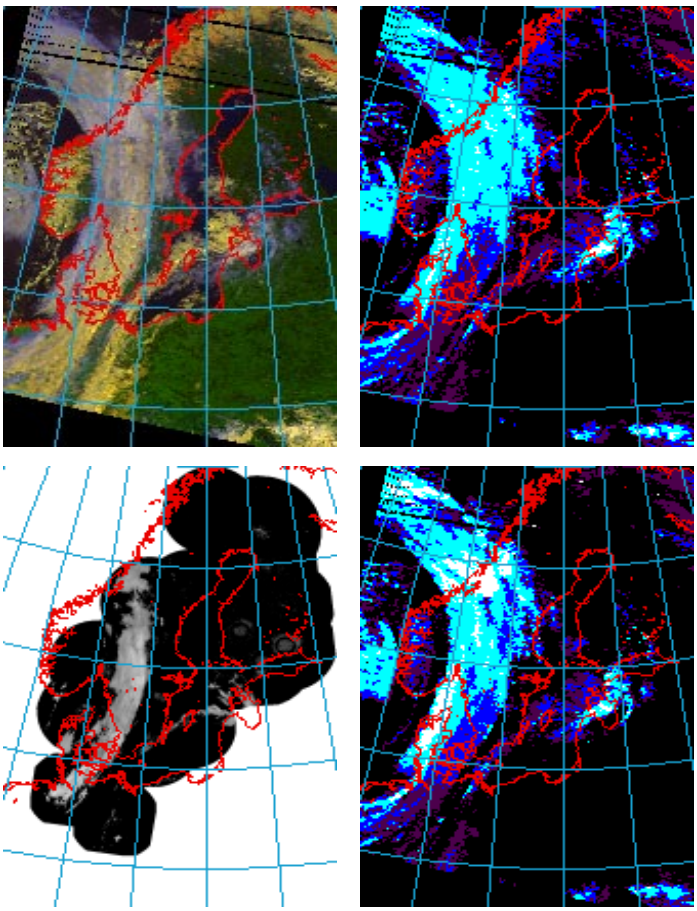

Figure 6-9: AVHRR NOAA15 overpath 22 May 1999, 06:39UTC. Upper left RGB composite AVHRR (0.6μm,0.9μm,11μm).Upper right: total precipitation probability for day time algorithm (magenta 10%, dark blue 20%, cyan 30%, white40% and above). Lower right as before, but for the night time algorithm. This case represents one of the few cases were the night-time algorithm performed superior to the day-time algorithm. Lower left BALTRAD radar composite for 6:30UTC.

6.4 Validation

Most aspects of validation are already implicit in the method, since the output is derived as precipitation likelihood. Visual inspection of the performance for cases lying within the seasons covered by the input data, showed a performance in agreement with expectations based on probability tables and histograms. The performance does however strongly depend on the synoptical situation. In some cases a lot of the area assigned to precipitation likelihood 10% coincides with radar echoes, whereas for other cases the 10% likelihood class is completely echo free and even the 20% class will contain only few echoes. Applying the night-time algorithm to winter cases gave a clear overestimation of precipitating area. It seems however possible to adjust the performance of the algorithm by selecting a coefficient "*a*" of about 260 instead of 280 in equations 6.1 and 6.2:

$$PIday = a(Tsurf) - T11 + b^* \ln(R0.6/R3.8) \quad (6.1)$$

and

$$PInight = a(Tsurf) - T11 + b^* (T11-T12) \quad (6.2)$$

This suggests that there is a potential of improvement and higher adaptability to different situations when "a " is for example made dependant on the ground temperature to account for seasonal and local variations. This hypothesis is strengthened by winter case studies which showed for a number of cases that the precipitation delineation was further improved when reducing the coefficient more in the northern than in the southern part of the Baltic. To achieve valid statistical results the retuning taking into account ground temperature dependence does of course need to be performed on a data set sampling the yearly cycle.

The statistical performance of the prototype in its current form can be measured by looking at the cumulative frequency of rain and no rain events in relation to assigned overall rain probability as given in Table 6-6.

6.4.1 Known problems

- The area of precipitation is over estimated. This problem is inherent in the methodology. It might however be reduced in extend with a finer calibration of the method as outlined below:
  - Make the PI dependent of surface temperature
  - Derive probabilities depending on cloud type or groups of cloud type.
- The overall precipitation likelihood is giving values smaller than intuitively expected. This problem is mainly related to the problem of overestimated area. Other contributions might be miss-locations between radar and satellite, which will have a stronger effect when the collocation is performed on pixel level (as in the current data set). In future tuning activities using some kind spatial averaging will be considered
- The current algorithm has not yet been tuned for winter conditions and has not been tested yet in southern Europe

6.5 Remaining work

The current prototype of the PC product is not yet sufficiently developed to serve as an operational algorithm. cipated to be ready July 2000)

Table 6-7 summarises deficiencies, planned remedy, estimated manpower and expected date of completion. The tasks below can be attempted, as soon as the processing chain has been adjusted to run from AAPP output (anticipated to be ready July 2000)

Table 6-7: Development planned after MTR.

Deficiency	Remedy	Resources	Ready by
Probability tables for prototype not derived on cloud type output. More accurate specifications of probabilities likely when creating separate index tables according to cloud type	Run CT scheme on historic data for a one year period.	2mm	Oct. 2000
Tuning to surface temperature dependence, including adaptation to winter season	Best performed together with task above. Otherwise possible to run statistics on one year data set coupled with surface temperature offline. This would require additional 0.5mm for data handling.	0.5mm	Oct. 2000
Validation and possibly revised tuning according to Spanish Radar data to cover representative cases over the product output area	Acquire and process a representative set of Spanish radar data, Validation, tuning	1.5mm	Tuning of the algorithm can be attempted after of in parallel to the above mentioned tasks
Adaptation to 1.6µm channel data	Can be attempted when a sufficient period of NOAA-L data is available	1mm	Probably not attempted before operational phase

7 Prototyping the AVHRR/AMSU Precipitating Clouds product – PC-2

7.1 Overview

7.1.1 Objectives

The Precipitating Clouds product provides information within every satellite FOV on the presence of precipitation and, in addition, indicates precipitation intensities, although only in very general terms.

The estimates will be given in precipitation likelihood in different intensity classes. When only IR/VIS information is considered, the estimates of precipitation intensity are somewhat arbitrary since only very intensive convective features have distinct spectral signatures. In mid – and northern latitudes a large fraction of the precipitation falls from stratiform clouds, were the coupling between brightness temperature and precipitation rate is not as strong. In these latitudes it is not always straightforward to delineate precipitating from possibly precipitating areas, but it is possible to identify many cloudy areas with very low precipitation likelihood with good confidence. The additional use of microwave data gives a more direct measurement of precipitation, but there are also uncertainties when using MW data. There is for example only little skill in retrieving small precipitation rates and the quality of the product varies depending whether it was retrieved over land, sea or coast. However, areas of medium to high precipitation can be delineated with better confidence. Combining both MW and IR/VIS estimates gives a marked improvement over their separate performances.

Both the AVHRR component and the AMSU component of the scheme are based on statistical estimates and have been developed and tuned using Radar data composites as precipitation ground truth. The AVHRR part of the scheme is, except for differences in the output, identical with the scheme for SEVIRI, which has been developed using AVHRR for prototyping. For details of description of the algorithm please see section 7.2. Updates to the AVHRR part are only given when they refer to differences between the AVHRR and SEVIRI scheme. The EPS PC scheme can be configured to run in two modes: one using AVHRR only and another mode using both AVHRR and AMSU.

7.1.2 Background

A precipitation product based on AVHRR data has been available at SMHI for several years as one output from the SCANDIA cloud classification scheme. As for all other VIS/IR schemes, the area of posssible instantaneous precipitation is overestimated since no direct physical coupling between precipitation and the VIS and IR cloud top signatures exists.

Microwave window channels on the other hand are strongly sensitive to scattering caused by precipitation sized frozen particles (see Bennartz and Petty 1999) and to emission from liquid rain drops. The latter can be sensed only against the radiatively cold background of ocean, whereas scattering caused by large frozen particles can in principle be retrieved over most surfaces. We have chosen to develop a precipitation retrieval making use of the scattering signature of frozen precipitation sized particles to be able to improve our estimates from VIS/IR over land and coast as well as over sea. Most scattering based algorithms reported in the literature were developed for SSM/I data and also make use of polarisation differences.

This can unfortunately not be applied to AMSU, but we could show that the 150GHz channel of AMSU-B allows to identify precipitation with a significantly higher accuracy than the 89GHz channel. Also the fairly high spatial resolution of AMSU-B compared to other MW sensors facilitates the retrieval of precipitation.

Development and archiving of BALTRAD radar composites made it recently possible to put the development of both VIS/IR and AMSU retrievals on a statistically solid basis.

7.1.3 SAFNWC Product requirements

A condensed description of the prescribed SAFNWC Precipitating Cloud product is given in the following sub-sections referring to the SAFNWC SP (section 3.1) and the descriptions and corresponding user requirements given in the SAFNWC URD 1.1. The description of the actual product is given in section 7.1.4.

The PC product will be available in two versions – one based solely on AVHRR data (denoted *A*) and one based on both AVHRR and AMSU data (denoted *A/A*).

7.1.3.1 Source

A:

- The PC product shall be derived from the complete AVHRR data set comprising of spectral channels at 0.6 μm, 0.9 μm, 1.6 μm, 3.7 μm, 10.8 μm and 11.9 μm. [TBC] (**UR-7.4.2.2.1**)

A/A:

- The PC product shall be derived from the complete AVHRR data set, comprising of spectral channels at 0.6 μm, 0.9 μm, 1.6 μm, 3.7 μm, 10.8 μm and 11.9 μm [TBC], and some selected AMSU window channels [TBD]. (**UR-7.4.2.3.1**)

7.1.3.2 Product description

- The PC product shall consist of a numerical value for the precipitation probability for the pixels identified as cloudy by the CMa and CT products within three precipitation intensity classes: no precipitation (R<0.1 mm/h), light precipitation and heavy precipitation. The threshold value for separating light from heavy precipitation is [TBD]. (**UR-7.4.2.2.2**)

- The following probability classes shall be used: 0-10%, 10-20%, 20-40%, 40-60%, 60-80% and >80% [TBC]. (**UR-7.4.2.2.4**)

7.1.3.3 Quality control

- No separate quality flag shall be included in the PC product. Provision of the probability of precipitation in each of the intensity classed will give an indication of the uncertainty of the estimate. (**UR-7.4.4.1**)

7.1.3.4 Product output content and format

No specification other than under 1.1.3.2 was given, for actual output see 1.1.4.3.

7.1.3.5 Time constraints

15 min after availability of data.

7.1.3.6 Internal product dependency

Products CT and CTT/H are needed as input to the algorithm.

7.1.3.7 Chosen method

Statistical scheme making use of IR/VIS and MW spectral features and forcing parameters derived from NWP data (SP, section 2.2.1.2.2).

7.1.3.8 Auxiliary and ancillary data

The chosen scheme will use the following input data for the dynamic definition of essential thresholds:

- Sun and satellite zenith and azimuth angles (four angles in total) associated with the AVHRR image. Mapped on AVHRR images at full horizontal resolution.
- NWP output (analyses or short-term (less than 12 hours) forecasts):
  -Temperature at several levels (most frequent in the lower troposphere including the surface in order to resolve and detect near-ground temperature inversions)

  -Water vapour content (the total amount and for several individual layers, TBC)

  -Near-surface wind speed (TBC during prototyping)

  -Forecasted snow accumulation (TBC during prototyping).

  All NWP data shall be mapped on AVHRR images at full horizontal resolution.
- Static threshold data (previously determined empirically or with the aid of RTM calculations)
- Other auxiliary data sets:

  -Land/sea mask (bit map)

  -Elevation map

  -Snow/ice cover map (TBC)

  -Surface type map (TBC) (SP, section 2.2.1.3.1)

7.1.4 Prototype description

A summary of the PC product in its present prototype stage is described in the following sub-sections. The same sub-division as in section 7.1.3 is used. If there are no deviations from the prescribed product definitions, or any additional information on the product, only a reference to the corresponding sub-section in 7.1.3 is given.

More details on the developed product are given in section 7.2.

7.1.4.1 Source

AVHRR/3 - all channels.

Input to the PC module are all the AVHRR spectral channels with exception of the 0.9 μm channel. In cloudy areas this channel is highly correlated with the 0.6μm channel and does not seem to contribute additional information on precipitation. It was however used in the Cloud Mask product to delineate clouds from different surfaces. For the 1.6μm channel we did not yet have enough data available to put the algorithm development on a statistically significant basis. The mandatory channels for the current algorithm are: 0.6μm, 3.7μm (1.6μm), 11μm and 12μm. To account for production for NOAA-L before an 1.6μm algorithm is implemented, the night time algorithm will be switched on when the 1.6μm channel is present instead of the 3.7μm channel. The availability of channels is checked on pixel basis and being translated in a quality flag on pixel basis. If mandatory AVHRR channels are missing, the product is assigned a missing data value on pixel basis

For the A/A product the same AVHRR algorithm is used as in the AVHRR-only Product.

The use of AMSU channels depends on the scene type (land/sea/coast). The mandatory use of AMSU channels is decided depending on scene type on a pixel by pixel basis . Over Land a scattering index derived from 23GHz AMSU-A and the 150GHz AMSU-B channels is used, over sea a scattering index derived from 89GHz and 150GHz AMSU-B channels is applied. Over coastal areas the estimate is blended form land and sea scattering indices according to the fraction of land within the AMSU-B FOV. If a mandatory AMSU channel is missing, a missing data value will be set for the respective AMSU-B FOV. If no valid AMSU precipitation estimate is encountered for a product pixel, the AVHRR only algorithm will be switched on and the processing flag for that pixel will contain the relevant information.

7.1.4.2 Product description

The product gives the likelihood of precipitation in different intensity classed. In the development work for the A/A product it proved advantageous to further sub-divide the light precipitation class into a very light/possible precipitation class and a light to moderate class according to the thresholds given in Table 7-1. The output is thus given in 4 intensity classes:

Table 7-1: Intensity thresholds for precipitation classes

Class	Type of precipitation	Minimum rain rate, mm/h	Maximum rain rate, mm/h
0	No precipitation	0.0	0.1
1	Risk for/light precipitation	>0.1	0.5
2	Light/moderate precipitation	>0.5	5.0
3	Intensive precipitation	>5.0	∞

Results from prototyping suggest to chose a finer resolution of probability classes than given in the user requirements. Due to the fact that the precipitating area is generally overestimated by IR/VIS methods, high precipitation probabilities are seldom reached when not considering MW data. About half of the precipitation events of the AVHRR algorithm are in areas which are assigned precipitation likelihoods between 5%-25%. Therefore we have chosen to use the precipitation probability classes given in Table 7-2.

Table 7-2: Probability intervals

100-95% assigned to	100%
>95-85% assigned to	90%
>85-75% assigned to	80%
>75-65% assigned to	70%
>65-55% assigned to	60%
>55-45% assigned to	50%
>45-35% assigned to	40%
>35-25% assigned to	30%
>25-15% assigned to	20%
>15- 5% assigned to	10%
> 5- 0% assigned to	0%

7.1.4.3 Quality Control

Even though there is no quality flag as such, the generation of the product depends on availability and quality of many input components. A processing flag described in the next section provides more detailed information on the product.

7.1.4.4 Product output content and format

The product output is given for the three classes indicating precipitation (class 1-3) as unsigned characters. The gain and intercept (floats) are used to convert from counts to percent probability. The probability of no precipitation can be derived as $100\%-\Sigma P_i$, where P_i are the probabilities of precipitation classes one to three.

Additionally a processing flag similar to the processing flag of the cloud type product is given. It provides information for each pixel on the available and used data, the applied algorithm, the scene type and quality of cloud type and the AMSU estimate. It is divided into general processing information, AVHRR specific and AMSU specific information. Details are given in the following tables:

Table 7-3: General processing flag

Bit #	Meaning of the bit – 1/0
0	Processed/non-processed
1	AMSU missing/not missing
2	AVHRR missing/not missing
3	AMSU used/not used
4	CT used/not used
5	AVHRR solar channels used/not used

Table 7-4: AVHRR specific processing flag

Bit #	Meaning of the bit – 1/0
0	AVHRR processed/non processed
1	AVHRR land/no land
2	High terrain/no high terrain
3	NWP data missing/not missing
4	AVHRR cloudtype low quality/no low quality

Table 7-5: AMSU specific processing flag

Bit #	Meaning of the bit – 1/0
0	AMSU processed/non processed
1	AMSU land/no land
2	AMSU coast/no coast
3	AMSU snow or ice detected/no snow or ice detected
4	AMSU lprocessing low confidence/AMSU processing ok

7.1.4.5 Coverage and resolution

North of the 50N parallel - depending on local radio horizon. (The product quality cannot be guaranteed below latitude 50N, but the algorithm will work anywhere). Full AVHRR (1 km) resolution can be specified not only for the AVHRR, but also for the AVHRR/AMSU version.

7.1.4.6 Time constraints

The general constraint that all products can be generated within 15 minutes from availability of the data will be fulfilled. See also section 7.3.1.

7.1.4.7 Internal product dependency

The production depends on the completion of the cloud type product. Instead of using the cloud height product we performed the actual development of the prototype using the original 11 μm and 12 μm brightness temperatures. This deviation from original plans was made necessary because of the delay in the development of the cloud height product. However it also provided us with the possibility to more directly tackle dependencies on semi-transparency.

7.1.4.8 Chosen method

According to the science plan a statistical scheme making use of IR/VIS and MW spectral features and forcing parameters derived from NWP data was to be chosen (SP section 2.2.1.2.2). However the original idea to incorporate large scale forcing parameters derived from NWP fields with a short lead time was dropped since in the statistical scheme we could not really secure that the final product would be dominated by satellite derived information in all cases. Since we managed to develop an AMSU retrieval which also works well over land and even coast, the need for incorporating information from NWP fields was reduced.

7.1.4.9 Auxiliary and ancillary data

From the list of auxiliary data given in 7.1.3.8, only the following information gets used:

For the AVHRR processing:

- Sun and satellite zenith and azimuth difference angles (three instead of 4 angles in total, since only the azimuthal difference between sun and satellite is output of the AAPP processing) associated with the AVHRR image. Mapped on AVHRR images at full horizontal resolution.
- NWP output (analyses or short-term (less than 12 hours) forecasts):
  - Surface temperature

- Other auxiliary data sets:
  - Probability lookup tables relating spectral features to precipitation derived from collocated AVHRR/Radar data, depending on surface temperature.
  - This last requirement is a prerequisite to the statistical scheme, but has not been explicitly mentioned in previous documentation.

The AMSU processing is done on AMSU-B fields of view. In the current prototype the only auxillary data needed are:

- Land/sea mask
- Scanning geometry
- Probability lookup tables relating MW spectral features to precipitation derived from collocated AMSU-B/Radar data

The current algorithm has been derived using a data set covering the Baltic in the period April to September 1999. Adopting the algorithm to winter conditions might necessitate additional inclusion of any of the following inputs to the AMSU scheme (TBC):

NWP output:
- integrated water vapour content
- surface temperature
- accumulated snow cover
- sea ice

Auxiliry data:
- snow cover map
- ice cover map

We will however try to keep the AMSU algorithm independent from NWP information if that proves to be possible for winter conditions as well.

7.2 Detailed algorithm description

7.2.1 Algorithm outline

The PC algorithm can be logically divided in three steps:

- AVHRR retrieval (always performed) using the cloud type classification and the correlations of AVHRR spectral features with precipitation.
- AMSU retrieval: performed independently on original AMSU –B resolution.
- Merging of the AVHRR and AMSU retrievals (always performed when AMSU data is considered)

The description of each of the processing steps is given in the sections below. An overview of the dataflow in the PC scheme is illustrated in Figure 7-1.

7.2.1.1 AVHRR retrieval

See chapter 6.2.

7.2.1.2 AMSU retrieval

To design a MW precipitation retrieval that works over land and sea and, we chose to base the retrieval on the scattering signatures of frozen precipitation sized particles. Since land and sea differ significantly in their surface emissivities, algorithms for land and sea have to be developed separately. It is essential for the quality of the retrieval that the fraction of land and water within each MW footprint is accurately described. The land/sea fraction within each AMSU footprint was determined by degrading a high resolution land/sea mask to AMSU resolution. Bennartz (1999a) shows, that the quality of this estimate depends crucially on the navigation accuracy.

Different possible scattering indices from window channel combinations of AMSU-A and AMSU-B were evaluated. It was shown that the 150GHz channel exhibits a much higher potential to identify precipitation according to its scattering signature than the 89GHz channel (see section 7.2.2.2). For the value range of the scattering index, precipitation probabilities have been derived from collocated radar data, which has been convolved to AMSU-B resolution (Bennartz 1999b, Bennartz and Michelson, 1999).

The algorithm had to be constructed in a way that it would even work over the highly structured, inhomogeneous terrain of the Baltic. Depending on the coverage of AMSU-A and AMSU-B FOVs with land coast and sea, different channel combinations had to be selected. The scattering indices are constructed as the difference of a lower frequency AMSU-A or AMSU-B channel and the 150GHz AMSU-B channel plus a correction term empirically correcting for scan angle dependence. The later was found by regressing the scattering index for all precipitation free observations against the local zenith angle.

The scattering indices for different scene types are:

AMSU-A water or coast, AMSU-B land:

$$S_{l1} = (T_{89} - T_{150}) - (0.158 + 0.0163\theta) \qquad (7.1)$$

AMSU-A land (and AMSU-B land):

$$S_{l2} = (T_{23} - T_{150}) - (1.7428 + 0.0776\theta) \qquad (7.2)$$

AMSU-B water:

$$S_s = (T_{89} - T_{150}) - (-39.2010 + 0.1104\theta) \qquad (7.3)$$

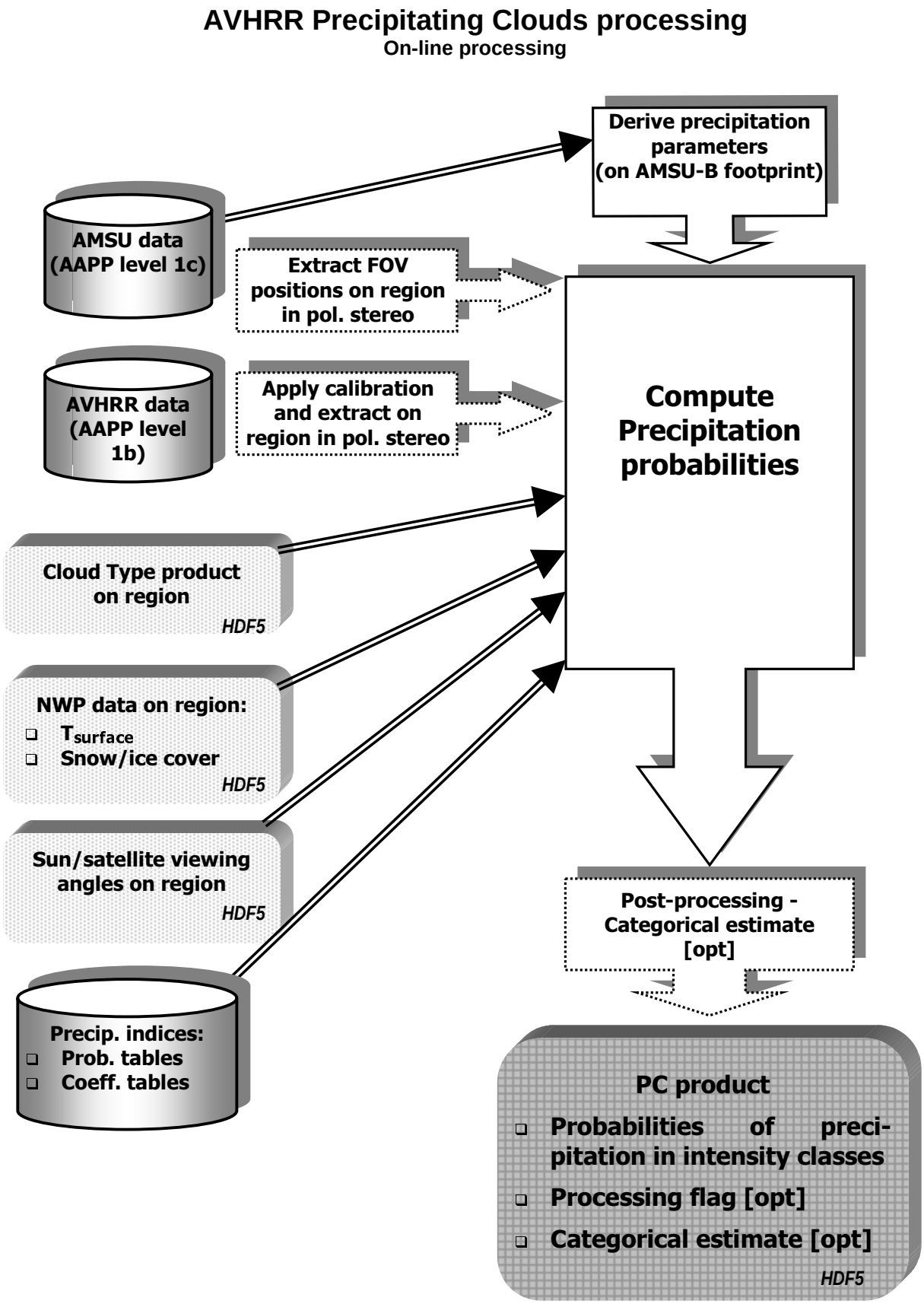

Figure 7-1: AVHRR Precipitating Clouds On-line processing

where θ, given in degrees, is the local zenith angle and T denotes the brightness temperatures of the respective channel. Note that there is a considerable offset for T_{89} and T_{150} over water, which is also corrected for. This correction is probably the least general part of the set of algorithms, since it is supposed to be strongly dependent on e.g. the water vapour path and atmospheric temperature, and may thus not be valid for other regions with completely different atmospheric conditions, such as tropics. It can, however, be generalised by adjusting the offset to the observed mean difference between T_{89} and T_{150} for a given area.

Coastal areas are defined as containing a land fraction between 1% and 95% . For discussion of this choice of thresholds see Appendix 9.1.2,"Precipitation Analysis from AMSU", section 3.2. The land fraction is determined by convolving a high resolution land/sea mask to the AMSU-B footprints. For coastal areas the probabilities are determined as composite from the land and sea estimates, weighted by the land fraction:

$$S_c = (1 - l)S_s + lS_{l1} \qquad (7.4)$$

where *l* is the fraction of land within the FOV. The weighted average according to the fraction of land in the footprint also automatically weights the zenith angle and offset corrections for the land and sea parts, so regardless of fraction of land in the footprint, a precipitation free scene has an average scattering index of 0K. This assumption is valid because of the observed linear dependence of MW brightness temperature on land fraction within each FOV. . There is a linear dependence of MW brightness temperature on the land fraction within the FOV (see Figure 7-2).

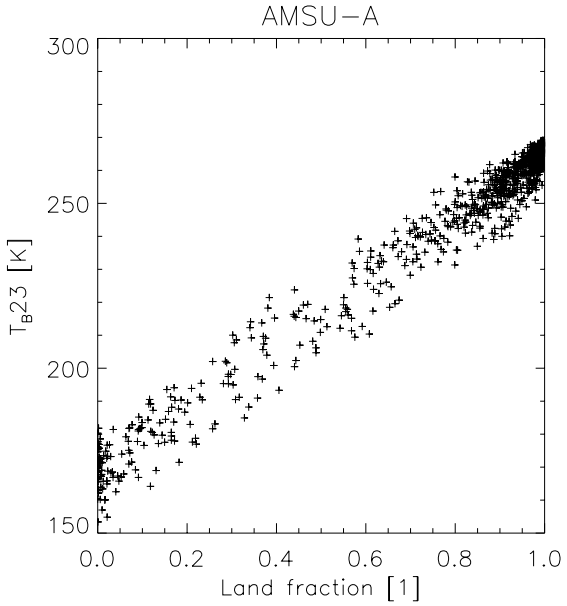

Figure 7-2: Dependence of the AMSU-A brightness temperatures at 23.8GHz on the fraction of land surface within the footprint.

Scattering signatures are not only sensitive to precipitation, but also to snow or ice covered ground. Since the algorithm has been developed on a period excluding the winter season, we had only few test cases with snow cover available. Snow and ice screening according to the algorithms of Grody et.al. (1999) has been incorporated. Additionally the scattering signature

of the 183∓ 7GHz shows potential to discriminate between snow and precipitation. If snow or ice is detected, a flag is set in the processing. The detection of snow and ice, as well as the general tuning to winter conditions, will be revisited after the end of the winter season, when a representative winter data set will be available.

Input to the AMSU module are the level 1c AMSU A and B files created by AAPP and a land sea mask file. Output from the scheme are precipitation probabilities and processing flags indicating whether any of the processing steps failed (convolution or calculation of the scattering index), or whether the snow/ice flag was set. The output is given for original AMSU-B FOV. If running the A/A algorithm is configured, this module is run before the AVHRR retrieval is started to have results available for a pixel by pixel processing of the specified region. An overview of the AMSU algorithm is given in Figure 7-3.

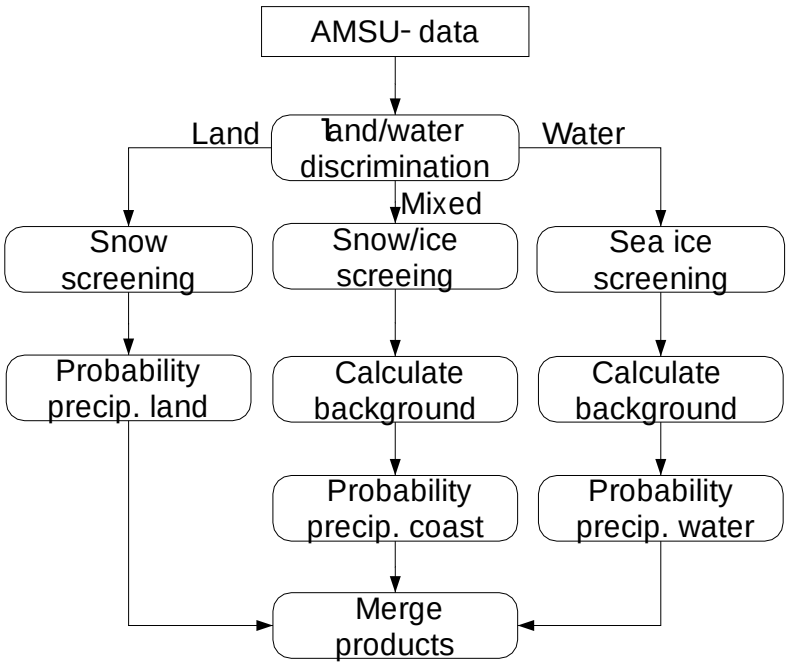

Figure 7-3:Overview of the AMSU algorithm.

7.2.1.3 Merged AVHRR/AMSU retrieval

For each pixel the likelihood of precipitation from the AVHRR algorithm is considered. If the likelihood of precipitation is assigned a higher value than 0% (meaning that the likelihood of precipitation is not higher than 5%) the availability of an AMSU estimate is checked. For that the AMSU scan line and spot indices projected to the region are used. If an AMSU estimate is available and none of the AMSU flags indicate low quality, the AMSU estimate is taken.

Employing this method decreases the de facto spatial resolution of the output product, but the delineation of medium to strong precipitation gets considerably improved when using the MW channels (see section 7.2.2). On the other hand the AVHRR algorithm has a higher skill in delineating cloud free areas and cloudy areas with very low precipitation likelihood. The

way of combining AMSU and AVHRR data sets will be subject to more tuning, once the final AMSU and AVHRR algorithms, tuned on a full yearly cycle, are available.

7.2.2 Derivation of Indices

7.2.2.1 AHVRR

The AVHRR algorithm is described in section 6.2 for the SEVIRI prototype, which has been developed using AVHRR data. The only difference between the algorithms is the output of precipitation classes. The common processing with AMSU data in the EPS module suggested that a finer resolution of precipitation classes should be used by introducing a class of very light precipitation, for which the retrieval accuracy of the AMSU is not as high as for the other classes (see also section 7.4). The AVHRR itself however, has no skill in separating this class, as is illustrated for the AVHRR day time precipitation index in Figure 7-4.

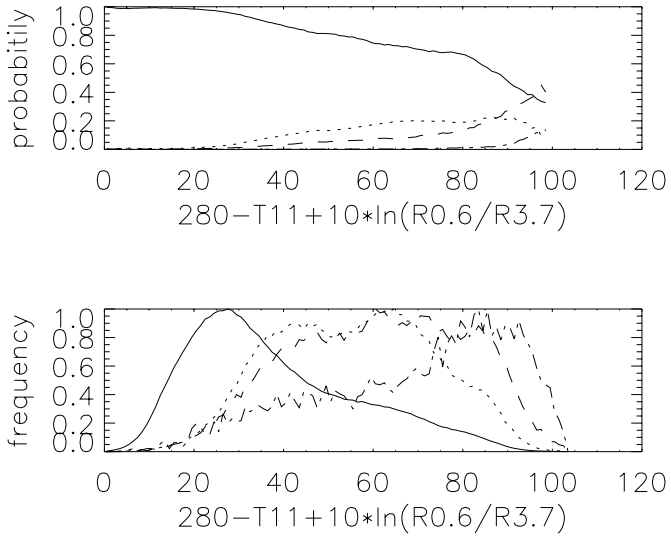

Figure 7-4: AVHRR precipitation index for day-time PI_{day}=280-T11+ 10*ln(R0.6μm/R3.8μm). Lower panel: normalised histogram for four different precipitation classes (solid line: no precipitation, dotted: light precipitation, dashed:light to moderate precipitation, dash-dot: heavy precipitation. Upper panel: same as above but for probability**.**

7.2.2.2 AMSU

Land

Different possible channel combinations were evaluated for their usefulness to retrieve precipitation. Over high emissivity land surfaces the impact of the signal of atmospheric emitters such as water vapour, cloud liquid water and liquid precipitation is small. The isolation of the scattering signal is simply performed using the difference between a low frequency channel (23GHz) and a high frequency channel (89GHz or 150GHz). We refer to these differences as scattering index at 89Ghz respective 150GHz (see equation (7.1)). For non precipitating situations it will be around zero, whereas for precipitation situations it will increase to values of more than 50, depending on the total amount of precipitation sized ice crystals within the field of view. The likelihood with which a given observation belongs to one of the above defined four classes (see Table 7-1) is derived using the radar data to subdivide the whole data set into 4 sub-classes according to the precipitation class thresholds.

From these data we derived histograms of the distribution of the scattering index for each of the four classes. Figure 7-5(upper panel) shows the histograms normalised to a peak value of 100 for the 89 GHz scattering index. From the histograms we derived the likelihood for which a given scattering index belongs to a certain class, under the constraint that for each scattering index the total probability has to be 100%. The resulting likelihoods are shown in the lower panel of Figure 7-2. While classes 0 (no precipitation) and 3 (precipitation greater than 5mm/hr) can be separated, classes 1 and 2 overlap strongly with each other and classes 0 and 3. The separation in the four classes can be enhanced if the 150GHz channel is used instead of the 89GHz channel. Figure 7-6 shows the histograms and corresponding likelihoods of the 150GHz channel. One can see that the separation of the classes 0 and 3 has now increased from 1K (for 89GHz) to 6K. Also the likelihood to classify a given observation as class 1 or 2 has increased in the range between zero and 7K.

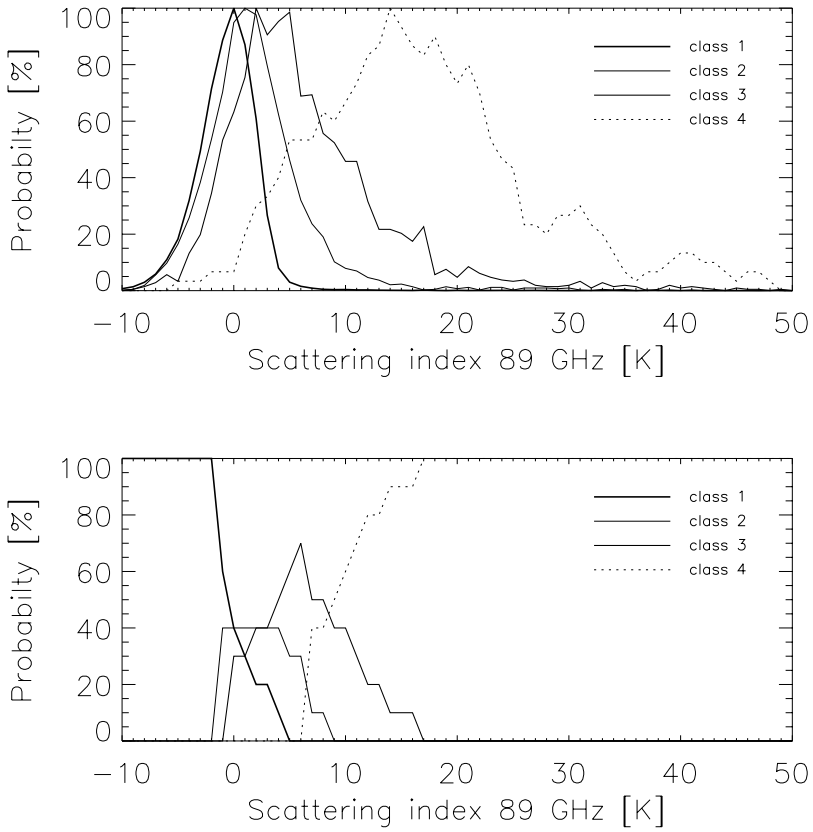

Figure 7-5: The upper panel shows histograms (normalized to a peak value of 100) of the distribution of the scattering index at 89 GHz over land for the four classes (please note that class 1 in the legend is referenced as class 0 in the rest of the document etc.). The observations were classified according to the radar derived convolved rain rate. The lower image gives the probability with which a given scattering index belongs to a certain class. **(***Class 1 with no precipitation has the leftmost peak and the other classes, going to the right, have their peaks in ascending order of precipitation intensities - 2, 3, 4 resp.).*

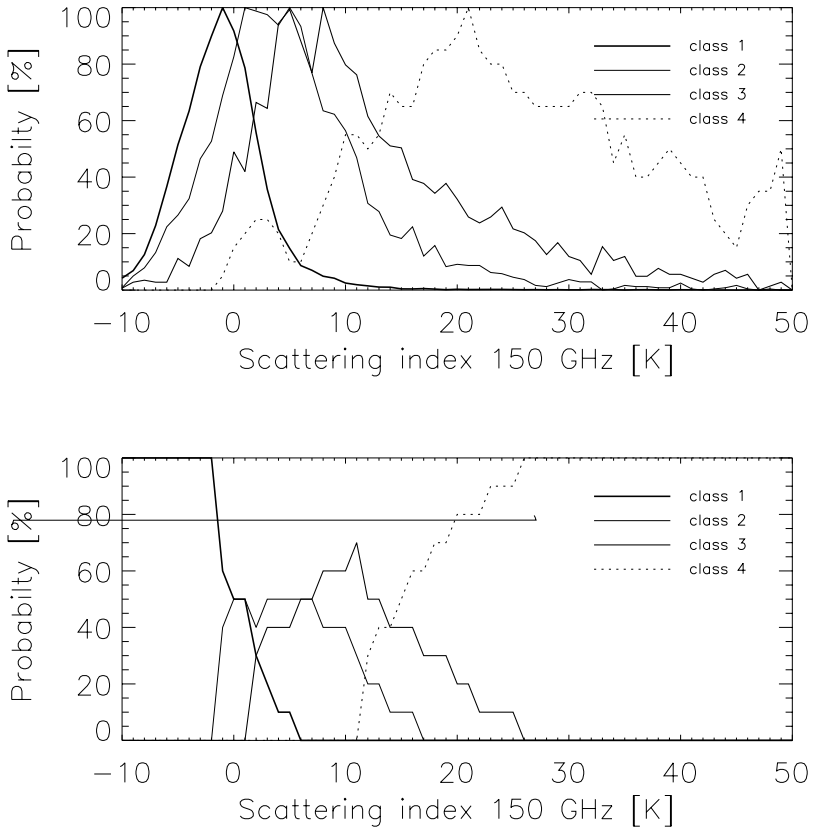

Figure 7-6: Same as Figure 7-5, but for the 150GHz scattering index over land.
(*Class 1 with no precipitation has the leftmost peak and the other classes, going to the right, have their peaks in ascending order of precipitation intensities - 2, 3, 4 resp.).*

Sea:

Over water surfaces it is both possible to derive precipitation information based on the emission signal from liquid precipitation and on the scattering signature of large frozen particles. An emission type algorithm based on thresholding the retrieved liquid water path has been tested. Emission type algorithms are however based on lower frequency AMSU-A channels. Due to the highly structured terrain in the Baltic, only 6% of the original vaidation dataset covers homogeneous water surface at the spatial scale of AMSU-A. We therefore decided to concentrate developing efforts on a scattering based algorithm over sea as well. Further details about the emission algorithm can be found in Appendix 9.1.2,"Precipitation Analysis from AMSU", section 3.4.1.

As for land surfaces, The different window channels of the AMSU-A and AMSU-B may be used in different combinations to obtain scattering indices. We investigated the combinations T_{23}-T_{89}, T_{23}-T_{150} and T_{89}-T_{150}. Although both the 89Ghz channel and the 150 GHz channel are affected by scattering, the latter turned out to give the best results. Figure 7-7, upper panel, shows the distribution of the observed scattering index derived from Equation (7-3). The lower panel shows the resulting probabilities. It can be seen that the dynamic range of the scattering indices over water surface is much larger than over land, which also leads to better classification results.

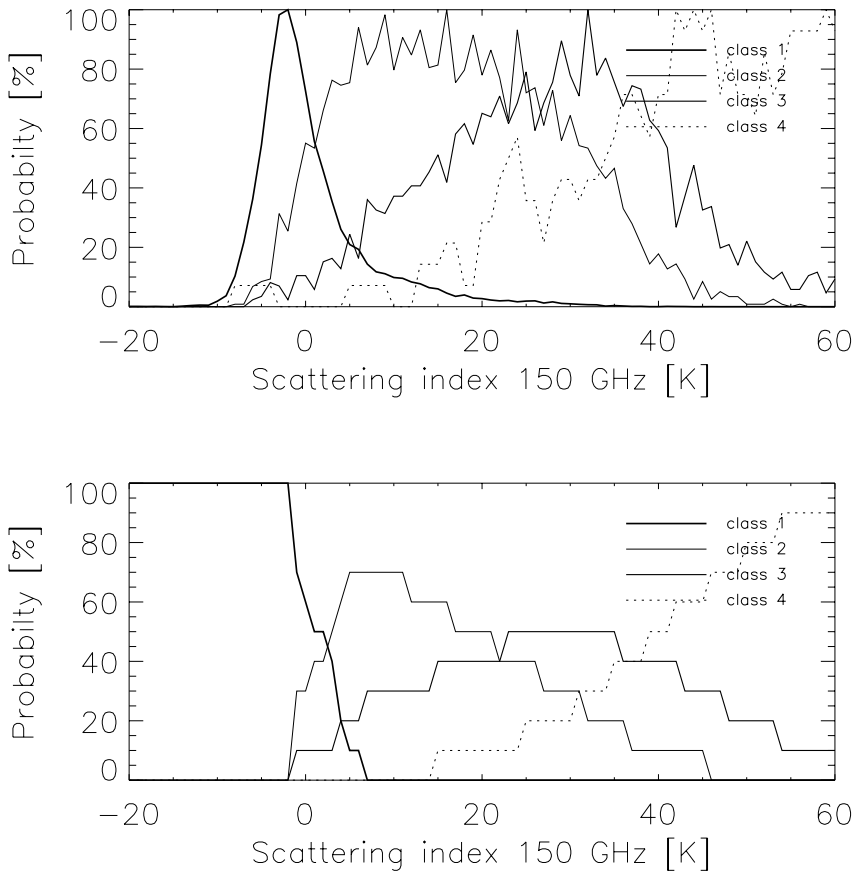

Figure 7-7: Same as Figure 7-5 but for the T_{89}- T_{150} scattering signal over sea.
(*Class 1 with no precipitation has the leftmost peak and the other classes, going to the right, have their peaks in ascending order of precipitation intensities - 2, 3, 4 resp.).*

Coast:

Coastal pixels consist of a mixed land/water signal. This influences both the observed brightness temperature and its sensitivity to precipitation. Our approach is to explicitly account for this mixing by weighting the observed scattering index as well as the derived probabilities with the fraction of land in the footprint. Figure 7-8 illustrates the approach. For 10% (15000pixels) of the coastal pixels in the data set we plotted the scattering index derived from Equation (7.4) against the fraction of land surface in the footprint. The lines indicate the regions were the different classes of precipitation prevail. Every observation below the lowest line would thus have a high probability to be precipitation free and every observation above the uppermost line would have the highest probability to belong to class 3.

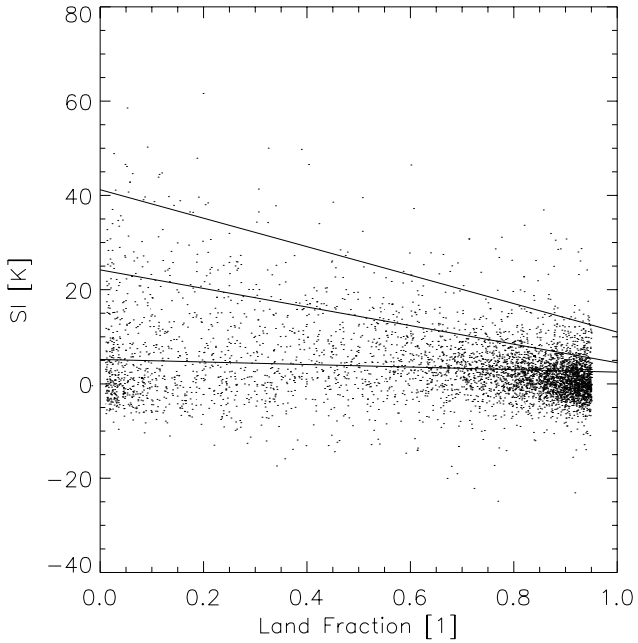

Figure 7-8: Visualisation of the precipitation classification for coastal pixels. The scattering index SI derived from Equation (7.4) against the fraction of land within the AMSU-B footprint is shown for 10% of the total pixels over coast. The lines give the threshold values between which the respective precipitation classes have the highest probability (e.g. below the lowermost line all observations are most likely to be precipitation free).

7.2.3 Processing flag

The processing flag (see section7.1.4.4) gives information about what information was used in the generation of the product, what parts of input data were missing, and which parts were rejected or not used because of bad quality. Especially when running the PC product in A/A mode this might give valuable information when evaluating the performance of the model. The processing flag is given as three independent parts (general, AVHRR, AMSU). Which flags should be generated, can be configured by the user.

7.2.4 The use of NWP data and their impact on quality

The PC makes use of the surface temperature. It is used in the calculation of the precipitation index PI from AVHRR data, mainly to account for seasonal differences in relating the 11μm brightness temperature to precipitation likelihood. The AMSU part of the algorithm employs no NWP data. If no AMSU estimate is available (either by configuration, missing data or at the edges of the swath), the same dependencies on NWP apply as given in section 6.2.3. If an AMSU estimate is available, it will substitute the AVHRR estimate in case that the AVHRR is giving a precipitation likelihood of 10% or more. Thus influences of NWP are restricted to situations with fairly low precipitation likelihood, where the decision whether it is raining or not according to AVHRR might be influenced by the actual NWP surface temperature value. The influence of NWP data quality on the combined AVHRR/AMSU product is thus marginal.

Another input which might come from NWP, if not provided from another source, is the use of snow and ice maps. The derivation of precipitation over snow and ice is problematic since these surface types sometimes exhibit scattering characteristics similar to precipitation. Where

snow and ice is flagged from ancillary data input, the AVHRR only algorithm is used. Ice and snow which is not detected in the NWP field, might thus lead to false precipitation echoes if AMSU is used.

7.3 Practical application

7.3.1 Implementation

The code is implemented in the C language with some interfaces to Python routines for the projection software for AMSU.

CPU and memory requirements depend on configuration (A versus A/A). All figures below are given for the hardware specified in section 3.3.1, and for a 1024 times 1024 pixel AVHRR region.

Processing from AVHRR only (including references to auxiliary data) required 39MB memory and 21.3 seconds at a CPU utilisation level of 42%.

When processing the AMSU data we currently process the complete overpath. Due to the convolution involved, this takes a substantial amount of time. However the processing of the AMSU overpath has to be performed once only, if several regions are to be processed. The figures are given for processing the 1024 times 1024 AVHRR pixel area and an AMSU-B overpath containing 190 scanlines. The memory required was 44MB and the processing time 4.19 minutes. Of that the processing of the AMSU overpath required 3.28 minutes and 4.5MB.

7.3.2 Product demonstration

For a demonstration of the AVHRR only module see chapter 6.3.2 of the SEVIRI prototype.

The following examples have not been prototyped with the final prototype, but using an offline prototype not embedded in the Nowcasting SAF software. The prototype embedded in the Nowcasting environment has been coded and is now in the testing phase.

The main difference in the processing of the presented examples as compared to the current nowcasting prototype, is that the matching of AVHRR and AMSU is not performed on AMSU pixel resolution, but with AVHRR convolved to AMSU-B resolution. Instead of the night-time algorithm for AVHRR (which includes the T11-T12 feature), just the 280-T11 feature was used for screening out precipitation. This was done to have a better traceability of effects of applying indices derived for full AVHRR resolution to the convolved data. As to be expected, precipitation masks thus applied seem to be slightly more stringent than when using the original resolution.

In all of the depicted cases it becomes obvious, that the ability to identify precipitation free pixels is improved by combining AVHRR and AMSU. Many areas in the AMSU with moderate scattering indices, indicating possible light precipitation, can be screened out that way. For an objective verification of the displayed cases see section 7.4. Using the AMSU data enables us to also to roughly estimate the intensity of the precipitation.

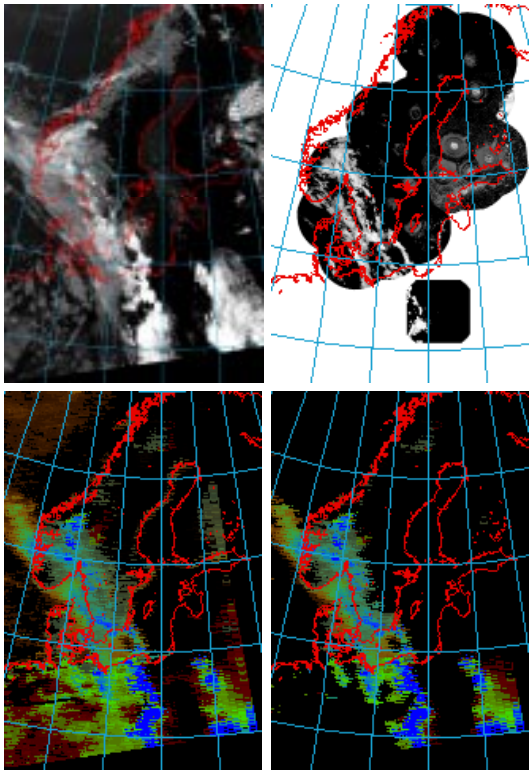

Figure 7-9: NOAA15 overpath 28 June 1999,17:45UTC. The upper left image shows the AVHRR channel 4 brightness temperature, the upper right image the collocated BALTRAD radar composite. The lower images give the result of the precipitation classification where class 1 (light/risk precipitation) is assigned red, class 2 green and class 4 blue. The lower left image shows the AMSU only classification, the lower right image the combined AVHRR/AMSU classification.

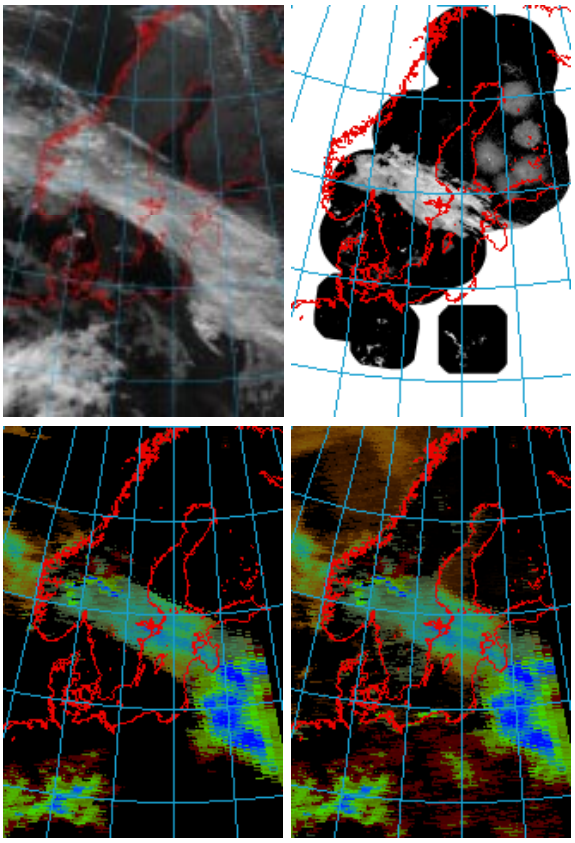

Figure 7-10: Same as Figure 7-9 but for 22 September 1999, 17:46UTC.

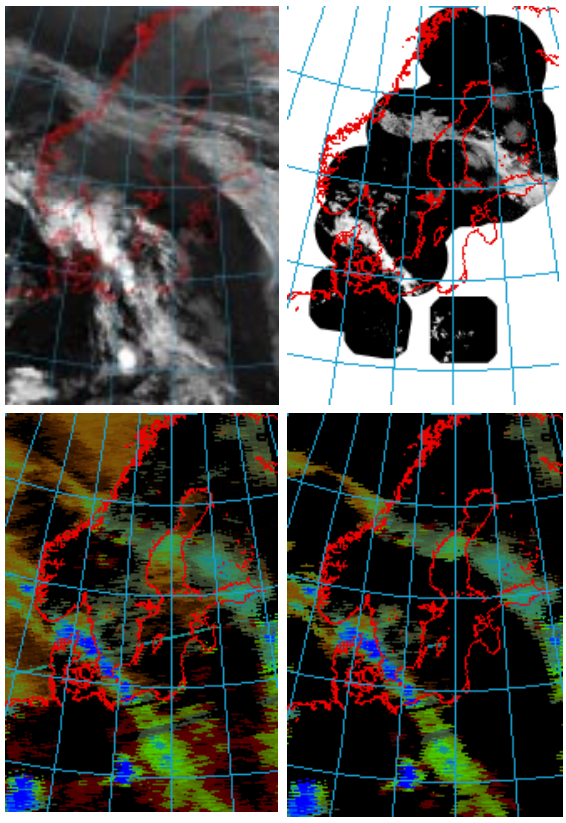

Figure 7-11: Same as Figure 7-9 but for 23 September 1999, 17:24UTC.

7.4 Validation

When using probability estimates, part of the verification is implicit in the scheme. Difficulties in applying a statistical scheme might arise though, when applying it on a data set for which it is not representative. In our case it proved that the scheme needs to be adjusted for use in winter conditions. This applies both to snow/ice screening and to tuning to different atmospheric conditions. We will revisit this issue in spring, after having a full yearly cycle of data available. Visual inspection of applying the AMSU scheme to the full NOAA paths covering Scandinavia down to the Mediterranean for a few summer and autumn cases, did however not indicate major portability problems.

Generally it can be stated, that the AMSU can very well detect light to strong precipitation, even for small alined features, which do not necessarily fill an AMSU footprint. The area of possible precipitation is slightly overestimated in areas close to precipitation. A seamless transition between land , coast and sea is achieved. Over some non-precipitating areas scattering indices which could also indicate light rain are found. Those areas can efficiently be screened out using AVHRR data.

Another way of demonstrating the ability of the scheme is to perform a hard-clustering by assigning each value to the class with the highest probability.(maximum likelihood classification) . In Table 7-6 the contingency tables for the 89Ghz and 150 GHz land algorithm are given. As to be expected from the histogram and probability figures (Figure 7-5and Figure 7-6), the 150GHz algorithm gives clearly better classification results.

Table 7-7 gives the hard-clustering for sea cases. Since the dynamic range of the signal is much larger than over land, there is also a better discrimination of precipitation. The performance of the coastal algorithm (Table 7-8) lies somewhere between the land and sea algorithm. An additional error source here are possible errors in the prescribed land fraction in the footprint, due to inaccuracies in navigation. However in most cases this effect is minor.

Table 7-6: Results of hard-clustering the probabilities for the land scattering algorithms. Upper panel using 89GHz scattering index. Lower panel using 150GHz scattering index.

Classified as/ Belongs to	Measurements in class	Class 0 [%]	Class 1 [%]	Class 2 [%]	Class 3 [%]
Class 0	42943	51.0	33.8	14.8	0.4
Class 1	3526	28.0	25.5	40.6	5.9
Class 2	2516	12.0	12.9	45.4	29.7
Class 3	129	0.7	1.6	14.0	83.7
Class 0	42943	73	22	2.4	0.2
Class 1	3526	11	33	26.7	8.3
Class 2	2516	5	8	36.1	31.9
Class 3	129	0	0	12.7	82.8

Table 7-7: Same as Table 7-6 but for scattering index over sea using the difference of the 89GHz and 150Ghz channels.

Classified as/ Belongs to	Measurements in class	Class 0 [%]	Class 1 [%]	Class 2 [%]	Class 3 [%]
Class 0	34176	82.8	15.8	1.4	0.0
Class 1	3503	15.6	54.0	28.4	2.0
Class 2	2295	3.7	31.2	48.2	16.9
Class 3	94	1.3	6.7	25.3	66.7

Table 7-8: Same as Table 7-6 but for scattering index over coast (see equation (7.4))

Classified as/ Belongs to	Measurements in class	Class 0 [%]	Class 1 [%]	Class 2 [%]	Class 3 [%]
Class 0	130242	70.2	25.9	3.7	0.2
Class 1	13860	24.0	42.4	28.4	5.2
Class 2	9298	9.0	26.3	44.3	20.4
Class 3	354	5.1	8.1	25.6	61.2

To more objectively assess the benefit of using the AVHRR in combination with AMSU, a hard-clustering has been performed for the three example cases presented in section 7.3.2.

The upper panel of Table 7-9 shows the results for AMSU only, the lower panel for the combined simplified AVHRR/AMSU algorithm. Incorporating AVHRR decreases the misclassifications of precipitation free cases as light rain from 22% to 12%. On the other hand there is a very moderate increase in the numbers of missed precipitation.

Table 7-9: Results of hard-clustering using for the three cases presented in 7.3.2. Upper panel: AMSU only, lower panel: AMSU/AVHRR

Classified as/ Belongs to	Measurements in class	Class 0 [%]	Class 1 [%]	Class 2 [%]	Class 3 [%]
Class 0	11140	73	22	5	0
Class 1	1244	11	33	43	13
Class 2	587	5	8	35	52
Class 3	13	0	0	0	100
Classified as/ Belongs to	**Measurements in class**	**Class 0 [%]**	**Class 1 [%]**	**Class 2 [%]**	**Class 3 [%]**
Class 0	11140	84	12	4	0
Class 1	1244	15	29	42	14
Class 2	587	6	7	35	52
Class 3	13	0	0	0	100

7.4.1 Summary of results

- When using the AVHRR algorithm alone, the area extent of precipitation is overestimated and there is no capability to estimate intensity. Tuning is needed to take both into account the surface temperature and the cloud type (see section 6.4).
- The AMSU algorithm performs well over land, coast and sea, giving also the possibility to roughly estimate precipitation intensity. Tuning is needed for winter conditions. When using AMSU data only, there are many cases where the algorithm assigns probabilities of light rain to non precipitating areas.
- The last mentioned shortcoming of the AMSU scheme can be markedly improved when combining AVHRR and AMSU, even with a simplified AVHRR algorithm taking only into account the T11 brightness temperature.

7.5 Remaining work

For the AVHRR algorithm refinements as outlined in section 6.5 are needed. The AMSU algorithm needs further tuning to winter cases (1 man-month). Finally some fine-tuning on how to best blend AVHRR and AMSU may be needed.

8 Conclusions and future activities

8.1 Summary of results from prototyping

Considerable progress in the prototyping of the SMHI NOAA/EPS and MSG/SEVIRI algorithms has been reached prior to MTR. This concerns especially the CMa, CTy and PC products. A major part of the prototyping work has been devoted to the fundamental CMa product.

The achievements can very shortly be summarised by the following:

Product CMa:

- A prototype is developed which is currently executed on a routine basis in a pre-operational computer environment.
- A complex threshold algorithm structure is applied (see Figure 3.3) in order to achieve an optimal adaptation to the current variations due to geography, illumination and meteorological conditions.
- Thresholds are dominantly defined in a dynamical way by utilisation of RTM cloud free radiance simulations, and have been verified against a large dataset of manually collected training targets.
- The algorithm have been successfully validated against a large database with Synop observations (section 3.4)

Product CT:

- A prototype is developed but not yet tested in an operational manner.
- The algorithm basically separates cloud types by use of thresholds, which are functions of viewing angles and vertical temperature profiles from NWP models, and by use of texture features.
- Thresholds have been defined by help of the training targets.

Product CTTH:

- A prototype version has been developed treating exclusively the opaque clouds.

Product PC SEVIRI:

- A prototype is developed, but not yet tested in an operational manner.
- Prototyping has been performed with a limited version, not taking into account the cloud type product as input. Results suggest that further tuning on the cloud type is needed and that an adaptation to winter conditions has to be performed.

Product PC AVHRR/AMSU:

- AMSU: An algorithm to retrieve precipitation likelihood based on the scattering signature of frozen precipitation sized particles has been developed. It works well over sea, coast and land for the identification of light to medium and intensive precipitation. Main shortcoming is that in certain cases spurious very light precipitation is reported. Tuning to winter conditions still has to be performed.
- AVHRR: Prototyping has been performed with a limited version, not taking into account the cloud type product as input. Results suggest that further tuning on the cloud type is needed and that an a adaptation to winter conditions has to be performed.
- AVHRR/AMSU: A limited prototype has been used to test the performance. Results for the combined product looked very good and deficiencies of both the AVHRR and AMSU algorithms were overcome.
- A prototype integrating all the above components in the SMHI pre-operational environment has been developed but not yet tested in an operational manner.

8.2 Remaining prototyping and validation tasks

For the CTTH product, parts of the prototyping work still remains uncompleted. Deviations from the development plan in Table 1.2 (section 1.3) can also be seen for the co-ordinated activities between SMHI and Météo-France (Step 3 in Table 1.2). The implications of those deviations are discussed later in section 8.4. .

For the other products, minor remainders from prototyping can be noticed.

A summary of the remaining work related to prototyping is given in the following with references to specific work packages in the updated project plan (UPP):

Product CMa:

- Finalise the definition and implementation of the aerosol flag algorithm.

Product CT:

- Definition of algorithm for the cloud phase flag -WP242241.
- Definitions of algorithm for the separation of cumuliform and stratiform cloud types (optional) – WP242241.
- Basic validation of prototyping results –WP242241.

Product CTTH:

- The prototype algorithm for opaque clouds will be implemented during spring 2000 – WP242233.
- Remaining development for the semi-transparent correction will be a limited effort of three man months between June and October 2000 to try to develop and implement the window-technique –WP242233.

Product PC SEVIRI:

- Probability tables for prototype to be derived on cloud type output –WP242243.

- Increase accuracy for the specifications of probabilities by creating separate index tables according to cloud types –WP242243.
- Tuning to surface temperature dependence, including adaptation to winter season–WP242243.
- Validation and possibly revised tuning according to Spanish Radar data to cover representative cases over the product output area–WP242243.

Product PC AVHRR/AMSU:

- For the AVHRR algorithm, tuning is needed to take both into account the surface temperature and the cloud type–WP242243.
- The AMSU algorithm needs more tuning for winter conditions–WP242243.
- Tuning of the combined algorithms for AVHRR and AMSU–WP242243.

8.3 Problems encountered

The discrepancies between SMHI achievements and the Project Plan (delay and tasks not fulfilled) are in essence due to the following factors:

1. Being a pilot SAF, the SAFNWC suffered from a very lengthy RADR process and unclear responsibilities as regards the host tasks (e.g. exchange of Project manager).

2. Some important, overall aspects of the EPS products have required considerable extra efforts from SMHI's part (See 2.1 regarding the EPS Software Package and 2.3 concerning the AVHRR level 1b data input).

3. Initial staffing problems at SMHI delayed the development work significantly.

4. SMHI has not been able to find a supplier of the necessary GOES imagery for the prototyping tasks.

5. The required effort for developing four NOAA/EPS products and one MSG/SEVIRI product and the contributions to the development of three additional MSG/SEVIRI products was heavily under-estimated.

6. The relevance and definition of WP's in the PP have in many cases not corresponded to the actual tasks. The actual amount of administrative tasks are not at all reflected in the PP.

8.4 Results of the co-operation between SMHI and Meteo-France

8.4.1 Details of the planned co-operation

According to the SAFNWC PP a rather close co-operation between SMHI and Meteo-France (CMS) was envisaged at the start of the SAFNWC project. This co-operation should cover three different aspects:

1. Harmonisation of cloud product output.
   (products CMa, CT and CTTH)
2. Adaptation of the SEVIRI CMa and CT algorithms to conditions at high latitudes.
   (SMHI to modify code for GOES prototype – WP242234, WP242321)
3. Sharing of tasks for the prototyping of the CTTH product.
   (SMHI to prototype window technique on NOAA and GOES and Meteo-France to prototype radiance rationing technique on GOES – WP242235, WP242322)

8.4.2 Achieved results

The first of the previously listed co-operation aspects has been realised at the time of the SAFNWC MTR. The cloud products output are consistent whether the source is SEVIRI or AVHRR. The second and third aspects were well prepared by the Meteo-France project team. Software code and accompanying material were made available to SMHI in connection with several bi-lateral meetings. An extended stay of one of the SMHI project team members at CMS further facilitated the conditions for the co-operation. Despite these facts, it has not been possible for the SMHI project team to complete the planned common prototyping tasks during the period defined in the PP. The reasons for this are mentioned earlier (8.4). Another factor is that the SMHI project team has given the highest priority to the prototyping of the NOAA/EPS products (according to the development strategy outlined in section 1.3).

8.4.3 Consequence for activities after MTR

. Due to the limited time remaining in the SAFNWC project, Meteo-France and SMHI have agreed to propose a removal of the two particular tasks from the remaining work packages in the UPP (*WP242234, WP242235, WP242321 and WP242322).*

The recommendations in sections 3.5 and 4.6 for a possible upgrading of the MSG/SEVIRI CMa and CT modules in the future must consequently be considered as suggestions for the phase following after the end of the SAFNWC project; the operational phase. The same is true for a possible incorporation of a complementary MSG/SEVIRI CTTH method based on the window technique. *We think that it is reasonable to conduct major validation of both the MSG/SEVIRI and the NOAA/EPS schemes over the same region (as envisaged for the operational phase in URD – **UR-7.2.4.4**)* before decision is taken of any software update. Such a methodology would give a more efficient harmonisation of the two schemes since it is not obvious that possible modifications must affect only the MSG/SEVIRI scheme. Also the NOAA/EPS scheme might need to adapt to features of the MSG/SEVIRI scheme. The initial set-up aiming exclusively at the adaptation of the MSG/SEVIRI scheme was in this respect not completely logical.

8.5 Plans for SEVIRI/AVHRR Final development

The MTR defines in principle the end of the basic SAFNWC prototyping work and accordingly, all of SMHI's products should by now be available in validated prototype form. This is not really the case for all products. However, it is envisaged that SMHI's tasks will eventually be in phase with the overall SAFNWC time schedule at the time of the integration phase (see UPP):

- The SEVIRI PC final prototyping and validation (WP242243) will be ready by October 2000 and implemented in the SMHI pre-operational environment (WP242323) according to schedule and thereby be delivered to the host as planned (WP243140).

- The AVHRR/CMa and CT products are in the near future in line with the PP.
- The AVHRR/AMSU PC final prototyping and validation (WP242243) will be ready by October 2000.
- The AVHRR CTTH final prototyping and validation (WP242233) will be ready by May 2000 (opaque clouds) and by October 2000, if quality is acceptable, with semi-transparency correction.

Dependant on an immediate solution for the (at the moment missing) integration task of the EPS Software Package, all AVHRR products can be in phase with the overall SAFNWC time schedule. Most urgent is the need for a EPS Software library which must be available at the latest in September 2000 in order to avoid delays in this and forthcoming phases (Pre-operational product validation and Software delivery to host).

Acknowledgements

The authors wish to thank Ralf Bennartz of the Free Univeristy of Berlin, Otto Hyvärinen of FMI and Øystein Godøy of DNMI, who have all contributed to the development of the prototype algorithms described in this report. Each of them stayed at SMHI during a short period, the visit being financed partly from the Visiting Scientist budget of the SAFNWC.

Thanks go also to Pia Hultgren of the Swedish Airforce, who indirectly has contributed to this work via the pilot study using the MSMS database for validating SCANDIA model.

Last but not least, the authors are grateful to Marcel Derrien and Herve Le Gléau at CMS, Météo-France for their generosity despite the often difficult conditions for co-operation. We have had fruitful discussions on the detailed content of the Cloud Products and algorithm development in general at several bi-lateral meetings.

A Appendices

A.1 Applicable documents

A.1.1 EUMETSAT SAFNWC planning and specification documents

ADD	Architectural Design Document
ICD	Interface Control Documents (requested input to MTR)
PP	Project Plan
UPP	Updated Project Plan (requested input to MTR)
SP	Science Plan (part of PP)
SRD	Software Requirements Document
URD	User Requirements Document, Issue 1.1 (SAF/NWC/INM/URD/1.1), 52 pp.

All documents are available at the SAFNWC host at http::/www.inm.es/wwg except documents ICD and UPP.

A.1.2 SMHI SAFNWC visiting scientist reports

VSci-1 Godøy, Ø., 1998: Cloud classifications in cold winter situations in northern Europe, SMHI Reports Meteorology, No. 94, September 1998.
Available at http://www.smhi.se/saf.

VSci-2 Hyvarinen, O., Karlsson, K.-G. and Dybbroe, A., 1999: Investigations of NOAA AVHRR/3 1.6 μm imagery for snow, cloud and sunglint discrimination, SMHI Reports Meteorology, No. 92, July 1999.
Available at http://www.smhi.se/saf.

VSci-3 Bennarz, R., Thoss, A., Dybbroe, A. and Michelson, D., 1999: Precipitation analysis from AMSU, SMHI Reports Meteorology, No. 93, November 1999. Available at http://www.smhi.se/saf.

A.1.3 Additional SMHI reports from SAFNWC prototyping

SMHI_1 Hultgren, P., Dybbroe, A. and Karlsson, K.-G., 1999: SCANDIA-its accuracy in classifying low clouds, SMHI Reports Meteorology, No. 91.

SMHI_2 Dybbroe, A. and Hultgren, P., 1999: The SMHI database Matching Satellite, Model and Synop data (MSMS) – User's manual – Ver1.00. Available at http://www.smhi.se/saf.

SMHI_3 Dybbroe, A., 1998: The AVHRR interactive training manager application – User's manual – Ver. 1.00, Available at http://www.smhi.se/saf.

SMHI_4 Dybbroe, A., 2000: The AVHRR cloud mask scheme of the SAFNWC, Presented at the 1999 Meteorological Satellite Data User's Conference in Copenhagen, September 6th-10th. Proceedings book in press. Available at http://www.smhi.se/saf.

SMHI_5 Karlsson, K.-G., A. Thoss, and A. Dybbroe. High resolution cloud products from AVHRR and AMSU. SAF Training workshop - Nowcasting and Very Short Range Forecasting, December 9th-11th, 1998. Eumetsat proceedings. ISBN 92-9110-030-7. pp. 180-190. Available at http://www.smhi.se/saf.

A.1.4 SMHI documents in relation to the "Python Issue"

SMHI_6 Moberg, M. and A. Dybbroe., 1998: Python in the NWCSAF? Paper prepared by SMHI on request from the SAFNWC steering group. Available at http://www.smhi.se/saf.

SMHI_7 Bolin, H., A. Dybbroe, and D. Michelsson., 1997: "SAF-ware" using Python: a modern and cost-effective development and production environment. A paper prepared by SMHI on request from the SAFNWC steering group. Available at http://www.smhi.se/saf.

SMHI_8 Bolin, H., 1997: Python in Remote Sensing. A paper prepared by SMHI on request from the SAFNWC steering group. Available at http://www.smhi.se/saf.

A.2 References

Arkin, P.A.,1979: The relationship between fractional coverage of high clouds and rainfall accumulations during GATE over the B-scale area. *Mon. Wea. Rev*.,**107**,1382-1387.

Ba. M.B. and A.Gruber, 1997:Satellite retrieval of hourly mean rain rate by synergistic use of Solar reflected Irradiance (3.9μm) and brightness temperature (11μm) derived from GOES-8. Proc. of the 1997 Meteorological Satellite Data Users Conference, Sep 29 – Oct 3,1997, Brussels, Belgium. Eumetsat.

Baum, B.,A., Q. Trepte, 1999: A grouped Threshold Approach for Scene Identification in AVHRR Imagery. *J. Atmos. Oceanic.Technology*., **16**, 793-800.

Bennartz, R., 1999a: On the use of SSM/I measurements in coastal regions. *J. Atmos. Oceanic.Technology*.,**16**, 417-431.

Bennartz, R., 1999b:Optimal convolution of AMSU-B to AMSU_A. *J.Atmos.Oceanic Technology*, in press.

Bennartz, R. and D.B. Michelson, 1999: Correlation of precipitation estimates from spacebourne passive microwave sensors and weather radar imagery for BALTEX PIDCAP. *Int. J. Remote Sensing*, submitted.

Bennartz, R., and G. Petty, 1999: The sensitivity of microwave remote sensing observations of Precipitation to ice particle size distributions. *J.Appl.Meteorol*. (Submitted).

Berendes, T.A., K.S. Kuo, A.M. Logar, E.M. Corwin, R.M. Welch, B.A. Baum, A. Pretre and R.C. Weger., 1999: A comparison of paired histogram, maximum likelihood, class elimination, and neural network approaches for daylight global cloud classification using AVHRR imagery. *J. Geoph. Res*., **104**, 6199-6213.

Chedin, A., N. A. Scott, C. Wahiche and P. Moulinier, 1985: *J. Clim. Appl. Meteor*., **24**, 124-143.

Derrien, M., Farki, B., Harang, L., LeGleau, H., Noyalet, A., Pochic, D. and Sairouni, A., 1993: Automatic cloud detection applied to NOAA-11/AVHRR imagery, *Rem. Sens. of Env.*, **46**, 246-267.

Derrien, M., L. Lavanant, and H. Le Gléau., 1988: Retrieval of the top temperature of semi-transparent clouds with AVHRR. *Proceedings of the IRS'88*, Lille (France), Deepack Publ., Hampton, pp. 199-202.

Evenden, Gerald I., 1990: Cartographic Projection Procedures for the Unix environment – A User's Manual. U.S. Geological Survey Open-File Report 90-284.

Eyre, J.R., 1991:A fast radiative transfer model for satellite sounding systems, *ECMWF Technical Memorandum*, No. 176.

Fischer, J., and H. Grassl, 1991: Detection of cloud top heights from backscattered radiances within the oxygen A band. Part 1: Theoretical study. *J. Appl. Meteorol*., **30**, 1245-1259.

Grody, N. C.,F. Weng and R. Ferraro,1999:Application of AMSU for obtaining hydrological parameters. Proc. of the fourth conference on microwave radiometry, Florence, Italy, March 1999, in press.

Inoue, T., 1985: On the temperature and effective emissivity determination of semi-transparent Cirrus clouds by bi-spectral measurements in the 10 μm window region, *J. Meteorol. Soc. Jpn.*, **63**, 88-99.

Karlsson, K.-G., 1996: Cloud classifications with the SCANDIA model, *SMHI Reports Meteorology and Climatology*, No. 67, 36 pp.

Karlsson, K.-G., 1997: Cloud climate investigations in the Nordic region using NOAA AVHRR data, *Theor. Appl. Climatol.*, **57**, 181-195.

Karlsson, K.-G. and Liljas, E., 1990: The SMHI model for cloud and precipitation analysis from multispectral AVHRR data, *SMHI PROMIS Reports*, No. 10, 74 pp.

Masuda, K., Takashima, T. and Takayama, Y., 1988: Emissivity of pure and sea waters for the model sea surface in the infrared window regions, *Rem. Sens. Environment*, **24**, 313-329.

Menzel, W.P., Smith, W.L. and Stewart, T.R., 1983: Improved cloud motion wind vector and altitude assignment using VAS, *J. Clim. Appl. Meteorol.*, **22**, 377-384.

Michelson, D.B., 2000:BALTEX radar data center products and their algorithms. RMK,SMHI,Norrköping,Sweden. (In preparation).

Prata,A.J., 1989: observations of volcanic ash clouds in the 10-12 mm window using AVHRR/2 data. *Int. J. Rem. Sens.*, **10**, 751-761.

Putsay, M., M. Derrien, H. Le Gléau and G. Monnier., 2000: *Comparison of two methods to estimate he cloud top temperature and pressure for NOAA-AVHRR and HIRS data*. Presented at the 1999 Meteorological Satellite Data User's Conference in Copenhagen, September 6th-10th. Proceedings book in press.

Rosenfield, D., and G. Gutman, 1994: Retrieving microphysical properties near the tops of potential rain clouds by multispectral analysis of AVHRR data. *Atmos. Res.*, **34**, 259-283.

Roujean, J.-L., Leroy, M. and Deschamps, 1992: A bi-directional reflectance model of the earth's surface for the correction of remote sensing data, *J. Geophys. Res.*, **97**, 20 455-20468.

Saunders, R. and Kriebel, K.T., 1988: An improved method for detecting clear sky and cloudy radiances radiances from AVHRR data, *Int. J. Rem. Sens.*, **9**, 123-150.

Smith, W.L., Woolf, H.M., Nieman, S.J. and Achtor, T.H., 1993: ITPP-5 – The use of AVHRR and TIGR in TOVS data processing, *Proc. Seventh International TOVS Study Conference, Igls, Austria, 10-16 Feb. 1993*, 443-453.

Snyder, John P., 1982: Map Projections Used by the U.S. Geological Survey. *Geological Survey bulletin 1532*. U.S. Department of the Interior.

Stowe, L., McClain, E.P., Carey, R., Pellegrino, P. and Gutman, G.G., 1991: Global distribution of cloud cover derived from NOAA/AVHRR operational satellite data, *Adv. Space Res.*, **11**, 51-54.

Tanré, D., Deroo, C. and Duhaut, P., 1990: Description of a computer code to simulate the satellite signal in the solar spectrum, the 5S code, *Int. J. Rem. Sens.*, **11**, 659-668.

de Valk, P., A. Feijt, J. Roozenkrans, and S. van der Veen., 2000: Cloud field Characterisation based on Meteosat Imagery and NWP model data. Presented at the 1999 Meteorological Satellite Data User's Conference in Copenhagen, September 6th-10th. Proceedings book in press.

Vermote, E., D. Tanre, J.L. Deuze, M. Herman, and J.J. Morcrette., 1997: 6S User's Guide version 2.

A.3 Acronyms

6S	Second Simulation of the Satellite Signal in the Solar Spectrum (RTM)
AAPP	ATOVS and AVHRR Processing Package.
AVHRR	Advanced Very High Resolution Radiometer (NOAA and EPS satellites)
AMSU	Advanced Microwave Sounding Unit (NOAA satellites)
APOLLO	AVHRR Processing scheme Over cLoud Land and Ocean
ASII	Automatic Satellite Image Interpretation, SAFNWC product 10
ATOVS	Advanced TIROS Operational Vertical Sounder
BRDF	Bi-directional Reflectance Distribution Function
BALTRAD	BALTEX Radar Network
CLAVR	Clouds from AVHRR
CMa	The Cloud Mask product
CMS	Centre de Meteorologie Spatiales (Météo-France, Lannion)
CRR	Convective Rainfall Rate, SAFNWC product 5
CTTH	The Cloud Top Temperature and Height product
CT	The Cloud Type product
EPS	EUMETSAT Polar System
FOV	Field-of-view
GOES	Geostationary Operational Environmental Satellite (USA)
GTOPO30	Global 30-Arc-Second Elevation Data Set
HLC	High Level Clouds (Cirrus including Nimbostratus and Cumulonimbus)
HIRLAM	HIgh Resolution Limited Area Model (developed by NMSs of the Nordic countries, the Netherlands, Ireland and Spain)
IFU	Frauenhofer Institut fuer Atmosphaerische Umweltforschung
INM	Instituto Nacional de Meteorología de España
IR	Infrared spectral region
LLC	Low Level Clouds (Fog, Stratus, Stratocumulus and Cumulus)
LMD	Laboratoire de Meteorologie Dynamique (Research facility in France)
LUX	Luminance Utilisee en eXploitation (CMS cloud classification scheme)
MOMO	Matrix Operator Model (RTM)
M-F	Météo-France
MLC	Medium Level Clouds (Altocumulus, Altostratus, Cumulus congestus)
MSG	Meteosat Second Generation

MSMS	The SMHI database Matching Satellite, Model and Synop data
MW	Microwave spectral region
NOAA	National Oceanographic and Atmospheric Administration (USA)
NMS	National Meteorological Service
NWP	Numerical Weather Prediction
PC	The Precipitating Clouds product
PGE	Product Generation Element
proj	USGS Cartographic projection library, available in C-code.
RGB	Colour composite images based on red, green and blue colour components
RTM	Radiative Transfer Model
RTTOV	Radiative Transfer model for TOVS radiance simulations (RTM)
SAF	Satellite Application Facility
SAFNWC	The SAF for support to NoWCasting and very short range forecasting
SAFOSI	The SAF for Ocean and Sea Ice monitoring
SCANDIA	The SMHI Cloud Analysis model using Digital AVHRR data
SEVIRI	Spinning Enhanced Visible and Infrared Imager (MSG satellites)
SMHI	The Swedish Meteorological and Hydrological Institute
SP	Science Plan
TBUS	TIROS Bulletin - United States (orbit prediction)
TIGR	TOVS Initial Guess Retrieval database
TOVS	Tiros Operational Vertical Sounder (on NOAA satellites)
UPP	(SAFNWC) Updated Project Plan
UR	User Requirement
URD	User Requirement Document
USGS	The United States Geological Survey, belonging to the ministry of interior
ZAMG	Zentralanstalt für Meteorologie und Geodynamik, Vienna.

A.4 Auxiliary data (used by the algorithms)

In the following a short description is given of the various kinds of auxiliary data sources which are used as input to the PGE's.

A.4.1 Land use (including land/sea mask)

The delineation of land and open water on a scale comparable to the sensors FOV is essential for all PGE's except for the SEVIRI and AVHRR Precipitating Clouds products. In addition the Cloud Mask utilise the actual land cover characterisation (or land use) within the AVHRR FOV.

The "Global 1km USGS Land Cover Characterisation database" (see http://edcwww.cr.usgs.gov/landaac/glcc/glcc_na.html) was chosen. This global dataset was generated in a joint effort of the U.S. Geological Survey (USGS), the University of Nebraska-Lincoln (UNL) and the European Commisions Joint Research Centre (JRC). Data are derived from one year of 1km AVHRR data (April 1992 till March 1993) and has a 1-km nominal resolution. The data are available on a continent-by-continent basis and share the same map-projections (Interrupted Goode Homolosine and Lambert Equal Area). From the continental datasets 6 different global thematic maps representing a different landscape based on a particular classification legend are available.

The regional data for the PGE's are based on the "Euroasia" (optimized for Europe) and "North America" datasets in the Azimuthal Equal Area projection. We use the 24 classes *USGS Land Use/Land Cover Scheme* (hereafter USGS-LU). Figure A.1 shows the Euroasia dataset using our own colour legend.

The land sea separation and resolution of lakes and water inlets has proven superiour compared to the pre-existing land-sea mask (restricted European coverage) used in the operational AVHRR environment at SMHI as well as the *Remote Sensing Forest Map of Europe*[2] (hereafter FM) also based on AVHRR data. However, both the USGS-LU and the FM seem to suffer from the same limitations in classifying and distinguishing between different vegetation types in a consistent way. Both these maps depict serious discrepancies to reality, e.g. in the case of delineation of forest and open land. They both show a general strong bias of too much forest in the Scandinavian Peninsula and too little over continental Europe.

Remote Sensing Forest Map of Europe: A contribution of the ESA to the Worls Forest Watch (WFW) project of the International Space Year (ISY).

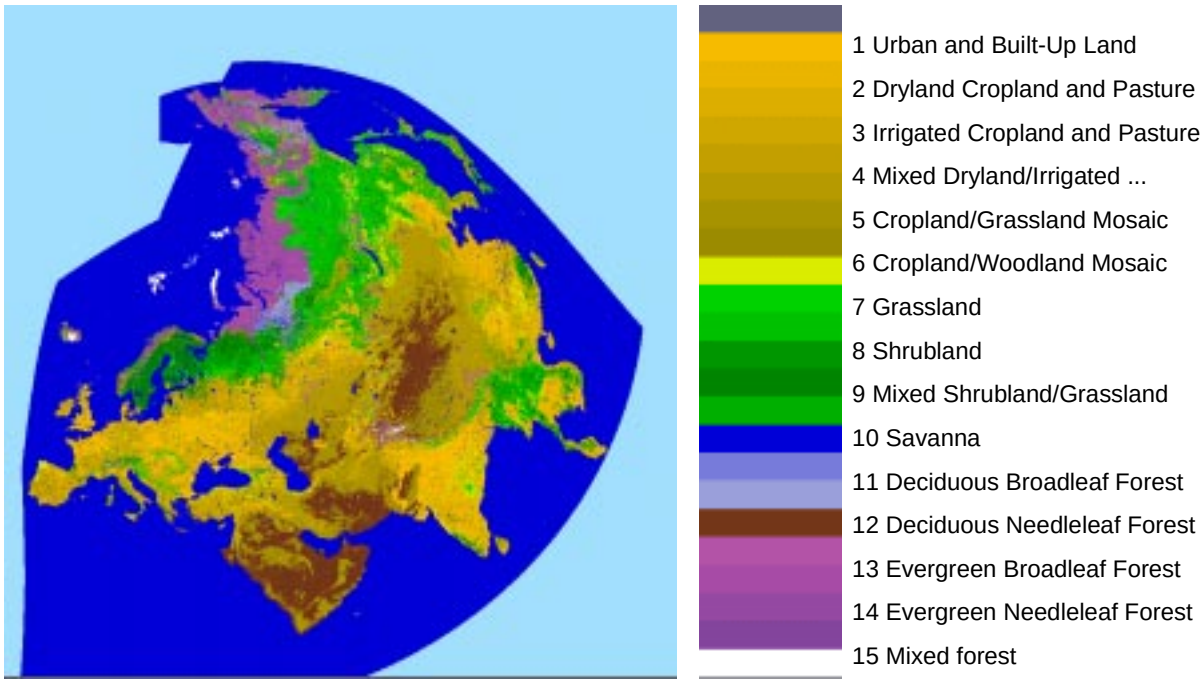

Figure A.1: The 24 classes USGS Land use scheme for the Euroasia area - Lambert Azimuthal Equal Area projection optimzed for Europe

The advantages of the USGS database over the Remote Sensing Forest map of Europe, as well as the general deficiencies of the AVHRR based datasets, is illustrated in Figure A.2. The data have been re-mapped to the same polar-stereographic map-projection. The reference is a 1 km land use dataset originating from the very high resolution (30 m) and accurate CORINE-3 database. This dataset has been compiled by Gerhard Smiatek at the Frauenhofer Institut fuer Atmosphaerische Umweltforschung (IFU) in Garmisch Partenkirchen, Germany. The area of interest here is the small forest “Grib Skov” west of the lake “Furesø” in Northern Zeeland, Denmark. The forest is placed too far east in the FM data and the lake is missing. In the USGS-LU data the lake seems correctly placed (comparison with accurate standard cartographic maps have been done) but the forest is slightly mis-placed and too little in size. The CORINE-3 data are both in the case of the lake and the forest more in agreement with reality.

A.4.2 Fraction of land

All PGE’s, except the SEVIRI PC and the AVHRR PC algorithms, needs information about the position of the footprint in relation to the coastal zone. There are two possible configurations of interest here:

1. The FOV may contain a mixture of land and open water
2. The footprint is near the coast and due to inaccuracies in the satellite navigation the true surface cannot be determined with a high confidence.

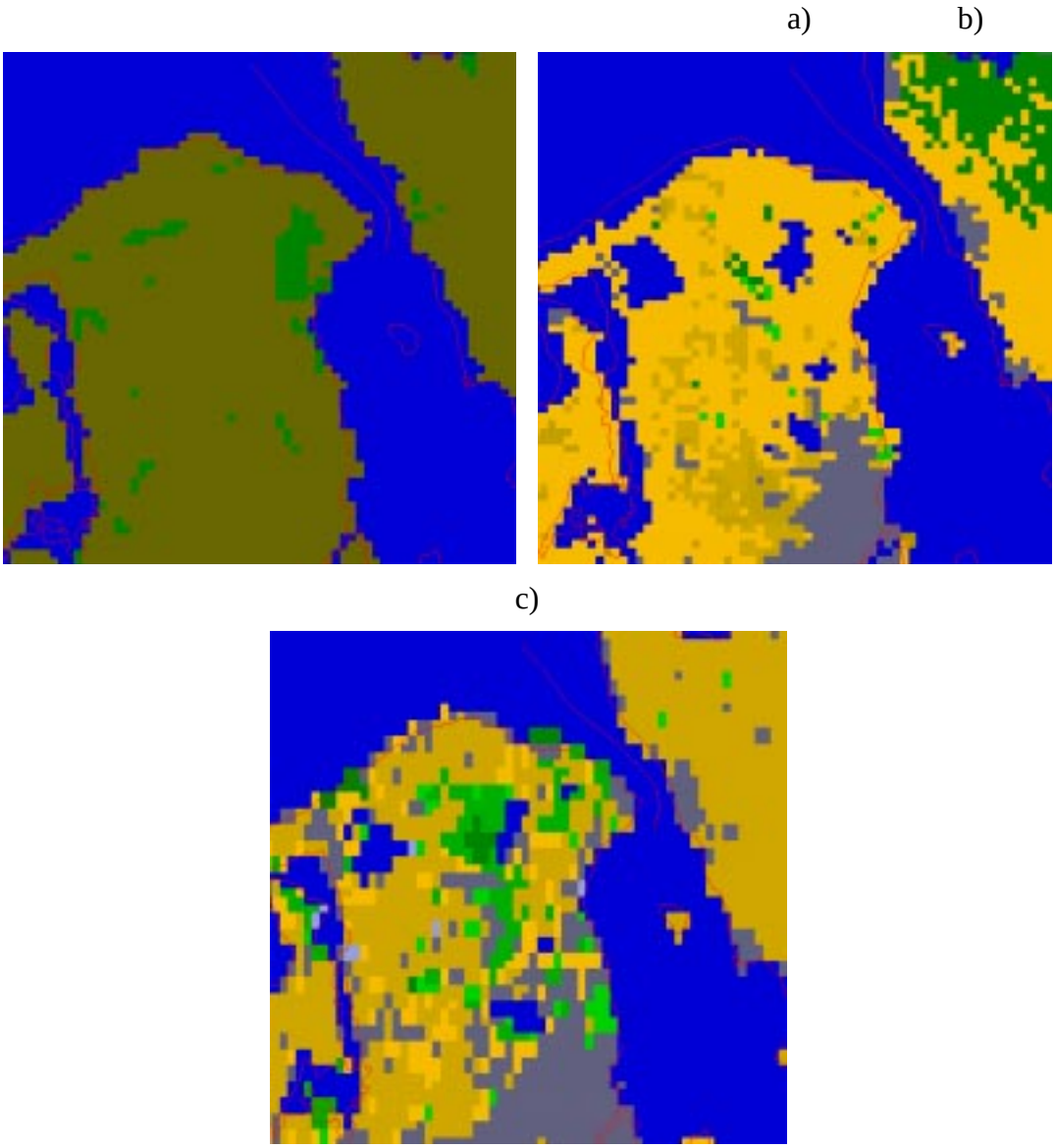

Figure A.2:North Zeeland (Denmark) as seen from the Remote Sensing Forest Map of Europe" (a), the USGS Land Use Characterization (b), and the Corine land use database.

The first point is of great importance for the AMSU retrieval due to the large FOV, whereas the last point is of importance mainly for the AVHRR-algorithms of the CMa and CT.

The *fraction of land* data is derived from the land use data presented above by calculating the local mean using a quadratic kernel of size 11x11 pixels.

A.4.3 DEM data

Digital elevation model data (hereafter *elevation*) are used in the all PGE's. Regional elevation maps in 1m resolution are derived from the *Global 30-Arc-Second Elevation Data Set* (GTOPO30) avaialble from the U.S. Geological Survey (http://edcwww.cr.usgs.gov/landdaac/gtopo30/gtopo30.html). GTOPO30 has a horizontal resolution of 30 arc-seconds, approximately 1km, and is compiled from different raster and

vector sources of topographic information. GTOPO is the result of an international collaborative effort led by the USGS.

The quality of the data has proven beyond the rather basic needs for topography information needed in all the PGE's.

A.4.4 NWP model data

In order to adapt the satellite retrievals as much as possible to the prevailing atmospheric environment we have chosen to utilise short range forecasts of a number of parameters, but mainly temperature and humidity, from available NWP models. Output from the 44km resolution limited area model HIRLAM at SMHI has been used during prototyping. The forecast parameters used by the PGE's are tabulated in Table A.1.

The HIRLAM output is given on a rotated longitude-latitude grid and data are stored using the GRIB-format. The surface temperature and humidity is extracted directly from the model-level data and re-mapped to a polar-stereographic map-projection using the Cartographic projection library, *Proj*, developed at the USGS. (See Snyder (1982) and Evenden (1990) for details on the various map projections and how they can be applied in the Unix environment.) The temperature and humidity at pressure levels and the total precipitable water are derived in a post-processing step before re-mapping.

Table A.1: NWP output parameters used by the five product generation elements

NWP output parameter	Used by
Surface temperature	PGE1b – 4b
Surface humidity	PGE3b
Surface pressure	PGE3b
Surface geopotential	PGE3b
Temperature at pressure levels	PGE1b-3b
Humidity at pressure levels	PGE3b
Total Precipitable water	PGE1b & PGE2b

The HIRLAM forecasts are available in 1-hour resolution, and a model run is ready three to four hours after time of analysis. However, only forecast lengths between 6 and 17 hours are allowed for, due to the inherent spin-up time of the model. The shorter and longer forecast lengths of this interval get less priority when identifying a valid model time.

A.5 Interactive training targets

A dedicated application was developed for the gathering of training and validation data. The application consists of a GUI-tool developed in Python and Tk/Tkinter and various I/O routines and help functions for browsing through and analysing the results. A description of the tool is described in detail in SMHI_3.

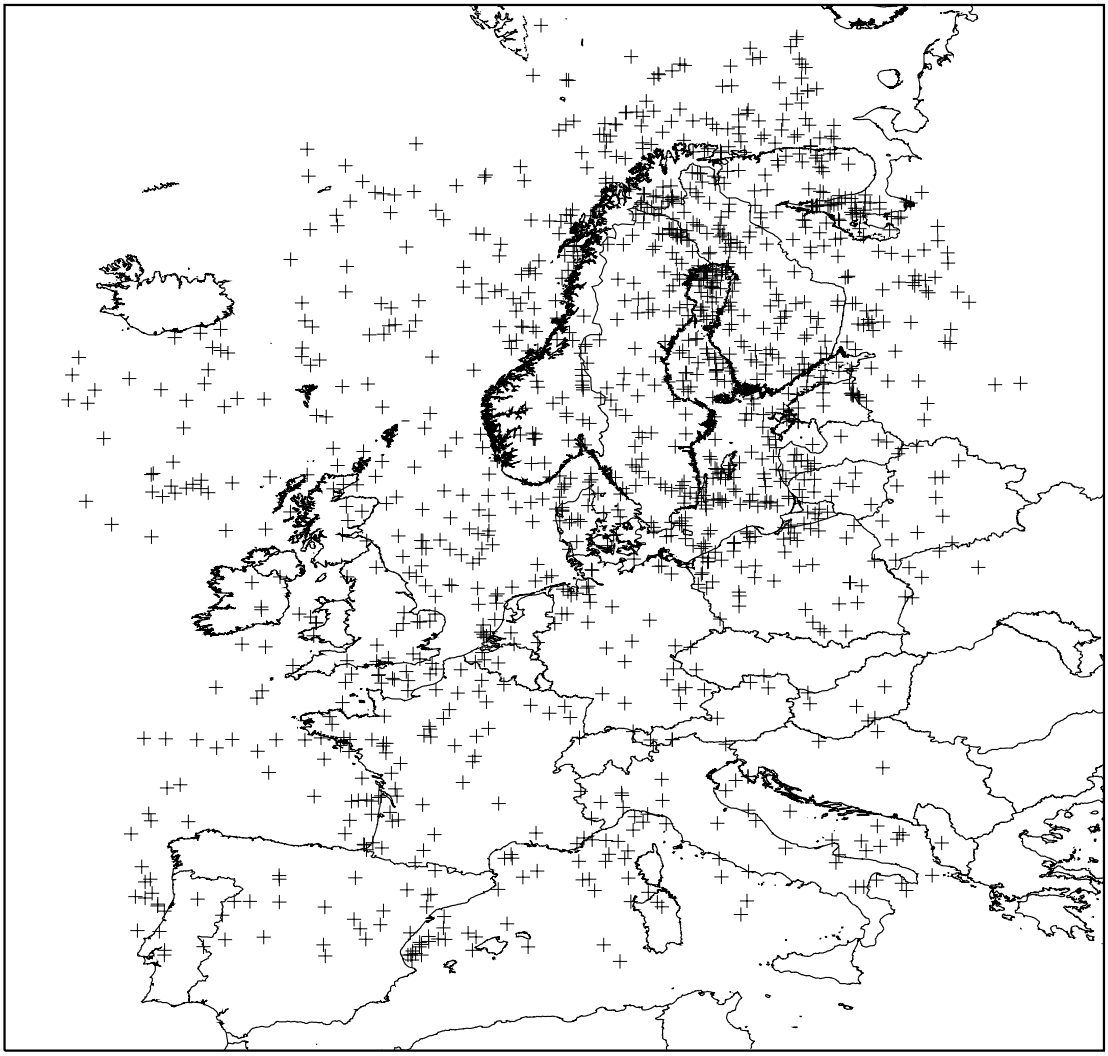

Figure A.3: All datasets of the training target database containing channel 3a data.

Mainly two operators, Gunhild Olofsson (SMHI) and Otto Hyvärinen (FMI) did the actual interactive collection of targets. In total the database consist of 3723 datasets. Here 2873 are for day cases, and 1353 contains the 1.6 μm channel data. A map of the geographical distribution of targets containing channel 3a data is hown in Figure A.3.

A.6 The database matching satellite, NWP model, and synop data (MSMS)

Software to automatically extract and co-locate satellite data, NWP model output and Synop reports in the SMHI environment was developed in the beginning of 1998. For each 3-hourly Synop report satellite data, of the NOAA AVHRR pass closest in time, are extracted over a small region (32 by 32 pixels) centred at the station. The vertical temperature and humidity profile and various surface parameters of a HIRLAM short range forecast at the grid point closest to the station is appended, and the information is stored in the database.

Data for a carefully selected set of Synop stations, known to provide reliable reports, has been gathered on a routine basis since June 6th, 1998. In addition to the quality criterion the stations were selected so as to cover most of northern Europe, that is Scandinavia and neighbouring countries, and so as to include inland, coastal and mountainous stations. In July 1999, the set of stations was extended to include more stations in central Europe, and also some Arctic stations (Bjørnøya and Svalbard).

The MSMS database contains today 81 Synop stations distributed over central and northern Europe. The total number of matchup's per month until the end of 1999 is given in Table A.2. The grand total until the end of 1999 is 104899.

Table A.2: Summary of contents in the MSMS database (end of 1999)

Month	Jun-98	Jul-98	Aug-98	Sep-98	Oct-98	Nov-98	Dec-98
Number	1148	2937	2555	2891	3078	1962	4013
Month		Jan-99	Feb-99	Mar-99	Apr-99	May-99	Jun-99
Number		5818	4503	6020	7010	6601	7540
Month		Jul-99	Aug-99	Sep-99	Oct-99	Nov-99	Dec-99
Number		9572	9739	6111	10403	8868	4130

More details on the MSMS database can be found in the MSMS User's Manual [SMHI_2].

A.7 *The AMSU, AVHRR, weather radar matchup database*

In the framework of the SAFNWC, SMHI has been building up a database for validating satellite retrievals at high latitude. It consists of NOAA-15 overpaths, processed with AAPP, and of BALTRAD Radar composites (described in more detail in the following section). Since 1 April 1999, the following input has been archived continuously:

Locally received NOAA-15 overpaths, processed with AAPP:

- AVHRR, level1b
- AVHRR, level 1c (local format) at reduced resolution (every 5th pixel in every 5th line)
- AMSU-A, level1c
- AMSU-B, level1c

BALTRAD radar composites containing radar reflectivity factor data (dBZ).

For the development presented in this report a subset spanning 1 April –30. September 1999 has been used. Only overpaths for which radar echoes were reported have been considered.

For the development of the AMSU precipitation algorithm 140 overpaths have been used. For the development of the AVHRR precipitation retrieval 110 overpaths were used (selection criterion was that at the overpath had to contain at least some pixels for which the sun stood more than 10 degree above the horizon.

For comparing AMSU and radar data, the radar data was convolved to AMSU-A and AMSU-B resolution respectively. The principle of the methodology is outlined in Bennartz (1999a) and Bennartz and Michelson (1999).

The distribution of the AMSU data in land, coast and sea is given in Table A.3.

Table A.3: Total amount of AMSU data used in the development.

	Total number of pixels	Land [%]	Coast [%]	Sea [%]
AMSU-A	115165	43.8	50.0	6.2
AMSU-B	1046797	50.5	39.9	11.6

A.7.1 BALTRAD radar data

The Baltic Sea Experiment (BALTEX) is a European regional project within the Global Energy and Water Cycle Experiment. (GEWEX), with contributions from 10 countries within the Baltic Sea's drainage basin. The BALTEX Main Experiment commenced it's so-called Pilot Phase on 1 April 1999. The BRIDGE Base-Line Period commenced on 1 October 1999 and is presently scheduled to last until 28 February 2002.

Within the Framework of BALTEX, a Radar Data Centre (BRDC) has been established at SMHI for collecting data from as many radars in, or proximate to the BALTEX Region as possible, deriving homogeneous data sets and archiving the data sets. During the BRIDGE Pilot Phase, data was available from 25 radars in six countries. Most of these radars operate at C-band (5cm), while two operate at X-band (3cm). The majority of the radars have Doppler capacity. Their maximum operational ranges are 200-250km and the horizontal resolution of the data is commonly 2km. With the exception of four radars, which produced reduced depth data, reflectivity factor data is available in 8-bit depth.

Those products being produced at the BRDC are presented in Michelson (2000). For the collocations with AMSU, the radar data has been corrected for their range dependence and bias adjusted using gauge adjustments (Koistenen and Puhakka, 1981; Michelson, 2000).

A.8 RTM simulations

A.8.1 TIGR dataset

The IR radiative transfer simulations for the derivation of IR-thresholds for the Cloud Mask and Type are done on a global dataset of atmospheric radiosoundings taken from the TIGR-3 database, and kindly provided by Noelle A. Scott at LMD. See Chedin et al. (1985).

The TIGR atmospheric profiles suffer from having no surface temperature. Therefore simulations were done setting the surface temperature, needed as input to the RTM, in steps of [+5K;0K;-5K] around the temperature at the lowest level (at 1000 hPa).

A.8.2 AVHRR spectral response functions

The RTM simulations for the derivation of cloud free TOA radiances need as input the spectral response of the given sensor channel. These normalised response functions, or filter functions, have been obatined by NOAA and from the 6S code. The curves shown in Figures A.4 and A.5 are valid for NOAA 15.

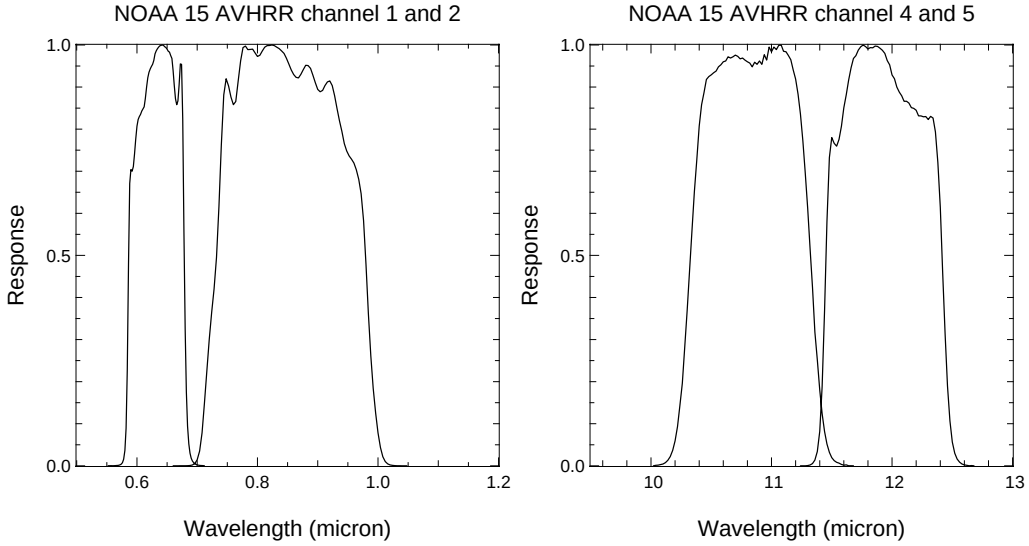

Figure A.4:The AVHRR spectral reponse functions for channels 1, 2, 4 and 5 for the NOAA 15 satellite.

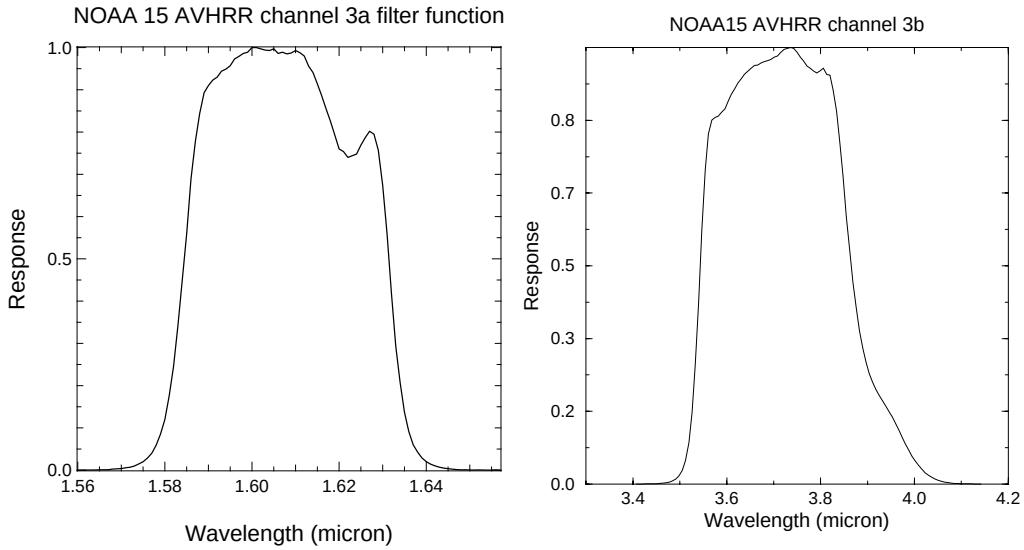

Figure A.5: The AVHRR spectral response functions for channels 3a and 3b for the NOAA 15 satellite.

A.8.3 RTTOV

RTTOV is a fast radiative transfer model intended for the assimilation of satellite sounder or imager radiances in a variational assimilation scheme (for example a 4D-Var scheme of a NWP model).

Even though the RTTOV model was specifically developed for sounding channels (HIRS) it allows for the processing of several sensors including the AVHRR and Meteosat. Besides the emissivity the model takes as input the vertical temperature and humidity (and optionally the ozone) profile specified at 40 standard levels, and the surface temperature, humidity and pressure.

The first version of RTTOV (RTTOV-3) is described by Eyre (1990). The RTTOV code, including the gas transmittances at AVHRR and GOES channels, used in this development was kindly made available from Pascal Brunel at CMS, Meteo-France. The obtainded code has been sligthly modified at CMS to allow surface emissivities different from one, and also the ozone treatment has been improved.

The latest version (RTTOV-5) has recently been obtained from ECMWF. Documentation can be found in a technical memorandum of the ECMWF (see Saunders et al., 1999).

A.8.4 6S

6S is a radiative transfer model enabling the simulation of visible to near infrared satellite signals for pre-defined or user-defined spectral channels, taking into account the absorption due to atmospheric gasses and the aerosol scattering, and allowing for non-lambertian surface conditions. The gasses considered are water vapour, CO2, O3, O2, NO2, CH4, and CO. A number of BRDF models are available to choose from. Also spectral channels from a number of satellite sensors (including AVHRR on NOAA 12,14, and 15) are prepared for via the description of the spectral response functions. Clouds are not considered.

6S is the improved version of 5S developed by the Laboratoire d'Optique Atmosphérique in the mid eighties.

We optained the version 4.1 of the computer code and associated documentation from the ftp-site kratmos.gsfc.nasa.gov (person of contact is Eric Vermote, eric@kratmos.gsfc.nasa.gov).

The code was easy to install, the manual (Vermote et al., 1997) is well written, and the program is easy to use.

A.8.5 MODTRAN

MODTRAN is the follow on to the radiative transfer model LOWTRAN7. MODTRAN is developed at the Phillips Laboratory Geophysics Directorate, U.S.A. It is a rather extensive and complex model, and therefore requires much computation time. The model coveres the spectrum from the visible to the infrared, and accounts for a wide varity of atmospheriic effects (gaseous absorption, aerosol scattering and clouds).

We obtained the version 3.7 of the source code and the associated documentation via ftp, after contacting Gail Andersson at the Phillips Laboratory (mail: gandersson@plh.af.mil).

We used the MODTRAN mainly to check the consistency of our simulations with RTTOV. See section below. For cloudy simulations, useful especially in the development of the PC product we used the Matrix Operator Model (MOMO).

A.8.6 Modtran/RTTOV comparisons

We made a comparison study simulating cloud free radiances for a number of standard atmospheres using RTTOV and Modtran. Deviations in brightness temperatures in nadir view were small (within ~1K) but increasing to a bias around 10% towards the edge of the AVHRR swath. Though significant this discrepancy was not found critical and therefore the RTTOV model, being both faster and much easier to handle, was used throughout the development with derivations of cloud free IR thresholds.

A.9 Defining the Channel 3.7μm reflectance

The monochromatic reflectivity (or reflectance) ρ_λ is the ratio of the reflected (backscattered) radiance to the incident radiance. In the case of solar reflection one can write:

$$\rho_\lambda = \frac{L_\lambda}{\mu_0 L_{\lambda 0}}$$

where L_λ is the measured radiance, $L_{\lambda 0}$ is the incoming solar radiance, and μ_0 is the cosine of the solar zenith angle θ_0.

Assuming the solar radiance is independent of direction, the equation for the reflectance can be written in terms of the solar flux $F_{\lambda 0}$:

$$\rho_\lambda = \frac{L_\lambda}{\frac{1}{\pi}\mu_0 F_{\lambda 0}}$$

For 3.7μm channel the outgoing radiance is due to solar reflection and thermal emission. Thus in order to determine a 3.7μm channel reflectance, it is necessary to subtract the thermal part from the satellite signal. To do this, the temperature of the observed object is needed. The best candidate available is the channel 4 brightness temperature, since most objects behave approximately as blackbodies in this spectral interval.

The 3.7μm channel reflectance, $\rho_{3.7}$ for simplicity, can thus be written as

$$\rho_{3.7} = \frac{L_{3.7} - \varepsilon_{3.7}\int_0^\infty \Phi_{3.7}(\lambda) B_\lambda(T_{11}) d\lambda}{\frac{1}{\pi}\mu_0 F_{3.7,0}} \qquad (1)$$

where $L_{3.7}$ is the measured radiance at 3.7μm, $\Phi_{3.7}$ (λ) is the 3.7μm channel spectral response function, B_λ is the Planck function, and T_{11} is the 11μm channel brightness temperature.

If the observed object is optically thick (transmittance =0)

$$\varepsilon_{3.7} = 1 - \rho_{3.7}$$

and using this in equation (1) one gets:

$$\rho_{3.7} = \frac{L_{3.7} - \int_0^\infty \Phi_{3.7}(\lambda) B_\lambda(T_{11}) d\lambda}{\frac{1}{\pi}\mu_0 F_{3.7,0} - \int_0^\infty \Phi_{3.7}(\lambda) B_\lambda(T_{11}) d\lambda} \qquad (2)$$

If the satellite observation is given in brightness temperature, than the corresponding radiance can be derived by folding the spectral response with the Planck function:

$$L_{3.7} = L_{3.7} - \int_0^\infty \Phi_{3.7}(\lambda) B_\lambda(T_{3.7}) d\lambda$$

A.9.1 Determination of the solar flux

Values for the 3.7μm channel solar flux were derived from tabulated values of "reflected solar radiance by a perfect diffusive reflector" published on the Internet by Bryan A. Baum (http://asd-www.larc.nasa.gov/~baum/). See also Baum and Trepte (1999). For NOAA 12 the derivation looks like this:

$$F_{3.7,0} = \pi w_{3.7} \cdot 5.213 \frac{mW}{m^2 \cdot sr \cdot cm}$$

where $w_{3.7}$ is the equivalent width of the spectral response function. Since the width is needed in wavenumbers ($k=1/\lambda$) we have

$$w_{3.7} = \int_0^\infty \Phi_{3.7}(k) dk = \int_0^\infty \frac{\Phi_{3.7}(\lambda)}{\lambda^2} d\lambda$$

Thus for NOAA 12 $F_{3.7,0} = 4.4303 W/m^2$.

A.10 Derivation of effective cloud droplet radius

As a mean to assess the microphysical properties at cloud top independent of viewing geometry, we developed a retrieval scheme for the effective cloud droplet radius at cloud top. It is based on radiative transfer simulations of backscattered solar radiation in the 0.6μm and 3.7μm channels. The radiative transfer calculations were inverted using a neural back propagation network to retrieve the effective radius.

A.10.1 Radiative Transfer Model

We used the radiative transfer model MOMO of the Free University of Berlin (Fischer and Grassl, 1991, Fell, 1997). It is an adding and doubling model and thus incorporates scattering processes of all orders. The output is spectrally averaged radiances for discrete azimuthal, solar and viewing angles. The absorption of atmospheric gases was calculated using the HITRAN92 database (Rothman et al., 1992) and taken into account using an exponential sum fit of transmission functions (Armbruster and Fischer, 1996). Continuum absorption of water vapour was taken into account as contribution of far wings of absorption lines(Clough et al. 1989 and 1992) using coefficients of Clough (1996).

Both Rayleigh and Mie scattering are included in the model. The wave length dependence of the phase functions is explicitly taken into account. The zenithal and azimuthal dependence of the radiative transfer is decoupled by developing the azimuthal dependence into a Fourier series. Because of computing time constraints, only 50 Fourier terms have been taken into account. This necessitated that for strongly forward peaking phase functions it was necessary to perform a phase function truncation (Potter, 1970) and thus to add the truncated part of the forward peak to the direct solar term. The zenithal dependence on viewing and sun angle was taken into account with six Gaussian quadrature points (0˚, 19.11˚, 34.99˚, 50.74˚, 66.45˚ and 82.15˚).

A.10.2 Model atmosphere and clouds

All cloud RT simulations were performed for a mid-latitude summer atmosphere containing 56 layers (100m from ground to 2000m, 200resolution from 2000m to 6000m and 400m resolution from 6000 to 10000m plus 5 additional layers up to 100000m height). The atmospheres contained maritime aerosol with an optical thickness of 0.15. At the ground a water surface with zero albedo was assumed, which means that simulation results are not strictly valid for optically thin clouds, sunglint and land areas. Since we planned to perform the radius retrieval over land as well, we used only simulations for the inversion which resulted in a reflectivity of at least 0.4. The simulations were performed using NOAA11 filter functions. For the 0.6μm channel the half-power points were considered, the 3.7μm channel was split up into five wavelength intervals of 100nm each to account for the strong variation of the scattering properties for this wavelength band.

For the droplet size spectra a modified gamma-distribution according to Hansen (1971) with a standard deviation of 0.111 was chosen. All water and ice particles were considered as spherical. Clouds were implemented to be vertically homogeneous in extinction and effective radius. The simulation data set contains 624 simulations for effective radii between 4μm and 32μm (4, 6, 8....20, 24,28, 32). The extinction per kilometre is taken between 15 and 40. For each radius two realisations of extinction per kilometre are calculated by randomly selecting the cloud base (between 100m and 9600m) and cloud top (between 3000m and 10000m)

under the constraint that the cloud thickness has to be positive. The resulting maximum liquid water content is thus 1.25g/m^3, the resulting optical thickness varies between 7.5 and 400. Clouds which have a top warmer than -5°C are classified as pure water clouds and clouds with tops colder than -20°C as pure ice clouds. Between -5°C and -20°C the ice content is chosen randomly (0%,25%,50%,75%,100%), which results in an overrepresentation of mixed cloud phases as compared to phase distribution in real clouds, but gives the possibility to investigate possibilities to retrieve cloud phase. For each cloud simulation, results are available for all combinations of 6 sun angles, 6 viewing angles and 17 azimuth angles (between 0°-180°).

A.10.3 Neural network retrievals

The simulations were inverted using a back propagation network (courtesy of René Preusker, Freie Universitaet Berlin). The simulation data set of 624 simulations times 612 angles resulted in a simulated data set of 381888 simulated bi-spectral observations. From these a training and test data set of 10000 simulated observations each with reflectances in the 0.6 μm channel of at least 0.4, were extracted randomly for the training of the neural network.. This reflectivity threshold was introduced keeping in mind that the application of the effective radius was to identify precipitation cases. It was also necessary in order to be able to apply the retrieval over land and sunglint as well, and thus minimise detrimental influences of ground albedo variations. To achieve a satisfactory retrieval of the effective radius, it was necessary to feed the net with the full geometry information and use a hidden layer with a minimum of ten nodes. Best results were achieved when training the net with the 0.6- μm reflectance and the ratio of the 0.6 μm/3.7 μm reflectances. It was neither possible to simultaneously nor to separately retrieve the optical thickness of the cloud. This was probably due to thresholding the reflectivity, thus a large part of training data set was in a region where the 0.6 μm signal was almost saturated.

The final architecture of the net was:

- 5 input nodes (sun-satellite azimuth, sun angle, viewing angle, 0.6 μm reflectance, 0.6 μm/3.7 μm)
- 1 hidden layer with 10 nodes
- one output layer (effective radius)

Different versions of the network were trained for all cloud phases simultaneously and for each cloud phase separately. The network usually converged after ingesting about 7000 simulated observations.

The accuracy of the retrievals when applying them to the full simulation data set is given in the table below. Whereas the networks were trained without noise, a constant noise according to the NOAA channel specifications was added in the retrieval. Training the networks on noisy data as well might yield slightly better retrieval results. It became clear however, that for an efficient effective radius retrieval, the cloud phase should also be known. The bias in the table below is calculated as real radius minus retrieved radius. In applications to real data, only the network trained on all phases was used.

Applied neural net ▶ / Real phase ▼	Water phase	Ice phase	Mixed phase	All phases
Water	Bias 0.05 RMS 2.03	Bias 4.37 RMS 5.74	Bias 2.34 RMS 4.15	Bias 1.16 RMS 3.62
Ice	Bias –5.85 RMS 7.54	Bias 0.24 RMS 3.19	Bias –2.81 RMS 4.72	Bias -2.96 RMS 5.03
Mixed	Bias –2.83 RMS 4.93	Bias 2.99 RMS 4.74	Bias 0.21 RMS 3.64	Bias –0.42 RMS 3.94

Table 8-1: Performance of different versions of the neural networks when applying them to the whole simulation dataset, split up in cloud phases. Bias and root mean square differences are given.

A.10.4 Possible shortcomings of the methodology:

Simulation part:

- Mie scattering also applied for ice particles
- zero surface albedo not strictly applicable over land and sunglint, even for thick clouds.
- filter functions of NOAA 11 used, but applied to NOAA15
- possibly too low angular resolution
- cloud model with homogeneous drop size distribution and concentration throughout cloud.
- three dimensional effects not taken into account
- still debate on reasons (or existence) of "abnormal absorption" in clouds, which seems to lead to an overestimation of retrieved effective radius as compared to in situ measurements for several authors.
- model cloud data set might not have been fully representative of actual cloud type distribution in real data.

- Application to data:
  uncertainties in 0.6μm channel calibration (pre-launch).
- uncertainties when removing the thermal component of the 3.7 μm channel (methodology see Appendix A9)
- overall the retrieved effective radius seems overestimated, whereas the distribution of relative radius size looked realistic.

After studying the results of applying the effective radius retrieval on NOAA15 data we concluded however, that the prerequisite of large radii to initiate precipitation seems to be fulfilled, but that large droplet radii are not necessarily an indicator for precipitation (see also section 6.2). The simple radiance ratio of the 0.6μm/3.7μm seems to be a slightly superior predictor of precipitation than the effective radius retrieved with the technique mentioned above. Since it is computationally significantly cheaper not to retrieve the effective radius for large parts of a satellite scene, no further development time was invested in possible refinements of the effective radius retrieval.

A.10.5 References

Armbruster, W., J. Fischer, 1996: Improved method of exponential sum fitting of transmission functions to describe the absorption of atmospheric gases. Appl. Optics 35, No. 12, pp 1931-1941.

Clough, S.A., F.X. Kneizys, E.W Davies, 1989: Line shape and the water vapor continuum. Atmos. Res. , Vol. 23, pp 229-241.

Clough, S.A., M.J. Iacono, J.-L. Moncet, 1992: Line-by-line calculations of atmospheric fluxes and cooling rates: applications to water vapor. J. Geophys. Res., Vol. 97, pp15761-15785.

Clough, S.A., 1996: Personal communication.

Fell, F., 1997: Validierung eines Modells zur Simulation des Strahlungstransports in Atmosphäre und Ozean, Beiträge zur Fernerkundung, Heft 7, Institut fuer Weltraumwissenschaften, FU Berlin.

Fischer, J., H. Grassl, 1991: Detection of cloud top heights from backscattered radiances within the oxygen A band. Part 1: Theoretical study. J. Appl. Meteorol. Vol. 30, pp. 1245-1259.

Hansen, J.E., 1971: Multiple scattering of polarized light in planetary atmospheres. Part II: sunlight reflected by terrestrial water clouds. J. Atmos. Sci. Vol. 28, 1400-1426.

Potter, J.F., 1970:The delta functin approximation in radiative transfer theory. J. Atmos. Sciences, Vol. 27, 943-949.

Rothman, L.S., R.R. Gamache, R.H. Tipping, C.P. Rinsland, M.A.H. Smith, D. Chris Benner, V. Malathy Devy, J.-M. Flaud, C. Camy-Peyret, A. Perrin, A. Goldman, S.T. Massie, L.R. Brown, R.A. Toth, 1992: The HITRAN molecular database: editions of 1991 and 1992. J. Quant. Spectrosc. Radiat. Transfer, Vol. 48, 469-507.

A.11 The SMHI web site and product visualisation

A web site for the contribution of SMHI to the SAF projects in general was set up in October 1999 prior to the SAFNWC Demonstration Experiment where near real time products were demonstrated to the public during one month. The address of this site is **http://www.smhi.se/saf/**, and besides general information about the SMHI engagement in the SAF projects, and a description of the cloud and precipitation products developed for the SAFNWC, products are demonstrated in near real time as derived images.

Below we provide some derived images of the four products from the AVHRR/AMSU prototype algorithms, and give examples of how the products can be visualised for the user. However, it is important to stress that the products are not images but gridded data. At first hand the products are rather thought to be used digitally (exploring the full content also of the additional flags) as input to mesoscale analysis models or directly into objective Nowcasting schemes.

Therefore the colour look-up-tables used to display the products as images may be freely chosen by the user. Here we employ the same LUT's as used on the web site.

A.11.1 Cloud Mask

Below (see figure A.6) is an example of the cloud mask output displayed using orange colouring for the cloud filled pixels, and grey for the cloud contaminated pixels. A land-sea mask (in this case a land use map) can be used to devide the cloud free category into cloudfree land (green) and cloudfree sea (blue). Coast lines (white) have been added as overlay. Unprocessed data (outside AVHRR swath) have been assigned black.

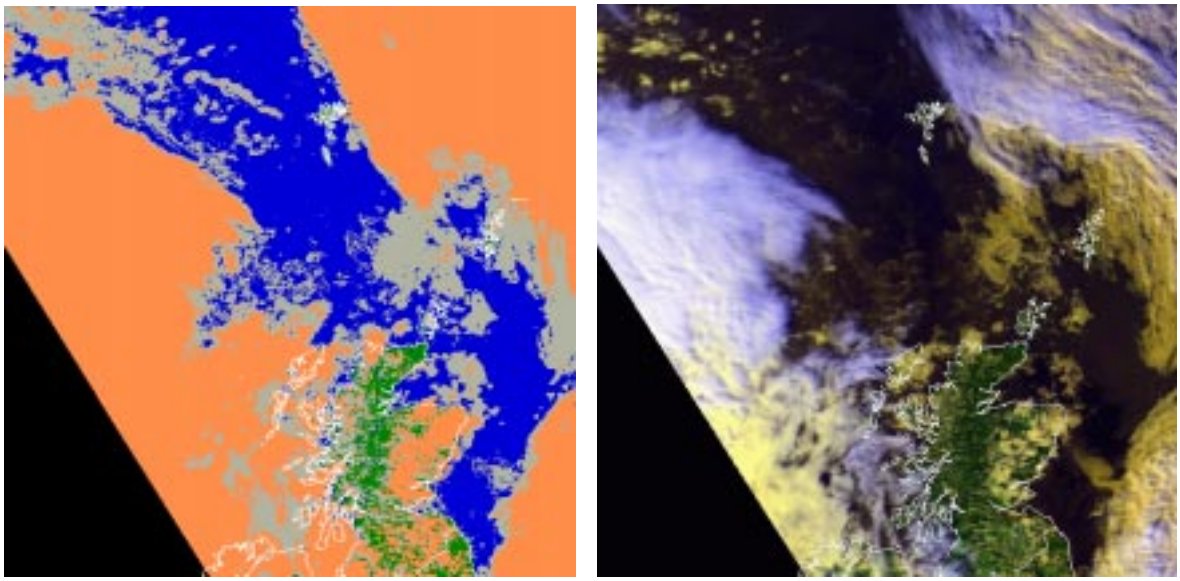

Figure A.6: Derived colour image showing the result of the Cloud Mask (left) for a NOAA 14 passage at 14:06 UTC September 5th, 2000, and the corresponding channel 1,2,4 RGB-composite image (right).

The example in figure A.6 only display all the information in the main output of the CMa, but it is also possible to utilise for instance the information in the processing flag and perhaps combine it with the main output in a useful way. In figure A.7 the bit number 9 of the processing flag, indicating a low quality (due to a value for a pixel in some feature being close

to the threshold determining the output) or risk for misclassification, is shown (purple) on top of the main output.

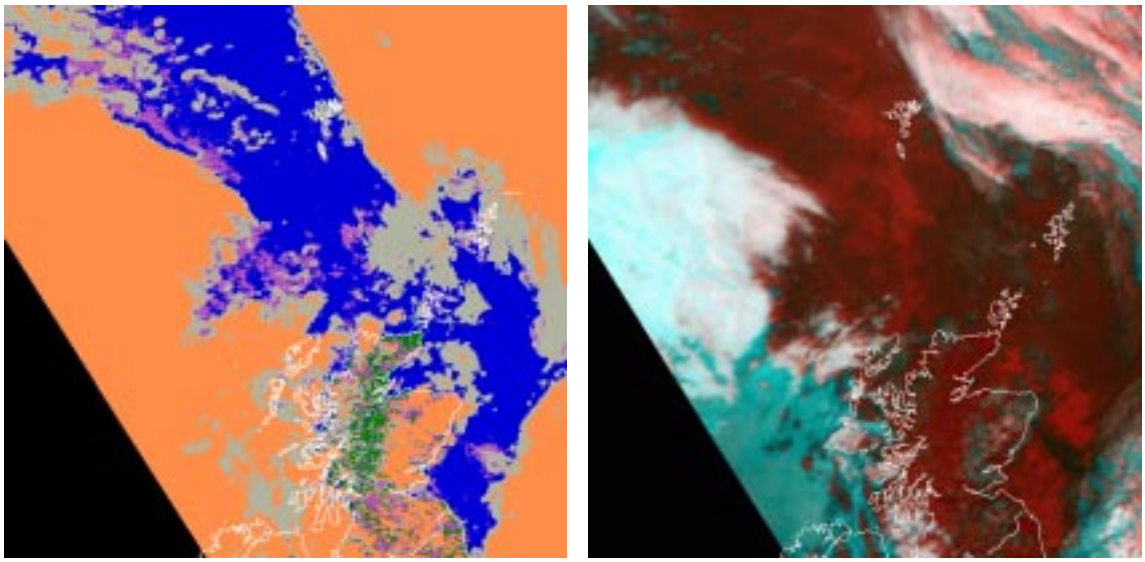

Figure A.7: Derived colour image showing the result of the Cloud Mask with the flag for low quality superimposed in purple (left) and the corresponding channel 3,4,5 RGB-composite image (right). The same satellite overpath as in A.6.

A.11.2 Cloud Type

For the current version of the CTy algorithm no discrimination of cumuliform and stratiform clouds is attempted. Thus the main output from the CTy algorithm is a classification into 16 classes (cloud types, surface, and unprocessed and unclassified). But as for the Cloud Mask, the product is a data product, containing more information than just the cloud types.

However, in figure A.8 we give examples of how information in the CTy product may be visualised for the user. One can choose to display all available classes or highlight one or a few cloud categories suitable for the application of interest. The example covers the same satellite scene as shown in figure A.6 and A.7.

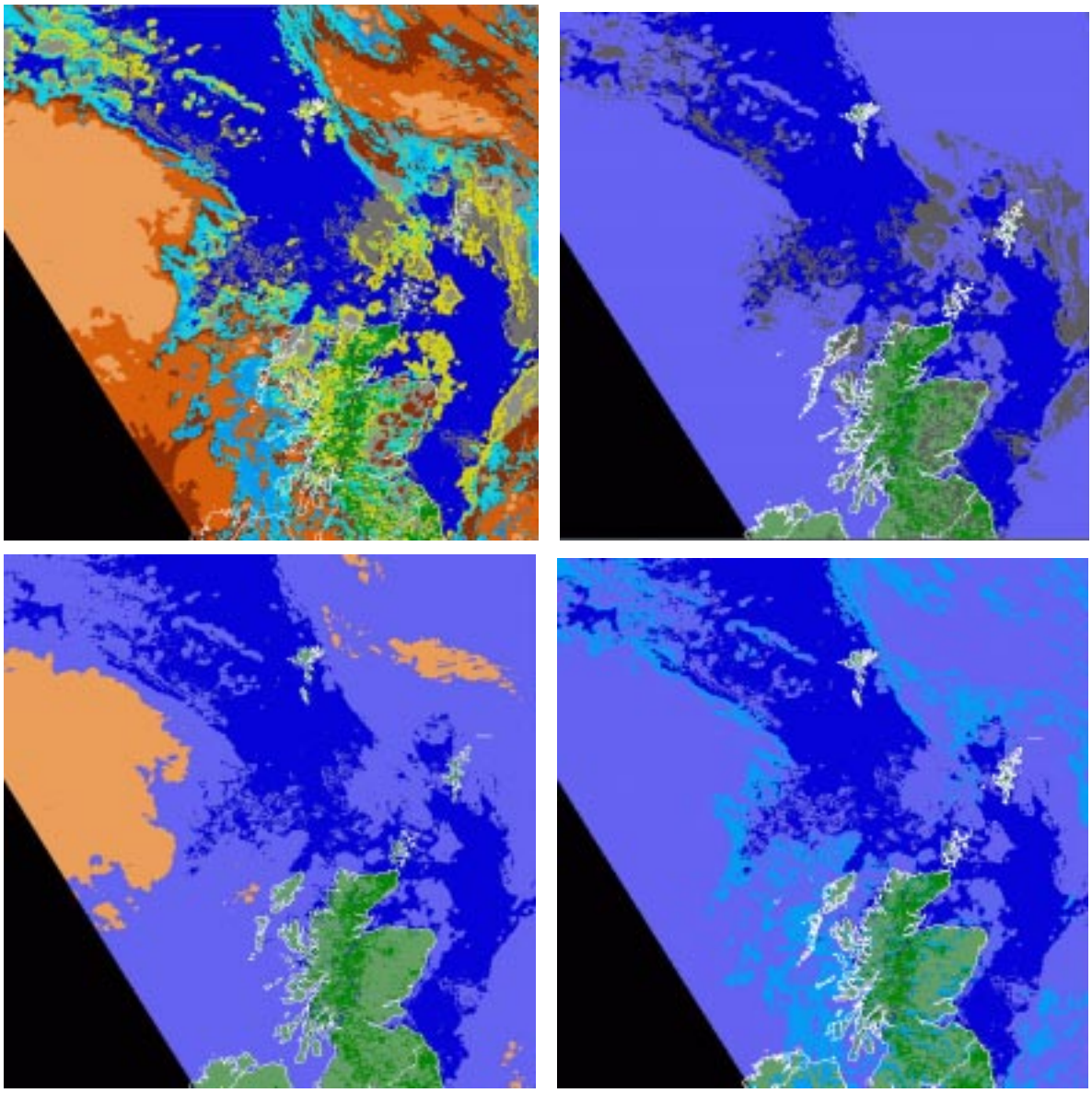

*Figure A.8: Four different image examples of the visualisation of the Cloud Type product. In the **upper left** all cloud categories are shown using the LUT specified in section 4.3. The **upper right** show the very low cloud and the low cloud category as dark grey, the **lower left** the very high cloud category (light orange), and in the **lower right** image only the four cirrus classes are highlighted (cyan). The same satellite overpath as in A.6.*

A.11.3 Cloud Top Temperature and Height

The CTTH product is more difficult to visualise. The product, if used as an image on the forecasters desk, will naturally be displayed in an interactive visualisation system, where individual pixel values (height and temperature) may be displayed while moving the mouse over the image. In figure A.9 we show an example image, however, of the Cloud Top Temperature of the opaque clouds as determined by the CTy. The temperature contrasts are shown using a linear grey scale. The lowest temperatures are -49.0 C (white) and the highest 9.0 C (dark grey). A land-sea mask (from the land use database) has been applied.

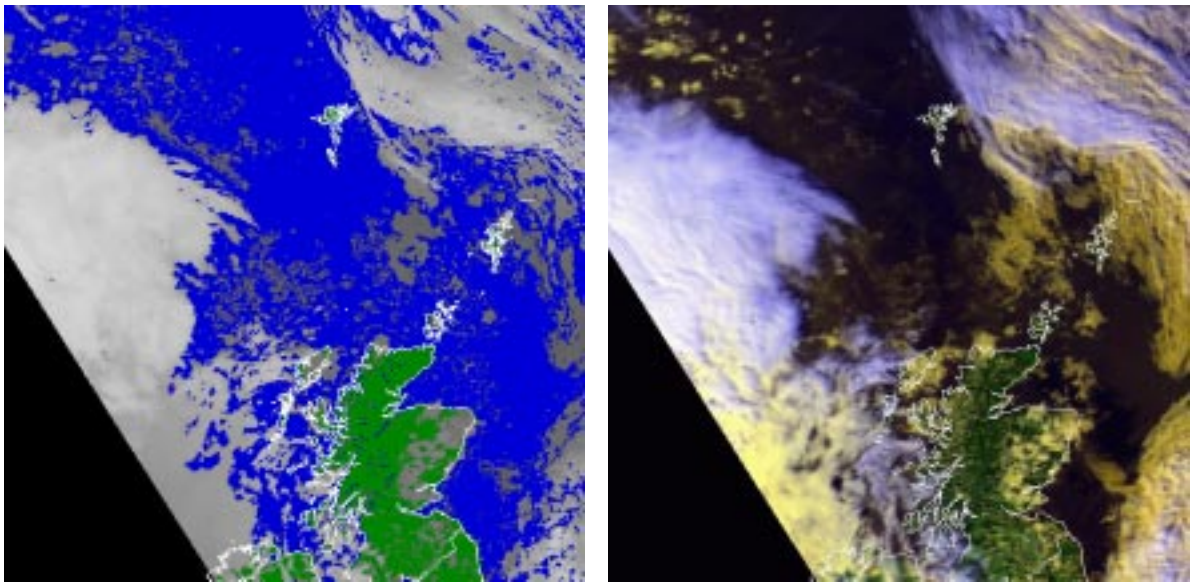

Figure A.9: Cloud Top Temperature image (left) giving temperatures of opaque clouds using a linear grey scale. Cold is white (minimum –49.0 C) and warm is shown dark grey to black (maximum 9.0 C).Please notice that opaque or fractional clouds are not visualised, To the right a channel 1,2,4 RGB-composite is added for comparison. The same satellite overpath as in A.6.

A.11.4 Precipitating Cloud

The precipitating cloud product contains the likelihood for three precipitation classes:

- Risk for/light precipitation (>0.1mm/h to 0.5mm/h)
- Light/moderate precipitation (>0.5mm/h to 5.0mm/h)
- Intensive precipitation (> 5.0mm/h)

The visualisation of the product is realised as an RGB composite assigning red to risk for/light precipitation, green to light/moderate precipitation and blue to intensive precipitation. Bright blue thus signifies a high risk for intensive precipitation whereas brown, green and grey scales signify a higher likelihood for light to moderate precipitation. A low likelihood of precipitation is given by almost black to dark brown colouring. In areas which have been assigned to be not raining, the land/sea mask is displayed as green (land) and blue (sea).

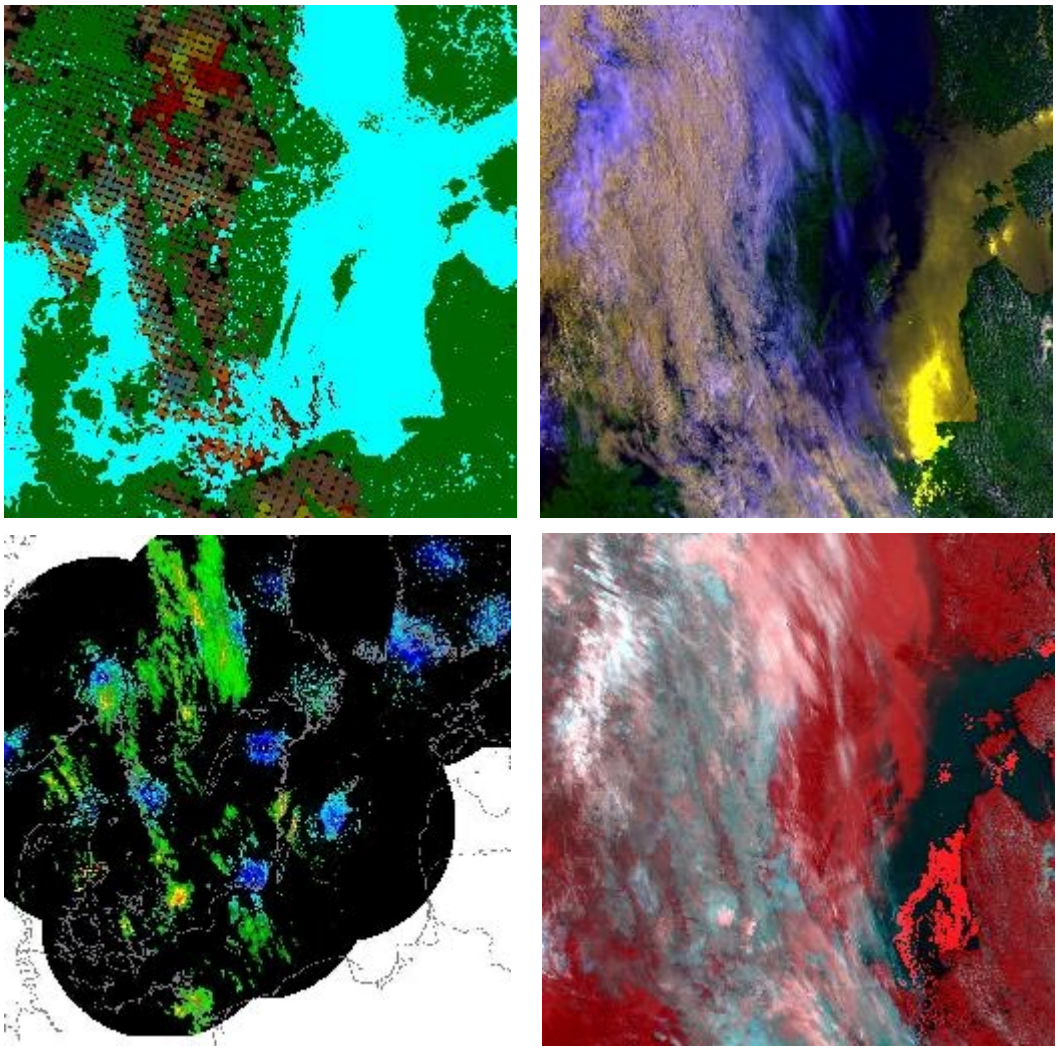

Figure A.10: Products for NOAA15 overpath18 June 2000, 07:39 UTC. ***Upper left:*** *PC product, RGB-composite of likelihoods for light, moderate and intensive precipitation (see text).* ***Lower left:*** *radar composite 7:45UTC, radar reflectivities [dBZ] displayed. Blue denotes very low intensities (mostly artefacts), green tones light to moderate intensities and yellow to red moderate to strong intensities.* ***Upper right:*** *RGB-composite of AVHRR channels 1, 2, 3.* ***Lower right:*** *RGB- composite of AVHRR channels 3,4,5.*

Two different examples of algorithm performance are presented. For the example 18 June 2000, it becomes quite obvious when studying the AVHRR RGB composites, that an AVHRR only algorithm would have failed in locating the mostly light precipitation correctly, whereas the AMSU located the precipitation quite accurately. For the example of the 27th of June 2000, the AMSU fails to detect fails to detect many small convective cells over the southern Baltic. This is caused by the fairly large fields of view for AMSU. On the other hand is the frontal precipitation over Sweden captured rather nicely, including the variations in intensity

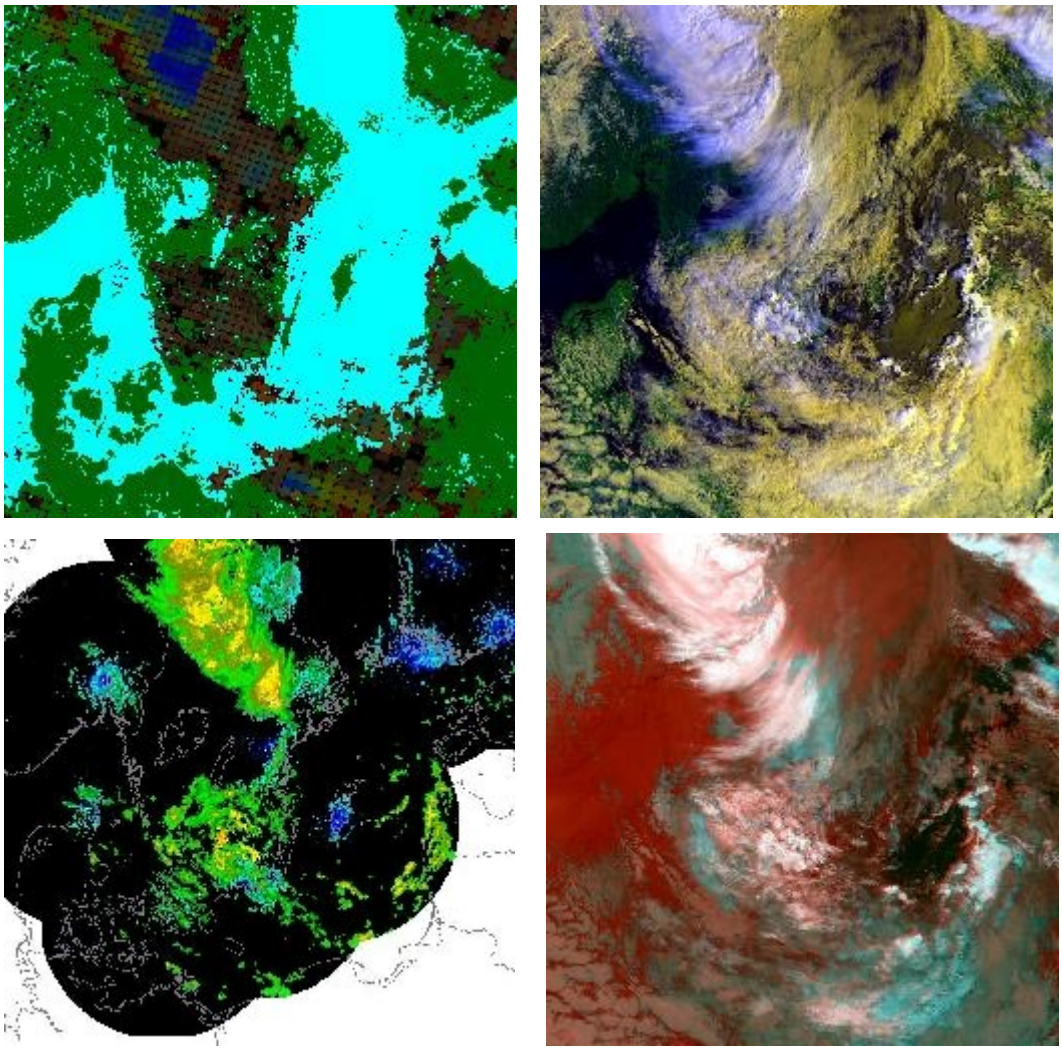

Figure A.11: Products for NOAA15 overpath 27 June 2000, 07:37 UTC. ***Upper left:*** *PC product, RGB of likelihoods for light, moderate and intensive precipitation (see text).* ***Lower left****: radar composite 7:30UTC, radar reflectivities [dBZ]displayed. Blue denotes very low intensities (mostly artefacts), green tones light to moderate intensities and yellow to red moderate to strong intensities.* ***Upper right:*** *RGB-composite of AVHRR channels 1, 2, 3.* ***Lower right:*** *RGB- composite of AVHRR channels 3,4,5.*